

Post-Newtonian observables for aligned-spin binaries to sixth order in spin from gravitational self-force and Compton amplitudes

Yilber Fabian Bautista,^{1,*} Mohammed Khalil,^{2,†} Matteo Sergola,^{1,‡} Chris Kavanagh,^{3,§} and Justin Vines⁴

¹*Institut de Physique Théorique, CEA, Université Paris–Saclay, F–91191 Gif-sur-Yvette cedex, France*

²*Perimeter Institute for Theoretical Physics, 31 Caroline Street North, Waterloo, ON N2L 2Y5, Canada*

³*School of Mathematics & Statistics, University College Dublin, Belfield, Dublin 4, Ireland, D04 V1W8*

⁴*Mani L. Bhaumik Institute for Theoretical Physics,*

University of California at Los Angeles, Los Angeles, CA 90095, USA

Accurate modeling of compact binaries is essential for gravitational-wave detection and parameter estimation, with spin being an important effect to include in waveform models. In this paper, we derive new post-Newtonian (PN) results for the conservative aligned-spin dynamics at next-to-next-to-leading order for the spin³ and spin⁴ contributions, in addition to the next-to-leading order (NLO) spin⁵ and spin⁶ contributions. One approach we follow is the Tutti Frutti method, which relates PN and gravitational self-force (GSF) results through the redshift and spin-precession invariants, by making use of the simple dependence of the scattering angle on the symmetric mass ratio. However, an ambiguity arises at the NLO spin⁵ contribution, due to transcendental functions of the Kerr spin in the redshift; this is also the order at which Compton amplitudes calculations are affected by spurious poles. Therefore, we follow an additional approach to determine the NLO spin⁵ and spin⁶ dynamics: using on-shell Compton amplitudes obtained from black hole perturbation theory. The Compton amplitude used in this work is composed of the unambiguous tree-level far-zone part reported in [Phys. Rev. D 109, no.8, 084071 (2024)], as well as the full, non-interfering with the far-zone, $\ell = 2$ partial wave contributions from the near zone, which are responsible for capturing Kerr finite-size effects. Other results in this paper include deriving the scattering angle of a spinning test body in a Kerr background from a parametrized worldline action, and computing the redshift and spin-precession invariants for eccentric orbits without an eccentricity expansion.

I. INTRODUCTION

Several analytical approximation methods exist for modeling the dynamics of compact binary systems in general relativity: the post-Newtonian (PN) approximation [1–5], which is an expansion in small velocities and large separations; the post-Minkowskian (PM) approximation [6–9], which is an expansion in large separations but for arbitrary velocities; and gravitational self-force (GSF) [10–13], which provides an expansion in the small mass-ratio but is valid for arbitrary velocities in the strong-field regime. Over the past two decades, remarkable advancements in the computation of PN and PM observables have been achieved using techniques inspired by quantum mechanics and particle physics, such as effective field theory (EFT) [3–5, 14–27], worldline quantum field theory [28–35], and scattering amplitudes [35–60]. Recently, there has also been work in applying and synergizing these methods with the self-force approach [61–63], and vice versa; i.e. using self-force for scattering calculations [64–66].

In the modern on-shell approach, compact objects are typically described as point particles interacting through the exchange and emission of gravitons, which resembles scattering problems in particle physics. This

description is of course an effective one as the extended nature of the compact object manifests when the energies of the exchanged gravitons are large enough to resolve the object’s finite-size structure. For instance, in a gravitational-wave scattering off a black hole (BH) scenario, the extended nature of the BH is elucidated starting at the fifth power of the ratio of the Schwarzschild radius to the wavelength of the graviton, i.e. $\sim (GM/\lambda)^5$, when tidal deformations [67, 68], and tidal heating effects start to take place [69, 70]. To capture these effects, the effective point-particle description needs to be extended by, for example, incorporating non-minimal operators in an EFT Lagrangian, which renormalize UV divergences appearing from considering the compact objects as point particles, in addition to capturing the extended nature of such objects through the coefficients of those operators [71–73].

A first-principle reconstruction of compact objects would naturally predict the values of the effective coefficients; this is however inaccessible at the moment. An EFT approach on the other hand uses a matching procedure to fix the value of such coefficients, but ignores the nature of how such values arise from a complete UV description. Although, an intermediate situation may arise in an EFT approach when a set of consistency rules, and perhaps hidden symmetries describing the compact objects, could emerge, providing alternative convenient ways to predict the values of some EFT coefficients. Well-known examples appeared in the literature when considering the amplitudes that describe

* yilber-fabian.bautista-chivata@ipht.fr

† mkhalil@perimeterinstitute.ca

‡ matteo.sergola@ipht.fr

§ chris.kavanagh1@ucd.ie

the linearized, isolated Kerr BH, where the uniqueness of its spin-multipole moments [74] can be recast in the simplest possible 3-point amplitude involving two massive spinning legs and one graviton [38, 75].

Analogous proposals appeared at the level of the Compton amplitude, among them is the minimal coupling proposals for low orders in spin, including the double copy [38, 41, 75–78], the spin-shift symmetry¹ [79–82], spin-resummed predictions from amplitudes with massive gauge symmetries and improved high energy behavior [83, 84], bootstrapped heavy-mass effective fields ansatz [85, 86], Neuman-Janis shifts and twistor dynamics [87–89], worldline and dynamical spin-multipole moments [90, 91], and superstring amplitudes [92, 93]. A proposal for effective amplitudes obtained directly from black hole perturbation theory (BHPT) computations appeared in Refs. [52, 94], with a recent connection to CFT [95]; the latter reference also discussed a separation of the tree-level Compton amplitude in an unambiguous far-zone contribution and a somehow more intriguing near-zone piece. These 3-point and Compton amplitudes are building blocks for the binary BH problem at lower orders in the PM expansion, and as such, are of primordial interest.

Identifying symmetries and consistency conditions is more cumbersome when the BH’s finite-size effects are present, the latter being naturally captured by near-zone contributions in the Teukolsky solutions. Although the near-zone contributions in the Compton amplitude have a unique spin-multipole expansion (SME)—as we show in Sec. III by matching a unique spin-5 and spin-6 covariant contact term to the leading $\ell = 2$ solutions of the Teukolsky equation in the near-zone region—it is ambiguous to separate a tree-level, point-particle contribution, from the BH finite-size contributions. This is because higher-order-spin contributions get mixed with dynamical tidal deformations, as we also observe in this work. Hence, in this paper we follow a somewhat intermediate approach where the Compton amplitude used to construct two-body observables is composed of the unambiguous tree-level far-zone contribution, as well as the unambiguous, non-perturbative (in the Kerr spin) complete $\ell = 2$ near-zone contribution, in turn capturing finite-size effects at first self-force order (1SF), and avoiding the ambiguities appearing when trying to extract a tree-level near-zone contribution. Analogous non-perturbative matching computations have been done in the absorptive sector, see for instance Refs. [69, 96].

More precisely, in this paper, we study the imprints of the aforementioned Compton amplitude on the conservative 2PM scattering angle, and indirectly on the redshift [97–107] and spin-precession frequency [108–

114]. Our work then provides an alternative approach to obtaining gauge-invariant observables from the, also gauge-invariant, scattering amplitudes. In particular, we show how several terms in such observables, obtained from a traditional GSF approach involving the reconstruction of the regular piece of the off-shell metric perturbation, can be obtained purely from the scattering amplitudes in a Kerr BH gravitational-wave scattering process. The Compton amplitude then serves as an “on-shell reconstruction” of the perturbation avoiding any subtlety related to gauge choices.

In addition to the scattering amplitudes approach, we also compute the aligned-spin dynamics using the Tutti Frutti method [115–118], which takes advantage of the simple dependence of the PM-expanded scattering angle on the symmetric mass ratio [119] to relate PN results valid for generic mass ratios to GSF results at lower orders in the mass ratio. The comparison of PN and GSF results is done through the redshift and spin-precession frequency; these gauge-invariant quantities are computed in the GSF literature by solving analytically the non-homogeneous Teukolsky or Regge–Wheeler–Zerilli equations in a PN expansion using, for example, the Mino-Sasaki-Tanaka (MST) method [120, 121], while in a PN calculation they can be computed from a Hamiltonian using the first law of binary mechanics [118, 122–126].

Using this method, we derive the aligned-spin dynamics at the next-to-leading PN order (NLO) spin⁵ and spin⁶ for generic orbits. However, computing the redshift and spin-precession invariants for eccentric orbits in terms of frequencies requires more PN information at lower orders in spin than the NLO. In particular, the NLO spin⁵ and spin⁶ contributions require information from the next-to-next-to-leading order (NNLO) spin³ and spin⁴ dynamics, which we derive in this paper for the first time. However, while we obtain the full NNLO spin³ contribution from existing GSF results, our result for the NNLO spin⁴ contribution contains one unknown coefficient that requires currently unavailable GSF results. We highlight the PN and spin orders derived in this work in Table I.

To perform the above calculations, we also needed to compute some results for a spinning test-body in a Kerr background. In particular, we computed the redshift and spin-precession frequency to sixth order in the Kerr spin for arbitrary eccentricities. We also derived the scattering angle of a spinning test body, to fifth order in its spin and sixth order in the Kerr spin, starting from the parametrized worldline action presented in Ref. [91], with generic Wilson coefficients. Then, we obtained constraints on the values of these coefficients by comparing the scattering angle with the one derived from a Compton amplitudes calculation, and with GSF results.

This paper is structured as follows:

- In Sec. II, we compute the redshift and spin-precession frequency from a parametrized PN

¹Although this was first proposed at the level of the two-body amplitude, it can be shown to be a consequence of the symmetry of the helicity-preserving gravitational Compton amplitude for low orders in spin.

Hamiltonian, for both circular and eccentric orbits, after relating its coefficients to those of an ansatz for the scattering angle. Then, we compare our results with GSF results to solve for the unknowns.

- In Sec. III, we use on-shell Compton amplitudes matched to BHPT to compute the 2PM scattering angle to sixth order in spin.
- In Sec. IV, we combine results from both approaches and discuss three possibilities to resolve an ambiguity in determining the NLO spin⁵ dynamics, in addition to confirming the unambiguous spin⁶ solution. Summary of our findings is provided in Table II.
- In Sec. V, we derive the scattering angle of a spinning test body from a worldline action with generic Wilson coefficients, and use GSF and Compton amplitudes results to constrain those coefficients.

We conclude in Sec. VI, and provide in Appendix A the test-body results for the redshift and spin-precession frequency to all orders in eccentricity, while Appendix B contains the full expressions of the BHPT-matched Compton coefficients. Most of our results are provided as electronic files in the Supplemental Material [127].

Notation

We use the metric signature $(-, +, +, +)$, and geometric units in which $c = G = 1$, but we write c and G explicitly for clarity in some PN and PM expansions.

For a binary with masses m_1 and m_2 , we assume that $m_1 \geq m_2$, and define the following combinations of the masses:

$$\begin{aligned} M &= m_1 + m_2, & \mu &= \frac{m_1 m_2}{M}, & \nu &= \frac{\mu}{M}, \\ q &= \frac{m_2}{m_1}, & \delta &= \frac{m_1 - m_2}{M}. \end{aligned} \quad (1)$$

For an aligned-spin binary with spins S_1 and S_2 , we define the spin lengths $a_i = S_i/m_i$, where $i = 1, 2$. The spin length of a Kerr BH is denoted a , with the dimensionless spin χ defined as $\chi = a/m_1$, and we define the quantity $\kappa = \sqrt{1 - \chi^2}$.

We also define the total energy $E = E_1 + E_2$ of the binary and effective energy E_{eff} via the energy map

$$\Gamma := \frac{E}{M} = \sqrt{1 + 2\nu(\gamma - 1)}, \quad (2a)$$

$$\gamma := \frac{E_{\text{eff}}}{\mu} = \frac{E^2 - m_1^2 - m_2^2}{2m_1 m_2}, \quad (2b)$$

where the Lorentz factor γ is related to the relative velocity v by

$$\gamma = \frac{1}{\sqrt{1 - v^2}}. \quad (3)$$

The azimuthal frequency is denoted Ω and the relativistic periastron advance is denoted k , from which we define the following variables:

$$x := (M\Omega)^{2/3}, \quad \iota := \frac{3x}{k}, \quad (4a)$$

$$y := (m_1\Omega)^{2/3}, \quad \lambda := \frac{3y}{k}. \quad (4b)$$

The redshift and spin-precession frequency are denoted z_i and Ω_{S_i} , while the spin-precession invariant is defined as $\psi_i := \Omega_{S_i}/\Omega$.

The magnitude of the canonical orbital angular momentum is denoted L , and is related to the relative position r , radial momentum p_r , and total linear momentum p via $p^2 = p_r^2 + L^2/r^2$. The Hamiltonian is denoted \mathcal{H} , and we define $u := M/r$.

In Sec. III, related to wave perturbations of spin-weight s off Kerr BH, we use the following notation:

$$\epsilon = 2Gm_1\omega, \quad (5)$$

which is the PM wave scattering parameter, with ω the energy of the scattered wave.

II. BOUND-ORBIT PN OBSERVABLES FROM SCATTERING AND GSF RESULTS

In this section, we derive new PN results at the NNLO for the S^3 and S^4 conservative dynamics, in addition to the NLO S^5 and S^6 dynamics. We follow the Tutti Frutti approach [115, 116, 118] by taking advantage of the simple dependence of the PM-expanded scattering angle on the mass ratio, which makes it possible to obtain NNLO PN results valid for arbitrary mass ratios from GSF results at first order in the mass ratio.

We first obtain a Hamiltonian whose coefficients are matched to a scattering angle ansatz parametrized by unknown coefficients that satisfy the mass-ratio dependence of the scattering angle. We then compute the redshift and spin-precession frequency from the Hamiltonian, for both circular and eccentric orbits in terms of the frequencies, and expand them to first order in the mass ratio. Finally, we express these gauge-invariant quantities in terms of the Kerr geodesic variables used in GSF calculations, and compare them to 1SF results to determine the unknown coefficients. In Sec. III, we discuss an alternative approach to fixing the scattering angle's free coefficients at NLO S^5 and S^6 using information from Compton amplitudes and BHPT computations.

For circular orbits, computing the redshift and spin-precession frequency in terms of the orbital frequency up to NLO S^n requires only the 1PN non-spinning contribution and the NLO $S^{m < n}$. However, for eccentric orbits, two frequencies exist: the radial and azimuthal frequencies, which agree at Newtonian order but differ starting at 1PN order. Therefore, expressing the redshift

TABLE I. This table summarizes the PN orders for the conservative dynamics at which each order in spin appears in the Hamiltonian, and the corresponding orders in x (which are the same as y and u_p) in the redshift z and spin-precession invariant ψ . We derive new PN results for the full NNLO S^3 , NLO S^5 , and NLO S^6 contributions (highlighted in green), in addition to the NNLO S^4 contribution (highlighted in orange) for which one unknown coefficient remains at $\mathcal{O}(\nu a_1^2 a_2^2)$. Note that the spin counting in this table follows the spin orders in the Hamiltonian, but since the spin-precession frequency involves a derivative with respect to spin, the spin orders in ψ are one power lower than the Hamiltonian.

Spin	LO	z	ψ	NLO	z	ψ	NNLO	z	ψ	N ³ LO	z	ψ	N ⁴ LO	z
S^0	0PN	x	–	1PN	x^2	–	2PN	x^3	–	3PN	x^4	–	4PN	x^5
S^1	1.5PN	$x^{5/2}$	x	2.5PN	$x^{7/2}$	x^2	3.5PN	$x^{9/2}$	x^3	4.5PN	$x^{11/2}$	x^4		
S^2	2PN	x^3	$x^{3/2}$	3PN	x^4	$x^{5/2}$	4PN	x^5	$x^{7/2}$	5PN	x^6	$x^{9/2}$		
S^3	3.5PN	$x^{9/2}$	x^3	4.5PN	x^4	x^4	5.5PN	$x^{13/2}$	x^5					
S^4	4PN	x^5	$x^{7/2}$	5PN	x^6	$x^{9/2}$	6PN	x^7	$x^{11/2}$					
S^5	5.5PN	$x^{13/2}$	x^5	6.5PN	$x^{15/2}$	x^6								
S^6	6PN	x^7	$x^{11/2}$	7PN	x^8	$x^{13/2}$								

and spin-precession invariants in terms of frequencies, which is needed for GSF comparisons (see e.g. Ref. [128]), requires including higher PN orders at lower orders in spin. In particular, the NLO S^5 and S^6 contributions require including the NNLO S^3 and S^4 , which in turn require the N³LO S^1 and S^2 contributions, in addition to the 4PN non-spinning contribution.

In Table I, we include all the PN orders needed to compute the NLO S^6 redshift and spin-precession frequency for eccentric orbits, while indicating the powers in $x := (M\Omega)^{2/3}$ at each order.

A. PN Hamiltonian and its relation to the scattering angle

For the Hamiltonian, we use a “quasi-isotropic” gauge [129], in which the aligned-spin Hamiltonian depends only on p^2 and r but not explicitly on L except as an overall factor for the odd-in-spin contributions.

We begin by writing down a general ansatz for the two-body Hamiltonian as

$$\mathcal{H} = \sum_{n=0}^6 \mathcal{H}_{S^n} + \mathcal{O}(S^7), \quad (6)$$

where each \mathcal{H}_{S^n} contains spin contributions of $\mathcal{O}(S^n)$. We fix the gauge freedom in the 0PM part of the Hamiltonian using the effective-one-body gauge, as in Ref. [129], which is given by

$$\mathcal{H}_{0\text{PM}} = M \sqrt{1 + 2\nu \left(\sqrt{1 + \mathbf{p}^2/\mu^2} - 1 \right)}. \quad (7)$$

The non-spinning part of the Hamiltonian in this gauge was provided to 3PN order in Ref. [129]. Schematically it reads

$$\mathcal{H}_{S^0} = Mc^2 + \left(\frac{\mathbf{p}^2}{2\mu^2} - Gu \right)$$

$$\begin{aligned} & + \frac{1}{c^2} \left[-\frac{1}{8}(1 + \nu) \frac{\mathbf{p}^4}{\mu^4} + \alpha_{11} G \frac{\mathbf{p}^2}{\mu^2} u + \alpha_{12} G^2 u^2 \right] \\ & + \frac{1}{c^4} \left[\frac{1}{16} (\nu^2 + \nu + 1) \frac{\mathbf{p}^6}{\mu^6} + \alpha_{21} G \frac{\mathbf{p}^4}{\mu^4} u \right. \\ & \left. + \alpha_{22} G^2 \frac{\mathbf{p}^2}{\mu^2} u^2 + \alpha_{23} G^3 u^3 \right] + \mathcal{O}(1/c^6), \quad (8) \end{aligned}$$

where $u := M/r$, the 0PM coefficients are the PN expansion of Eq. (7), and we obtained the coefficients α_{ij} through 4PN order by canonically transforming the Hamiltonian of Ref. [130]. We provide the Hamiltonian in the Supplemental Material.

The spin contributions can be organized for odd-in-spin terms as

$$\begin{aligned} \mathcal{H}_{S^n} = & \frac{L}{c^{1+2n}} \frac{\mathbf{a}^{(n)}}{r^{n+1}} \cdot \left[\alpha_{11}^{(n)} Gu \right. \\ & + \frac{1}{c^2} \left(\alpha_{31}^{(n)} G \frac{\mathbf{p}^2}{\mu^2} u + \alpha_{32}^{(n)} G^2 u^2 \right) \\ & + \frac{1}{c^4} \left(\alpha_{51}^{(n)} G \frac{\mathbf{p}^4}{\mu^4} u + \alpha_{52}^{(n)} G^2 \frac{\mathbf{p}^2}{\mu^2} u^2 + \alpha_{53}^{(n)} G^3 u^3 \right) \\ & \left. + \mathcal{O}(1/c^6) \right], \quad (9) \end{aligned}$$

with $n = 1, 3, 5$. For even-in-spin terms, a convenient parametrization is

$$\begin{aligned} \mathcal{H}_{S^n} = & \frac{\mu \mathbf{a}^{(n)}}{c^{2n} r^n} \cdot \left[\alpha_{01}^{(n)} Gu \right. \\ & + \frac{1}{c^2} \left(\alpha_{21}^{(n)} G \frac{\mathbf{p}^2}{\mu^2} u + \alpha_{22}^{(n)} G^2 u^2 \right) \\ & + \frac{1}{c^4} \left(\alpha_{41}^{(n)} G \frac{\mathbf{p}^4}{\mu^4} u + \alpha_{42}^{(n)} G^2 \frac{\mathbf{p}^2}{\mu^2} u^2 + \alpha_{43}^{(n)} G^3 u^3 \right) \\ & \left. + \mathcal{O}(1/c^6) \right], \quad (10) \end{aligned}$$

with $n = 2, 4, 6$. As summarized in Table I, we include the N³LO in \mathcal{H}_{S^1} and \mathcal{H}_{S^2} , the NNLO in \mathcal{H}_{S^3} and \mathcal{H}_{S^4} , and the NLO in \mathcal{H}_{S^5} and \mathcal{H}_{S^6} .

Let us explain our notation in Eqs. (9) and (10). To render the treatment of the spin sectors systematic, we introduced two $(n+1)$ -vectors

$$\begin{aligned} \mathbf{a}^{(n)} &:= (a_1^n, a_1^{n-1}a_2, a_1^{n-2}a_2^2, \dots, a_2^n), \\ \boldsymbol{\alpha}_{ij}^{(n)} &:= (\alpha_{ij}^{n0}, \alpha_{ij}^{(n-1)1}, \alpha_{ij}^{(n-2)2}, \dots, \alpha_{ij}^{0n}), \end{aligned} \quad (11)$$

whose number of entries increases with the spin order. The symbol $\mathbf{a}^{(n)}$ is a vector where each entry is a monomial of the form $a_1^k a_2^l$ such that $k+l = n$. $\mathbf{a}^{(n)}$ is dotted into another vector, $\boldsymbol{\alpha}_{ij}^{(n)}$, whose entries are coefficients that are matched to the scattering angle ansatz in the following subsection. The indices have the following meaning: α_{ij}^{lm} is a coefficient which multiplies a contribution proportional to $(v/c)^i G^j a_1^l a_2^m$. Although we employ Eqs. (9) and (10) through $\mathcal{O}(S^6)$, the same structure holds to arbitrarily high orders in spin.

Next, we compute the scattering angle from the Hamiltonian written in terms of the $\{\alpha\}$ coefficients. This is done by solving the equation $\mathcal{H} = E$ for the radial momentum $p_r^2 = \mathbf{p}^2 - L^2/r^2$, perturbatively in a PN expansion, and obtaining the scattering angle via [8]

$$\theta(E, L, \{\alpha\}) = -\pi - 2 \int_{r_{\min}}^{\infty} dr \frac{\partial}{\partial L} p_r(E, L, r, \{\alpha\}), \quad (12)$$

where r_{\min} is the turning point, obtained from the largest root of $p_r(E, L, r) = 0$.

It is important to note that L in the above equation is the magnitude of the canonical orbital angular momentum $L = |\mathbf{r} \times \mathbf{p}|$, corresponding to the Newton-Wigner spin-supplementary condition [131, 132], which is needed when working in a Hamiltonian formalism. However, in the scattering angle, it is more convenient to use the covariant angular momentum L_{cov} , corresponding to the covariant (Tulczyjew-Dixon) spin-supplementary condition [133–135], since the impact parameter $b = \sqrt{-b^\mu b_\mu}$ (the covariant initial separation of the binary) can be defined as

$$b := \frac{L_{\text{cov}}}{|\mathbf{p}|}. \quad (13)$$

The canonical and covariant angular momenta are related via the total angular momentum

$$\begin{aligned} J &= L + m_1 a_1 + m_2 a_2, \\ &= L_{\text{cov}} + E_1 a_1 + E_2 a_2, \end{aligned} \quad (14)$$

which is valid to all orders in spin. Solving this equation for L , leads to [74, 129]

$$L = \frac{\mu\gamma v}{\Gamma} b + M \frac{\Gamma - 1}{2} \left[a_1 + a_2 - \frac{\delta}{\Gamma} (a_1 - a_2) \right], \quad (15)$$

where Γ and $\gamma = 1/\sqrt{1-v^2}$ are given by Eqs. (2).

Thus, we can evaluate the scattering angle in Eq. (12) after replacing L by b such that

$$\theta(b, v, \{\alpha\}) = -\pi + 2 \frac{M\Gamma}{\mu\gamma v} \int_0^{1/b} \frac{du}{u^2} \frac{\partial}{\partial b} p_r(E, b, u, \{\alpha\}). \quad (16)$$

We note that this integral involves divergences which can be treated by taking the Hadamard partie finie at the unperturbed turning point [8, 136]. Finally, we equate the angle obtained from the Hamiltonian to an ansatz for the angle that satisfies the mass-ratio dependence of the PM-expanded scattering angle, as explained in the following subsection.

B. Scattering angle parametrization

The PM expansion of the scattering angle θ , in the center-of-mass frame scaled by the energy θ/Γ , has a simple dependence on the mass ratio that was proven in Ref. [119] (see also Ref. [129]) and extended to spin in Ref. [118]. The structure is such that at each n PM order for non-spinning binaries, θ/Γ is a polynomial in the symmetric mass ratio ν of degree $\lfloor (n-1)/2 \rfloor$. When spin is included, the angle also depends on the antisymmetric mass ratio $\delta := (m_1 - m_2)/M$, because of the symmetry under the exchange of the two bodies' labels. (See Refs. [118, 119, 137] for a more detailed discussion.)

We split the spin contributions to the scattering angle θ as

$$\theta = \sum_{n=0}^6 \theta_{S^n} + \mathcal{O}(S^7). \quad (17)$$

As discussed at the beginning of this section, computing the redshift and spin-precession invariants for eccentric orbits to NLO S⁵ and S⁶, in a form suitable for comparison with GSF results, requires information from the N³LO S¹ and S² contributions, in addition to the NNLO S³ and S⁴ contributions. In the following paragraphs, we overview the knowledge of each of these pieces, some of which are fully known and some of which we give in parametrized form.

The 3PN non-spinning contribution θ_{S^0} is given to 3PN order by Eq. (4.32a) of Ref. [129], while the N³LO (4.5PN) S¹ contribution was derived in Refs. [118, 138–140] and is given by Eq. (7) of Ref. [138]. The N³LO (5PN) S² contribution was derived in Refs. [141–143], and is given by Eqs. (6.17)–(6.20) of Ref. [143]. Thus, the scattering angle completely determines the N³LO S¹ and S² contributions to the Hamiltonian.

In Ref. [38] (see Eq. (1.12) there), the authors obtained the fully-relativistic one-loop (2PM) scattering angle of two Kerr BHs with aligned spins a_1 and a_2 . As explained there, this angle is to be trusted only through spin order $\mathcal{O}(a_1^n a_2^m)$ where *both* n and m are less than or equal 4. This is because higher spin terms are affected by spurious

poles inside the Compton amplitudes which constitute the needed cuts.

In Sec. V B, we derive the scattering angle of a spinning test body to 6PM order and fifth order in spin, starting from the parametrized worldline action of Ref. [91] in terms of generic Wilson coefficients. Our result reduces to the 2PM angle of Ref. [38] at fourth order in spin, after setting the Wilson coefficients to their values for BHs [117].

Therefore, because of the structure of the scattering angle discussed above, the test-body scattering angle at 2PM order yields the full NLO (4.5PN) S^3 and NLO (5PN) S^4 dynamics for aligned spins, which were later derived for generic spins in Refs. [144–146]. We write the S^3 part of the scattering angle through NNLO as

$$\theta_{S^3} = \theta_{S^3}^{\text{test}} + \theta_{S^3}^{3\text{PM},4.5\text{PN}} + \theta_{S^3}^{3\text{PM},5.5\text{PN}}, \quad (18)$$

where $\theta_{S^3}^{\text{test}}$ is obtained from the cubic-in-spin part of the test-body scattering angle (102), $\theta_{S^3}^{3\text{PM},4.5\text{PN}}$ is the 4.5PN part of the 3PM contribution, while $\theta_{S^3}^{3\text{PM},5.5\text{PN}}$ includes the 5.5PN part at 3PM order. The term $\theta_{S^3}^{3\text{PM},4.5\text{PN}}$ is known from the NLO S^3 Hamiltonian, which only includes 2PM terms at 4.5PN order, and we parametrize the unknown term $\theta_{S^3}^{3\text{PM},5.5\text{PN}}$ as

$$\begin{aligned} \frac{\theta_{S^3}^{3\text{PM},5.5\text{PN}}}{\Gamma} &= \frac{G^3 M^3}{b^6 v} \left[(f_{30} + \delta g_{30} + \nu h_{30}) a_1^3 \right. \\ &\quad + (f_{21} + \delta g_{21} + \nu h_{21}) a_1^2 a_2 + (f_{30} - \delta g_{30} + \nu h_{30}) a_2^3 \\ &\quad \left. + (f_{21} - \delta g_{21} + \nu h_{21}) a_1 a_2^2 \right], \end{aligned} \quad (19)$$

where f_{ij} , g_{ij} and h_{ij} are some dimensionless coefficients independent of the mass, and we made use of the symmetry under the exchange of the two bodies' labels to reduce the number of unknowns in the above ansatz.

Similarly, we write the S^4 scattering angle as

$$\theta_{S^4} = \theta_{S^4}^{\text{test}} + \theta_{S^4}^{3\text{PM},5\text{PN}} + \theta_{S^4}^{3\text{PM},6\text{PN}}, \quad (20)$$

where $\theta_{S^4}^{\text{test}}$ is obtained from the quartic-in-spin part of Eq. (102) after setting the Wilson coefficients to zero, $\theta_{S^4}^{3\text{PM},5\text{PN}}$ is the known 5PN part of the 3PM contribution, and we write the unknown contribution $\theta_{S^4}^{3\text{PM},6\text{PN}}$ as

$$\begin{aligned} \frac{\theta_{S^4}^{3\text{PM},6\text{PN}}}{\Gamma} &= \frac{G^3 M^3}{b^7 v^2} \left[(f_{40} + \delta g_{40} + \nu h_{40}) a_1^4 \right. \\ &\quad + (f_{31} + \delta g_{31} + \nu h_{31}) a_1^3 a_2 + (f_{22} + \nu h_{22}) a_1^2 a_2^2 \\ &\quad \left. + (f_{31} - \delta g_{31} + \nu h_{31}) a_1 a_2^3 + (f_{40} - \delta g_{40} + \nu h_{40}) a_2^4 \right]. \end{aligned} \quad (21)$$

At NLO S^5 and S^6 , we parametrize the scattering angle as

$$\theta_{S^5} = \theta_{S^5}^{\text{test}} = \bar{\theta}_{S^5}^{\text{test}} + \Delta\theta_{S^5}, \quad (22a)$$

$$\theta_{S^6} = \theta_{S^6}^{\text{test}} = \bar{\theta}_{S^6}^{\text{test}} + \Delta\theta_{S^6}, \quad (22b)$$

where the full NLO can in principle be obtained from the test-body scattering angle (102) derived in Sec. V B. However, since it includes Wilson coefficients whose values for BHs are unknown, we split the NLO contributions into terms of order $\mathcal{O}(a_1^{\leq 4} a_2^{\leq 4})$, denoted $\bar{\theta}_{S^5}^{\text{test}}$ and $\bar{\theta}_{S^6}^{\text{test}}$, and terms with higher orders in spin, which we parametrize as

$$\frac{\Delta\theta_{S^5}}{\Gamma} = \frac{\pi G^2 M^2}{b^7 v} \left[(f_{50} + \delta g_{50}) a_1^5 + (f_{50} - \delta g_{50}) a_2^5 \right], \quad (23a)$$

$$\begin{aligned} \frac{\Delta\theta_{S^6}}{\Gamma} &= \frac{\pi G^2 M^2}{b^8 v^2} \left[(f_{60} + \delta g_{60}) a_1^6 + (f_{60} - \delta g_{60}) a_2^6 \right. \\ &\quad \left. + (f_{51} + \delta g_{51}) a_1^5 a_2 + (f_{51} - \delta g_{51}) a_1 a_2^5 \right]. \end{aligned} \quad (23b)$$

We stress that the above parametrization for the scattering angle is completely fixed by parity invariance, dimensional analysis and a well-behaved small-velocity expansion.

We solve for the f_{ij} and g_{ij} unknowns in the NNLO S^3 and S^4 parts from the 3PM test-body scattering angle in Eq. (102). Comparison with the ansatzes in Eqs. (19) and (21) yields the following values for the unknowns:

$$\begin{aligned} f_{30} &= -180, & g_{30} &= -100, \\ f_{21} &= -540, & g_{21} &= -100, \\ f_{40} &= 650, & g_{40} &= 400, \\ f_{31} &= 2600, & g_{31} &= 800, \\ f_{22} &= 3900. \end{aligned} \quad (24)$$

We solve for the remaining unknowns ($h_{30}, h_{21}, h_{40}, h_{31}$) using the 1SF redshift and spin-precession invariants, but h_{22} requires 1SF results that are unavailable in the literature, namely the redshift (or spin-precession frequency) to quadratic (linear) order in the secondary spin and quadratic order in the Kerr spin.

We also use 1SF results to solve for the unknowns in the NLO S^5 and S^6 scattering angle, and in Sec. V C, we relate those unknowns to the Wilson coefficients in the test-body scattering angle (102). Additionally, in Sec. III, we solve for them from gravitational-wave scattering.

C. First law of binary mechanics

Having related the coefficients of the Hamiltonian to the scattering angle ansatz, the next step is to compute the redshift and spin-precession invariants by making use of the first law of binary mechanics.

The first law was derived in Refs. [118, 122–126], and it is known for spinning binaries in eccentric orbits to first order in spin. It reads

$$dE - \Omega_r dI_r - \Omega dL = \sum_i (z_i dm_i + \Omega_{S_i} dS_i), \quad (25)$$

where Ω_r and Ω are the radial and azimuthal frequencies, respectively, I_r is the radial action, z_i is the redshift, Ω_{S_i} is the spin-precession frequency, and the subscript $i = 1, 2$ labels the two bodies.

The first law implies that the redshift and spin-precession frequency can be computed by taking derivatives of the Hamiltonian (energy) while keeping I_r and L constant, i.e.,

$$z_i = \left. \frac{\partial H}{\partial m_i} \right|_{I_r, L}, \quad \Omega_{S_i} = \left. \frac{\partial H}{\partial S_i} \right|_{I_r, L}. \quad (26)$$

However, it is difficult to express the Hamiltonian for spinning binaries in terms of the radial action, but we can still obtain a gauge-invariant quantity by taking an appropriate orbit average of the Hamiltonian derivatives, such as averaging over an eccentric orbit for aligned-spin binaries. (See, e.g., Sec. IV.A of Ref. [118] for the derivation.) In that case, we have

$$z_i = \left\langle \frac{\partial H}{\partial m_i} \right\rangle, \quad \Omega_{S_i} = \left\langle \frac{\partial H}{\partial S_i} \right\rangle. \quad (27)$$

In Sec. II E, we explain how to perform this average.

For circular orbits, the calculation of the redshift and spin-precession frequency is much easier, since in that case, the first law can be written as

$$d\mathfrak{M} \stackrel{\text{circ}}{=} \sum_i (z_i dm_i + \Omega_{S_i} dS_i), \quad (28)$$

where \mathfrak{M} is the system's free energy defined as

$$\mathfrak{M}(\Omega) := E(\Omega) - \Omega L(\Omega), \quad (29)$$

leading to

$$z_i = \frac{\partial \mathfrak{M}(\Omega)}{\partial m_i}, \quad \Omega_{S_i} = \frac{\partial \mathfrak{M}(\Omega)}{\partial S_i}. \quad (30)$$

It should be stressed that the first law in Eq. (25) is only valid to first order in spin. Meaning that, when computing the redshift and spin-precession frequency of the lighter object, m_2 , our results for z_2 and Ω_{S_2} are valid to linear order in S_2 , but to all orders in S_1 , since the primary object does not affect the derivatives $\partial/\partial m_2$ and $\partial/\partial S_2$ in Eq. (27).

In the following subsection, we first perform the calculation of the redshift and spin-precession frequency for circular orbits, which is enough to solve for all the unknowns in the scattering angle, except for h_{22} , which as explained above, requires 1SF results unavailable in the literature. Then, in Sec. II E, we perform the calculation for eccentric orbits to obtain additional constraints that confirm our results.

D. Redshift and spin-precession invariants for circular orbits

To obtain $\mathfrak{M}(\Omega)$ for circular orbits, we solve Hamilton's equations

$$\dot{p}_r = -\frac{\partial}{\partial r} \mathcal{H}(r, p_r = 0, L) = 0, \quad (31a)$$

$$\dot{\phi} = \frac{\partial}{\partial L} \mathcal{H}(r, p_r = 0, L) = \Omega \quad (31b)$$

for $r(\Omega)$ and $L(\Omega)$, perturbatively in a PN expansion. We then substitute the solution in $E = \mathcal{H}(r, p_r = 0, L)$ to obtain $E(\Omega)$, yielding $\mathfrak{M}(\Omega)$ via Eq. (29). The redshift z_2 and spin-precession frequency Ω_{S_2} are simply obtained by differentiating $\mathfrak{M}(\Omega)$ as in Eqs. (30). For convenience, we define the spin-precession invariant

$$\psi_2 := \frac{\Omega_{S_2}}{\Omega}, \quad (32)$$

and express z_2 and ψ_2 as functions of $x := (M\Omega)^{2/3}$.

Next, we expand z_2 and ψ_2 to first order in the mass ratio $q := m_2/m_1$, by making use of the following variables:

$$y := (m_1\Omega)^{2/3} = \frac{x}{(1+q)^{2/3}}, \quad (33a)$$

$$\chi := \frac{a_1}{m_1}, \quad (33b)$$

setting $a_2 = 0$, and replacing δ and ν by

$$\delta = \frac{1-q}{1+q}, \quad \nu = \frac{q}{(1+q)^2}. \quad (34)$$

Our result for the redshift reads

$$U_2 := \frac{1}{z_2} = U_2^{(0)} + qU_2^{(1)} + \mathcal{O}(q^2), \quad (35a)$$

$$\begin{aligned} U_2^{(0)} = & 1 + \frac{3}{2}y + \frac{27}{8}y^2 + \frac{135}{16}y^3 + \frac{2835}{128}y^4 + \mathcal{O}(y^5) + \chi \left[-2y^{5/2} - 9y^{7/2} - \frac{135}{4}y^{9/2} + \mathcal{O}(y^{11/2}) \right] \\ & + \chi^2 \left[\frac{y^3}{2} + \frac{31}{12}y^4 + \frac{255}{16}y^5 + \mathcal{O}(y^6) \right] + \chi^3 \left[-\frac{79}{27}y^{11/2} - \frac{145}{6}y^{13/2} + \mathcal{O}(y^{15/2}) \right] + \chi^4 \left[\frac{3}{8}y^6 + \frac{4333}{1296}y^7 + \mathcal{O}(y^8) \right] \\ & + \chi^5 \left[\left(\frac{8f_{50}}{15} + \frac{8g_{50}}{15} + 14 \right) y^{15/2} + \mathcal{O}(y^{17/2}) \right] + \chi^6 \left[\left(\frac{16f_{60}}{35} + \frac{16g_{60}}{35} - 21 \right) y^8 + \mathcal{O}(y^9) \right] + \mathcal{O}(\chi^7), \end{aligned} \quad (35b)$$

$$\begin{aligned}
U_2^{(1)} = & -y - 2y^2 - 5y^3 + \left(\frac{41\pi^2}{32} - \frac{121}{3} \right) y^4 + \chi \left[\frac{7y^{5/2}}{3} + \frac{46y^{7/2}}{3} + 77y^{9/2} + \mathcal{O}(y^{11/2}) \right] \\
& + \chi^2 \left[-y^3 - \frac{86}{9}y^4 - \frac{577}{9}y^5 + \mathcal{O}(y^6) \right] + \chi^3 \left[y^{9/2} + \frac{1526}{81}y^{11/2} + \left(\frac{3h_{30}}{8} + \frac{72469}{648} \right) y^{13/2} + \mathcal{O}(y^{15/2}) \right] \\
& + \chi^4 \left[-2y^6 + \left(\frac{5h_{40}}{16} + \frac{506825}{7776} \right) y^7 + \mathcal{O}(y^8) \right] + \chi^5 \left[\left(-\frac{16f_{50}}{15} - \frac{16g_{50}}{5} - 47 \right) y^{15/2} + \mathcal{O}(y^{17/2}) \right] \\
& + \chi^6 \left[\left(91 - \frac{32f_{60}}{21} - \frac{352g_{60}}{105} \right) y^8 + \mathcal{O}(y^9) \right] + \mathcal{O}(\chi^7), \tag{35c}
\end{aligned}$$

while for the spin-precession invariant, we obtain

$$\psi_2 = \psi_2^{(0)} + q\psi_2^{(1)} + \mathcal{O}(q^2), \tag{36a}$$

$$\begin{aligned}
\psi_2^{(0)} = & \frac{3}{2}y + \frac{9}{8}y^2 + \frac{27}{16}y^3 + \mathcal{O}(y^4) + \chi \left[-y^{3/2} - \frac{y^{5/2}}{2} - \frac{15}{8}y^{7/2} + \mathcal{O}(y^{9/2}) \right] + \chi^2 \left[-\frac{y^3}{2} + \frac{7}{12}y^4 + \frac{37}{16}y^5 + \mathcal{O}(y^6) \right] \\
& + \chi^3 \left[-\frac{y^{9/2}}{2} - \frac{37}{108}y^{11/2} + \mathcal{O}(y^{13/2}) \right] + \chi^4 \left[-\frac{3}{8}y^6 + \mathcal{O}(y^7) \right] + \chi^5 \left[\left(117 - \frac{16f_{51}}{35} - \frac{16g_{51}}{35} \right) y^{13/2} + \mathcal{O}(y^{15/2}) \right] \\
& + \mathcal{O}(\chi^6), \tag{36b}
\end{aligned}$$

$$\begin{aligned}
\psi_2^{(1)} = & y^2 - 3y^3 + \mathcal{O}(y^4) + \chi \left[y^{3/2} + 0 \times y^{5/2} + \frac{16}{3}y^{7/2} + \mathcal{O}(y^{9/2}) \right] + \chi^2 \left[-3y^4 + \left(\frac{7409}{144} - \frac{3h_{21}}{16} \right) y^5 + \mathcal{O}(y^6) \right] \\
& + \chi^3 \left[y^{9/2} + \left(-\frac{5h_{31}}{32} - \frac{1051}{16} \right) y^{11/2} + \mathcal{O}(y^{13/2}) \right] + \chi^4 [0 \times y^6 + \mathcal{O}(y^7)] \\
& + \chi^5 \left[\left(\frac{16f_{51}}{21} + \frac{176g_{51}}{105} - 237 \right) y^{13/2} + \mathcal{O}(y^{15/2}) \right] + \mathcal{O}(\chi^6). \tag{36c}
\end{aligned}$$

Let us pause for a moment and interpret the expressions above in terms of amplitudes. The LO (NLO) PN contributions, corresponding to tree level (one loop) amplitude input appear in the redshift at order y^{n+1} (y^{n+2}) for even powers of spin χ^n , while for odd powers in spin χ^m , they appear at orders $y^{m+3/2}$ ($y^{m+5/2}$). For example, the tree level, spin-squared scattering data is contained in the $\chi^2 y^3$ piece, and the one loop S^5 information is in $\chi^5 y^{15/2}$. Similarly, in the spin-precession invariant, the LO (NLO) power counting goes as follow: for an even-in-spin term χ^n the LO (NLO) scattering data is in y^{n+1} (y^{n+2}) while for an odd-in-spin term χ^m the LO (NLO) is $y^{m+1/2}$ ($y^{m+3/2}$). Table I summarizes the powers in x , or y , of the PN and spin orders considered in this paper.

Having computed the redshift and spin-precession invariants, we can compare them to GSF results to solve for the unknowns. The test-mass limits (0SF parts) of these invariants are known to all PN orders, and are given by [112, 117]

$$\begin{aligned}
U_{0\text{SF}} = & \left[1 + \chi y^{3/2} - 3y(1 - \chi y^{3/2})^{1/3} \right]^{-1/2} \\
& \times \left(1 - \chi y^{3/2} \right)^{-1/2}, \tag{37a}
\end{aligned}$$

$$\psi_{0\text{SF}} = 1 - \left(\frac{1 + \chi y^{3/2} - 3y(1 - \chi y^{3/2})^{1/3}}{1 - \chi y^{3/2}} \right)^{1/2}. \tag{37b}$$

In Appendix A, we derive the 0SF redshift and spin-

precession invariants for eccentric orbits.

The 1SF contribution to the redshift was derived in Ref. [102] for a non-spinning secondary in a Kerr background to all orders in the Kerr spin and to 8PN order, while the spin-precession invariant was similarly derived in Ref. [112]. The results of both references are included in the Black Hole Perturbation Toolkit [147].

By comparing our results with GSF results, we obtain the following constraints at NNLO S^3 and S^4 :

$$1\text{SF } z : a^3 y^{13/2} (3h_{30} - 451) = 0, \tag{38a}$$

$$1\text{SF } \psi : a^2 y^5 (h_{21} - 371) = 0, \tag{38b}$$

$$1\text{SF } z : a^4 y^7 (2h_{40} + 631) = 0, \tag{38c}$$

$$1\text{SF } \psi : a^3 y^{11/2} (h_{31} + 446) = 0, \tag{38d}$$

leading to the solution

$$h_{30} = \frac{451}{3}, \quad h_{21} = 371, \tag{39a}$$

$$h_{40} = -\frac{631}{2}, \quad h_{31} = -446. \tag{39b}$$

The constraint at NLO S^5 from the 0SF redshift is

$$0\text{SF } z : a^5 y^{15/2} (4f_{50} + 4g_{50} + 105) = 0, \tag{40}$$

leading to the following relation:

$$f_{50} = -\frac{105}{4} - g_{50}. \tag{41}$$

The 1SF constraint from the redshift would be enough to determine the remaining unknowns, but at $\mathcal{O}(S^5)$, the 1SF redshift depends on transcendental functions of spin, and it is not clear how to translate that nonperturbative information into a PN spin expansion; we discuss possible ways of resolving this issue in Sec. IV. No constraints are available from the spin-precession frequency, since it would require a GSF calculation at fourth order of the secondary spin in a Schwarzschild background.

The NLO S^6 unknowns can be solved for with no ambiguity since no transcendental functions of spin appear at $\mathcal{O}(y^8)$ in the redshift or at $\mathcal{O}(y^{13/2})$ in the spin-precession invariant. Comparison with GSF results

yields the following constraints:

$$\text{0SF } z : a^6 y^8 (16f_{60} + 16g_{60} - 735) = 0, \quad (42a)$$

$$\text{0SF } \psi : a^5 y^{13/2} (16f_{51} + 16g_{51} - 4095) = 0, \quad (42b)$$

$$\text{1SF } z : a^6 y^8 (-160f_{60} - 352g_{60} + 9555) = 0, \quad (42c)$$

$$\text{1SF } \psi : a^5 y^{13/2} (80f_{51} + 176g_{51} - 24885) = 0, \quad (42d)$$

leading to the solution

$$\begin{aligned} f_{60} &= \frac{2205}{64}, & g_{60} &= \frac{735}{64}, \\ f_{51} &= 210, & g_{51} &= \frac{735}{16}. \end{aligned} \quad (43)$$

With the solutions obtained above, the NNLO S^3 and S^4 contributions to the scattering angle are given by

$$\begin{aligned} \frac{\theta_{S^3}}{\Gamma} &= -\frac{4GMa_+^3}{b^4 v} + \frac{\pi G^2 M^2}{b^5 v^3} \left[-\frac{3}{2} \delta a_- a_+^2 - \frac{21}{2} a_+^3 + \left(-\frac{3}{32} \delta a_-^3 - \frac{141}{32} \delta a_+^2 a_- + \frac{21}{32} a_+ a_-^2 - \frac{357 a_+^3}{32} \right) v^2 \right] \\ &+ \frac{G^3 M^3}{b^6 v^5} \left\{ -20 \delta a_- a_+^2 - 100 a_+^3 + \left[\left(\frac{100\nu}{3} - \frac{1400}{3} \right) a_+^3 - 200 a_- a_+^2 \delta + \frac{200}{3} \nu a_-^2 a_+ \right] v^2 \right. \\ &\left. + \left[-100 \delta a_- a_+^2 + \left(\frac{391\nu}{3} - 180 \right) a_+^3 + 20\nu a_-^2 a_+ \right] v^4 + \mathcal{O}(v^6) \right\} + \mathcal{O}(G^4), \end{aligned} \quad (44a)$$

$$\begin{aligned} \frac{\theta_{S^4}}{\Gamma} &= \frac{2GM}{b^5 v^2} a_+^4 (1 + v^2) + \frac{\pi G^2 M^2}{b^6 v^4} \left[\frac{15}{4} a_+^4 + \left(\frac{105}{16} \delta a_- a_+^3 + \frac{705}{32} a_+^4 - \frac{15}{32} a_-^2 a_+^2 \right) v^2 \right] \\ &+ \frac{G^3 M^3}{b^7 v^6} \left\{ 30 a_+^4 + [200 \delta a_- a_+^3 + a_+^4 (550 - 10\nu) - 40\nu a_-^2 a_+^2] v^2 + \left[400 \delta a_+^3 a_- + \left(\frac{261\nu}{16} - \frac{975}{4} \right) a_-^4 \right. \right. \\ &\left. \left. + \left(\frac{975}{2} - \frac{1893\nu}{8} \right) a_+^2 a_-^2 + \left(\frac{1625}{4} - \frac{1523\nu}{16} \right) a_+^4 + (h_{22}\nu + 3900) a_1^2 a_2^2 \right] v^4 + \mathcal{O}(v^6) \right\} + \mathcal{O}(G^4), \end{aligned} \quad (44b)$$

where we defined $a_+ := a_1 + a_2$ and $a_- := a_1 - a_2$. The NLO S^5 and S^6 contributions read

$$\begin{aligned} \frac{\theta_{S^5}}{\Gamma} &= -\frac{4GMa_+^5}{b^6 v} + \frac{\pi G^2 M^2}{b^7 v^3} \left\{ -\frac{45}{16} \delta a_- a_+^4 - \frac{315}{16} a_+^5 + \left[\frac{315 \delta a_-^5}{512} + \frac{1515}{256} \delta a_+^2 a_-^3 - \frac{3345}{512} \delta a_+^4 a_- + \frac{2625}{512} a_+ a_-^4 \right. \right. \\ &\left. \left. + \frac{3045}{256} a_+^3 a_-^2 - \frac{8715 a_+^5}{512} - a_1^5 \left(\frac{105}{4} + g_{50}(1 - \delta) \right) - a_2^5 \left(\frac{105}{4} + g_{50}(1 + \delta) \right) \right] v^2 + \mathcal{O}(v^4) \right\} + \mathcal{O}(G^3), \end{aligned} \quad (44c)$$

$$\frac{\theta_{S^6}}{\Gamma} = \frac{2GM}{b^7 v^2} a_+^6 (1 + v^2) + \frac{\pi G^2 M^2}{b^8 v^4} \left[\frac{105}{16} a_+^6 + \left(\frac{735}{64} \delta a_- a_+^5 + \frac{4515}{128} a_+^6 - \frac{105}{128} a_-^2 a_+^4 \right) v^2 + \mathcal{O}(v^4) \right] + \mathcal{O}(G^3), \quad (44d)$$

where we left the coefficient g_{50} in θ_{S^5} since there is more than one possibility of determining it from 1SF results, as explained in Sec. IV.

In the following subsection, we obtain additional constraints on the unknowns by comparing our results with eccentric-orbit GSF results. The solutions we obtain are consistent with the circular-orbit calculation.

E. Redshift and spin-precession invariants for eccentric orbits

For eccentric orbits, the redshift and spin-precession invariants can be computed using Eq. (27), by taking derivatives of the Hamiltonian, orbit averaging the result and expressing it in terms of frequencies. To perform such a calculation, we follow the method in Refs. [104, 113], by making use of the Keplerian parametrization for

the conservative dynamics [148]

$$r = \frac{M}{u_p(1 + e \cos \zeta)}, \quad (45)$$

where u_p is the inverse of the semi-latus rectum (scaled by the total mass), e is the eccentricity, and ζ is the relativistic anomaly.

The radial and azimuthal periods can be calculated from the Hamiltonian using

$$T_r := \oint dt = 2 \int_0^\pi \left(\frac{\partial \mathcal{H}}{\partial p_r} \right)^{-1} \frac{dr}{d\zeta} d\zeta, \quad (46a)$$

$$T_\phi := \oint d\phi = 2 \int_0^\pi \frac{\partial \mathcal{H}}{\partial L} \left(\frac{\partial \mathcal{H}}{\partial p_r} \right)^{-1} \frac{dr}{d\zeta} d\zeta, \quad (46b)$$

from which we define the gauge-independent variables

$$x := (M\Omega)^{2/3}, \quad \iota := \frac{3x}{k}, \quad (47)$$

where $\Omega = T_\phi/T_r$ is the orbit-averaged azimuthal frequency, and k is the fractional periastron advance computed from

$$k = \frac{T_\phi}{2\pi} - 1. \quad (48)$$

Then, we perform the orbit averages as follows:

$$z_i = \left\langle \frac{\partial \mathcal{H}}{\partial m_i} \right\rangle = \frac{1}{T_r} \oint \frac{\partial \mathcal{H}}{\partial m_i} dt, \quad (49a)$$

$$\Omega_{S_i} = \left\langle \frac{\partial \mathcal{H}}{\partial S_i} \right\rangle = \frac{1}{T_r} \oint \frac{\partial \mathcal{H}}{\partial S_i} dt, \quad (49b)$$

where we express the integrands as functions of the Keplerian parameters (u_p, e, ζ) , then evaluate the time integrals as

$$\langle f \rangle(u_p, e) = \frac{1}{T_r} \int_0^{2\pi} f(u_p, e, \zeta) \left(\frac{\partial \mathcal{H}}{\partial p_r} \right)^{-1} \frac{dr}{d\zeta} d\zeta, \quad (50)$$

for any function f .

The above steps yield the redshift and spin-precession invariants, $z_i(u_p, e)$ and $\psi_i(u_p, e)$, in terms of the gauge-dependent variables u_p and e . Therefore, we first invert the PN expansions for x and ι from Eq. (47) to obtain $u_p(x, \iota)$ and $e(x, \iota)$, which yield gauge-invariant expressions for $z_i(x, \iota)$ and $\psi_i(x, \iota)$. Note that the denominator of ι in Eq. (47) is of order 1PN, which effectively scales down the PN order such that, to obtain z_i and ψ_i , we need to include higher PN orders at lower spin orders, as summarized in Table I.

The next step is to expand $z_2(x, \iota)$ and $\psi_2(x, \iota)$ (of the lighter object) to first order in the mass ratio $q = m_2/m_1$ and zeroth order in the secondary spin a_2 , and we express the result in terms of the following variables:

$$y := (m_1\Omega)^{2/3} = \frac{x}{(1+q)^{2/3}}, \quad (51a)$$

$$\lambda := \frac{3y}{k} = \frac{\iota}{(1+q)^{2/3}}. \quad (51b)$$

To compare $z_2(y, \lambda)$ and $\psi_2(y, \lambda)$ with 1SF results, we need to write them in terms of the variables used in GSF calculations, which are the Kerr geodesic variables (u_p, e) . These are technically in a different gauge from the one we use in the PN calculations, but we use the same notation for simplicity. In Appendix A, we show how to derive the relations $y(u_p, e)$ and $\lambda(u_p, e)$. Typically, these relations are derived in the literature in an eccentricity expansion [104, 118, 149], but we were able to obtain them, in addition to the redshift and spin-precession frequency, without any eccentricity expansions.

In the test-mass limit, our result for the (inverse) redshift $U_2 := 1/z_2 = U_2^{(0)} + qU_2^{(1)} + \mathcal{O}(q^2)$ is given by

$$\begin{aligned} U_2^{(0)} = [\dots] &+ \chi^5 \varepsilon^3 u_p^{15/2} \left[-\frac{33\varepsilon^7}{2} + \frac{903\varepsilon^6}{4} - 513\varepsilon^5 \right. \\ &- \frac{7443\varepsilon^4}{8} + \frac{3659\varepsilon^3}{2} + \frac{14457\varepsilon^2}{4} - 84\varepsilon - \frac{32921}{8} \\ &\left. + \left(\frac{77}{10} - \frac{\varepsilon^6}{6} + \frac{7\varepsilon^4}{2} - \frac{21\varepsilon^2}{2} \right) (f_{50} + g_{50}) \right] \\ &+ \chi^6 \varepsilon^3 u_p^8 \left[-\frac{495\varepsilon^6}{16} + \frac{351\varepsilon^5}{2} - \frac{201\varepsilon^4}{16} - 612\varepsilon^3 \right. \\ &\left. + \left(\frac{33}{5} - \frac{\varepsilon^6}{7} + 3\varepsilon^4 - 9\varepsilon^2 \right) (f_{60} + g_{60}) \right. \\ &\left. - \frac{10485\varepsilon^2}{16} + \frac{17829}{16} \right], \quad (52) \end{aligned}$$

where the dots $[\dots]$ indicate lower PN contributions that are the same as the 0SF redshift derived in Appendix A (cf. Eq. (A4)), and to ease the notation, we defined the variable

$$\varepsilon := \sqrt{1 - e^2}. \quad (53)$$

Note that the 0SF eccentric-orbit redshift only depends on the sums $f_{50} + g_{50}$ and $f_{60} + g_{60}$, meaning that it cannot provide additional constraints on these unknowns than the circular-orbit comparison from the previous subsection; indeed, comparing $U_2^{(0)}$ with the 0SF result from Eq. (A4) leads to the same circular-orbit constraint in Eq. (42a).

At first order in the mass ratio, our result for the redshift reads

$$\begin{aligned}
U_2^{(1)} = & -\varepsilon^2 u_p - 2\varepsilon^4 u_p^2 + (5\varepsilon^6 - 9\varepsilon^5 + 4\varepsilon^4 - 5\varepsilon^3) u_p^3 + \left[\frac{27\varepsilon^7}{2} - 4\varepsilon^8 + 16\varepsilon^6 + \left(\frac{79}{6} - \frac{41\pi^2}{64} \right) \varepsilon^5 + 16\varepsilon^4 + \left(\frac{123\pi^2}{64} - 95 \right) \varepsilon^3 \right] u_p^4 \\
& + \chi \varepsilon^3 \left\{ (5 - 2\varepsilon) u_p^{5/2} + (-8\varepsilon^3 - 5\varepsilon^2 - 12\varepsilon + 43) u_p^{7/2} + \left(30\varepsilon^5 - \frac{581\varepsilon^4}{8} - \frac{27\varepsilon^3}{2} - \frac{307\varepsilon^2}{2} - 60\varepsilon + \frac{2853}{8} \right) u_p^{9/2} \right. \\
& + \left[\frac{1447\varepsilon^6}{8} - 32\varepsilon^7 + 68\varepsilon^5 - \left(\frac{9773}{24} + \frac{569\pi^2}{256} \right) \varepsilon^4 + 116\varepsilon^3 + \left(\frac{2189\pi^2}{128} - \frac{58253}{24} \right) \varepsilon^2 - 280\varepsilon + \frac{231391}{72} - \frac{13355\pi^2}{768} \right] u_p^{11/2} \left. \right\} \\
& + \chi^2 \varepsilon^3 \left\{ (\varepsilon - 2) u_p^3 + (\varepsilon^3 + 29\varepsilon^2 + 12\varepsilon - 56) u_p^4 + \left(21\varepsilon^4 - 35\varepsilon^5 + 7\varepsilon^3 + \frac{1011\varepsilon^2}{2} + 80\varepsilon - \frac{1363}{2} \right) u_p^5 + \left[121\varepsilon^7 - \frac{3689\varepsilon^6}{8} \right. \right. \\
& + \frac{153\varepsilon^5}{2} + \left(\frac{4403\pi^2}{4096} - \frac{4375}{24} \right) \varepsilon^4 - 96\varepsilon^3 + \left(\frac{54307}{8} - \frac{16767\pi^2}{2048} \right) \varepsilon^2 + 448\varepsilon + \frac{33875\pi^2}{4096} - \frac{175747}{24} \left. \right] u_p^6 \left. \right\} \\
& + \chi^3 \varepsilon^3 \left\{ \left(2\varepsilon^3 - \frac{37\varepsilon^2}{2} - 4\varepsilon + \frac{47}{2} \right) u_p^{9/2} + \left(12\varepsilon^5 + \frac{309\varepsilon^4}{4} - 27\varepsilon^3 - 588\varepsilon^2 - 40\varepsilon + \frac{2463}{4} \right) u_p^{11/2} \right. \\
& + \left[-130\varepsilon^7 + \frac{4749\varepsilon^6}{16} - \frac{283\varepsilon^5}{4} - \frac{2875\varepsilon^3}{4} - 280\varepsilon + \varepsilon^4 \left(\frac{45h_{30}}{64} + \frac{106811}{64} \right) + \varepsilon^2 \left(-\frac{105h_{30}}{32} - \frac{307453}{32} \right) \right. \\
& + \frac{189h_{30}}{64} + \frac{590739}{64} \left. \right] u_p^{13/2} \left. \right\} + \chi^4 \varepsilon^3 \left\{ (3\varepsilon^2 - 3) u_p^5 + \left(\varepsilon^5 - \frac{127\varepsilon^4}{2} + 44\varepsilon^3 + \frac{573\varepsilon^2}{2} - 276 \right) u_p^6 \right. \\
& + \left[50\varepsilon^7 + \frac{339\varepsilon^6}{4} - 197\varepsilon^5 + 1591\varepsilon^3 + \varepsilon^4 \left(\frac{75h_{40}}{128} - \frac{506211}{256} \right) + \varepsilon^2 \left(\frac{971975}{128} - \frac{175h_{40}}{64} \right) + \frac{315h_{40}}{128} - \frac{1843795}{256} \right] u_p^7 \left. \right\} \\
& + \chi^5 \varepsilon^3 \left\{ \left(\frac{27\varepsilon^4}{2} - \frac{47\varepsilon^3}{2} - \frac{239\varepsilon^2}{4} + 4\varepsilon + \frac{263}{4} \right) u_p^{13/2} + \left[\varepsilon^6 \left(f_{50} + \frac{5g_{50}}{3} - \frac{1697}{16} \right) - 4\varepsilon^7 + \frac{637\varepsilon^5}{2} - \frac{2763\varepsilon^3}{2} + 56\varepsilon \right. \right. \\
& + \varepsilon^4 \left(-\frac{77f_{50}}{3} - \frac{119g_{50}}{3} + \frac{2783}{16} \right) + \varepsilon^2 \left(91f_{50} + 133g_{50} - \frac{18899}{16} \right) - 77f_{50} - \frac{539g_{50}}{5} + \frac{29493}{16} \left. \right] u_p^{15/2} \left. \right\} \\
& + \chi^6 \varepsilon^3 \left\{ \left(3\varepsilon^3 + \frac{9\varepsilon^2}{2} - \frac{15}{2} \right) u_p^7 + \left[\varepsilon^6 \left(\frac{8f_{60}}{7} + \frac{12g_{60}}{7} - \frac{393}{16} \right) - \frac{327\varepsilon^5}{2} + \varepsilon^4 \left(-28f_{60} - 40g_{60} + \frac{20469}{16} \right) + 570\varepsilon^3 \right. \right. \\
& + \varepsilon^2 \left(96f_{60} + 132g_{60} - \frac{59355}{16} \right) - \frac{396f_{60}}{5} - \frac{528g_{60}}{5} + \frac{40503}{16} \left. \right] u_p^8 \left. \right\} + \mathcal{O}(\chi^7). \tag{54}
\end{aligned}$$

The 1SF contribution to the redshift for eccentric orbits in a Kerr background was derived in Ref. [107] up to 8PN order, without an eccentricity expansion to 3.5PN order, expanded in eccentricity to $\mathcal{O}(e^{16})$ through 6PN order, and to $\mathcal{O}(e^{10})$ at higher PN orders. Comparing Eq. (54) with the 1SF redshift from Ref. [107] leads to several constraints at each order in ε , leading to the same circular-orbit solutions in Eqs. (38) and (43).

For the spin-precession invariant, we obtain

$$\psi_2^{(0)} = [\dots] + \chi^5 u_p^{13/2} \left[-\frac{537\varepsilon^6}{16} + \frac{13029\varepsilon^4}{16} - \frac{34887\varepsilon^2}{16} + \frac{24267}{16} + \left(\frac{\varepsilon^6}{7} - 3\varepsilon^4 + 9\varepsilon^2 - \frac{33}{5} \right) (f_{51} + g_{51}) \right], \tag{55}$$

where the dots represent the lower order PN contributions in Eq. (A7). The 0SF eccentric-orbit spin-precession invariant produces one constraint on the sum $f_{51} + g_{51}$, which is the same as the circular-orbit constraint in Eq. (42b).

Our result for the spin-precession invariant at first order in the mass ratio reads

$$\begin{aligned}
\psi_2^{(1)} = & -u_p + \left(\frac{13}{4} - \varepsilon^2 \right) u_p^2 + \left[-\frac{\varepsilon^4}{2} + \left(\frac{123\pi^2}{256} - \frac{325}{16} \right) \varepsilon^2 - \frac{615\pi^2}{256} + 67 \right] u_p^3 + \left[\frac{628 \log u_p}{15} + \frac{31697\pi^2}{6144} - \frac{587831}{2880} + \frac{1256\gamma_E}{15} \right. \\
& + \frac{296 \log 2}{15} + \frac{729 \log 3}{5} + e^2 \left(\frac{268 \log u_p}{5} - \frac{164123}{480} - \frac{23729\pi^2}{4096} + \frac{536\gamma_E}{5} + \frac{11720 \log 2}{3} - \frac{10206 \log 3}{5} \right) \left. \right] u_p^4 \\
& + \chi \left\{ -\frac{1}{2} u_p^{3/2} + \left(\frac{\varepsilon^2}{8} - \frac{21}{4} \right) u_p^{5/2} + \left[\frac{43\varepsilon^4}{32} + \left(1 + \frac{123\pi^2}{256} \right) \varepsilon^2 + \frac{81}{16} - \frac{615\pi^2}{256} \right] u_p^{7/2} + \left[\frac{628 \log u_p}{15} + \frac{52225\pi^2}{6144} - \frac{2580077}{5760} \right. \right. \\
& + \frac{1256\gamma_E}{15} + \frac{296 \log 2}{15} + \frac{729 \log 3}{5} + e^2 \left(\frac{268 \log u_p}{5} - \frac{274889}{640} - \frac{39529\pi^2}{4096} + \frac{536\gamma_E}{5} + \frac{11720 \log 2}{3} - \frac{10206 \log 3}{5} \right) \left. \right] u_p^{9/2} \left. \right\} \\
& + \chi^2 \left\{ -u_p^2 + \left(2\varepsilon^2 + \frac{7}{4} \right) u_p^3 + \left[\frac{781}{16} - \frac{615\pi^2}{256} - \frac{5\varepsilon^4}{8} + \left(\frac{9}{2} + \frac{123\pi^2}{256} \right) \varepsilon^2 \right] u_p^4 + \left[\frac{628 \log u_p}{15} + \frac{5155\pi^2}{1536} + \frac{159179}{2880} + \frac{1256\gamma_E}{15} \right. \right. \\
& + \frac{296 \log 2}{15} + \frac{729 \log 3}{5} - \frac{3h_{21}}{16} + e^2 \left(\frac{268 \log u_p}{5} - \frac{15h_{21}}{16} - \frac{9441}{160} - \frac{22037\pi^2}{2048} + \frac{536\gamma_E}{5} + \frac{11720 \log 2}{3} - \frac{10206 \log 3}{5} \right) \left. \right] u_p^5 \left. \right\} \\
& + \chi^3 \left\{ -u_p^{5/2} + \left(\frac{5}{4} - \frac{\varepsilon^2}{8} \right) u_p^{7/2} + \left[\frac{477}{16} - \frac{615\pi^2}{256} - \frac{39\varepsilon^4}{16} + \left(\frac{123\pi^2}{256} - \frac{189}{8} \right) \varepsilon^2 \right] u_p^{9/2} + \left[\frac{628 \log u_p}{15} + \frac{5155\pi^2}{1536} - \frac{2922857}{5760} \right. \right.
\end{aligned}$$

$$\begin{aligned}
& + \frac{1256\gamma_E}{15} + \frac{296 \log 2}{15} + \frac{729 \log 3}{5} - \frac{5h_{31}}{32} + e^2 \left(\frac{268 \log u_p}{5} - \frac{25h_{31}}{32} - \frac{214929}{640} - \frac{22037\pi^2}{2048} + \frac{536\gamma_E}{5} + \frac{11720 \log 2}{3} \right. \\
& \left. - \frac{10206 \log 3}{5} \right) u_p^{11/2} \Big\} + \chi^4 \left\{ -u_p^3 + \left(\frac{\varepsilon^2}{4} + \frac{5}{4} \right) u_p^4 + \left[\frac{51\varepsilon^4}{16} + \left(\frac{59}{8} + \frac{123\pi^2}{256} \right) \varepsilon^2 + \frac{267}{16} - \frac{615\pi^2}{256} \right] u_p^5 \right. \\
& + \left[\frac{628 \log u_p}{15} + \frac{5155\pi^2}{1536} - \frac{22351}{2880} + \frac{1256\gamma_E}{15} + \frac{296 \log 2}{15} + \frac{729 \log 3}{5} + e^2 \left(\frac{268 \log u_p}{5} - \frac{196037}{320} - \frac{22037\pi^2}{2048} + \frac{536\gamma_E}{5} \right. \right. \\
& \left. \left. + \frac{11720 \log 2}{3} - \frac{10206 \log 3}{5} \right) \right] u_p^6 \Big\} + \chi^5 \left\{ -u_p^{7/2} + \left(\frac{\varepsilon^2}{4} + \frac{5}{4} \right) u_p^{9/2} + \left[\frac{93}{4} - \frac{615\pi^2}{256} - \frac{35\varepsilon^4}{32} + \left(\frac{123\pi^2}{256} - \frac{23}{16} \right) \varepsilon^2 \right] u_p^{11/2} \right. \\
& + \left[\frac{176f_{51}}{35} + \frac{72g_{50}}{5} + \frac{208g_{51}}{35} + \frac{628 \log u_p}{15} + \frac{5155\pi^2}{1536} - \frac{8434547}{5760} + \frac{1256\gamma_E}{15} + \frac{296 \log 2}{15} + \frac{729 \log 3}{5} \right. \\
& \left. + e^2 \left(\frac{152f_{51}}{7} + 52g_{50} + \frac{200g_{51}}{7} + \frac{268 \log u_p}{5} - \frac{3452929}{640} - \frac{22037\pi^2}{2048} + \frac{536\gamma_E}{5} + \frac{11720 \log 2}{3} - \frac{10206 \log 3}{5} \right) \right] u_p^{13/2} \Big\} \\
& + \mathcal{O}(\chi^6), \tag{56}
\end{aligned}$$

where γ_E is the Euler gamma constant. The PN contributions in $\psi_2^{(1)}$ written in terms of ε have been computed without an eccentricity expansion. However, the highest PN order at each order in spin (N³LO S¹, N³LO S², NNLO S³, NNLO S³, NLO S⁵, NLO S⁶—see Table I) has been computed in an eccentricity expansion, because it receives contributions from the 4PN non-spinning part of the Hamiltonian, in which the nonlocal-in-time contribution is only known in an eccentricity expansion. We wrote the $\mathcal{O}(e^2)$ expansion in the above equation, but in the Supplemental Material, we include the $\mathcal{O}(e^6)$ expansion of those terms, since we used the 4PN non-spinning Hamiltonian of Ref. [130], whose nonlocal part was expanded to $\mathcal{O}(e^6)$.

This mixing of the non-spinning and spin contributions from the Hamiltonian into the spin-precession frequency for eccentric orbits (when expressed in terms of frequencies) leads to unintuitive powers of u_p at high orders in spin (cf. Table I). For example, the first PN order in $\psi_2^{(1)}$ at $\mathcal{O}(\chi^5)$ is $u_p^{7/2}$, but the full information from the LO S⁶ part of the Hamiltonian is in the $\chi^5 u_p^{11/2}$ term, and the NLO S⁶ information is in the $\chi^5 u_p^{13/2}$ term.

Furthermore, note that the $e \rightarrow 0$ limit of the 1SF eccentric-orbit spin-precession invariant does not reduce to the circular-orbit result in Eq. (36). This is because the invariant was computed by fixing both the radial and azimuthal frequencies of the perturbed and unperturbed spacetime. Thus, even if the orbit in the unperturbed spacetime is circular, the orbit in the perturbed spacetime is not necessarily circular. (See Sec. III.B of Ref. [110] for an explanation of how to recover the circular-orbit spin-precession invariant from the eccentric-orbit result.)

The 1SF spin-precession invariant has not been derived in the literature beyond quadratic order in the Kerr spin [113]. Therefore, we can only solve for the NNLO S³ coefficient h_{21} using existing GSF results; the eccentric-orbit comparison leads to the same solution $h_{21} = 371$ that was obtained from the circular-orbit calculation.

III. SCATTERING ANGLE FROM COMPTON AMPLITUDE

In order to compute the green slots in the NLO column of Table I and provide a match to the scattering angle coefficients in Eq. (23), in this section we follow a scattering amplitude approach to the problem. The scattering angle receives contributions from the 1-loop triangle leading singularity [150], which uses as main ingredient the gravitational Compton amplitude, which we extract from BHPT solutions. We start this section by reviewing the Compton matching to Teukolsky solutions, and then show how such a matching completely fixes the scattering angle free coefficients. We leave to Sec. IV the comparison of the results obtained in this section with the ones obtained from the GSF approach discussed in the previous section.

A. Gravitational Compton Amplitude

For perturbations of spin-weight s off a Kerr BH whose spin parameter is $\chi = a_1/m_1 \equiv a/m$, Compton amplitudes are well known to be obtained from infinite sums of partial-wave amplitudes. Denoting γ as the angle formed between the direction of the incoming wave and the orientation of the BH's spin, and ϑ and φ as the polar and azimuthal angles defining a direction on the celestial sphere, this sum reads [151]

$${}_s\mathcal{A} = \sum_{\ell, m} \left[-{}_2S_{\ell m} \left(\gamma, 0; \frac{\varepsilon\chi}{2} \right) -{}_2S_{\ell m} \left(\vartheta', \varphi; \frac{\varepsilon\chi}{2} \right) {}_s\mathcal{A}_{\ell, m} \right]. \tag{57}$$

For the helicity-preserving amplitude, the angle $\vartheta' = \vartheta$, and the the partial wave modes are obtained via

$${}_s\mathcal{A}_{\ell m}|_{\text{HP}} = \frac{2\pi}{i\omega} \sum_{P=\pm 1} \left(s\eta_{\ell m} e^{2i(s\delta_{\ell m}^{P, \text{FZ}} + s\delta_{\ell m}^{\text{NZ}})} - 1 \right), \tag{58}$$

here ω is the energy of the wave perturbation. For the helicity-reversing scenario, the angle $\vartheta' = \pi - \vartheta$, and the

amplitude modes are instead

$${}_s\mathcal{A}_{\ell m}|_{\text{HR}} = \frac{2\pi}{i\omega} \sum_{P=\pm 1} P(-1)^\ell \left({}_s\eta_{\ell m} e^{2i({}_s\delta_{\ell m}^{P,\text{FZ}} + {}_s\delta_{\ell m}^{\text{NZ}})} - 1 \right). \quad (59)$$

Here, P is a parity label which appears explicit in the sum factors in Eq. (59), or implicit in the phase-shift for the modes in both Eqs. (58) and (59) due to the imaginary part of the Teukolsky-Starobinski constant². The sum over P is understood as the change from the parity to the helicity basis. Notice we have made explicit the separation of the near and far-zone contributions to the scattering phase-shift [68, 95], as we are interested in tracking the different imprints these components have on the two-body observables³. The conservative far- and near-zone contributions to the phase-shift read respectively [95]:

$${}_s\delta_{\ell m}^{P,\text{FZ}} = \underbrace{\frac{1}{2} \text{Im} [\partial_{M_3} F] - \frac{1-\kappa}{2} \epsilon + \frac{1}{2} \text{Arg}[A_s^P]}_{\text{rational}} + \underbrace{\epsilon \log(2|\epsilon|)}_{\text{tail}} + \underbrace{\frac{1}{2} \text{Arg} \left[\frac{\Gamma(\frac{1}{2}-\bar{\nu}-M_3)}{\Gamma(\frac{1}{2}-\bar{\nu}+M_3)} \right] + \frac{\pi}{2} \left(\ell + \frac{1}{2} + \bar{\nu} \right)}_{\text{transcendental}}, \quad (60)$$

and

$${}_s\delta_{\ell m}^{\text{NZ}} = \frac{1}{2} \text{Arg} \left[\frac{1 + e^{-i\pi\bar{\nu}} \mathcal{K}}{1 + e^{i\pi\bar{\nu}} \frac{\cos(\pi(M_3-\bar{\nu}))}{\cos(\pi(M_3+\bar{\nu}))} \mathcal{K}} \right]. \quad (61)$$

and goes by the name of tidal response function, as it captures the tidal deformability of the BH due to the wave perturbations.

The gravitational Compton amplitude is computed for wave perturbations of spin-weight $s = -2$. In Ref. [95], the tree-level contributions to the far-zone amplitude were presented up to 8th order in the Kerr

²Recall the Teukolsky-Starobinski constant is complex only for perturbations of spin-weight $s = -2$. This is the reason why the the helicity-reversing modes (59) vanish for non-gravitational perturbations.

³The near/far-zone separation here is a different separation compared to other splitting proposed in the literature, where the perturbation is divided not in two but in three regions: the far-zone ($r \gg r_+$) which agrees with the one here, the near-horizon region ($(r - r_+)\omega \ll 1$), and the near-zone which is the overlap between the near-horizon and the far-zone ($(r - r_+)\omega \ll 1$ and $r \gg r_+$). In our splitting, our near-zone compresses both the near horizon and the near-zone used for instance in Ref. [152].

⁴In the notation of Ref. [95], here $\bar{\nu} = \alpha$ in Eq. (15) of Ref. [95].

Here, we have used the dictionary relating gauge theory to Kerr BH parameters

$$\begin{aligned} M_1 &= i \frac{m\chi - \epsilon}{\kappa}, & M_2 &= -s - i\epsilon, \\ M_3 &= i\epsilon - s, & \Lambda &= -2i\epsilon\kappa, \\ \mathbf{u} &= -\lambda - s(s+1) + \epsilon(is\kappa - m\chi) + \epsilon^2(2 + \kappa), \end{aligned} \quad (62)$$

with λ and m the spheroidal and azimuthal eigenvalues respectively, and we recall that $\kappa := \sqrt{1 - \chi^2}$. We use the Matone relation [153, 154] to solve for the partial wave ‘‘shifted-renormalized angular momentum’’ parameter⁴, $\bar{\nu}$, given by

$$\mathbf{u} = \frac{1}{4} - \bar{\nu}^2 + \Lambda \partial_\Lambda F(M_1, M_2, M_3, \bar{\nu}, \Lambda), \quad (63)$$

where F is the so called Nekrasov-Shatashvili Function. An explicit evaluation of F up to $\mathcal{O}(\Lambda^9)$ was presented in Ref. [95], and we make use of it in the discussion below.

The amplitude modes in Eqs. (58) and (59) contain additionally absorptive contributions enclosed in the absorption probability $1 - ({}_s\eta_{\ell m})^2$, which we discard in this work. The conservative amplitude is then defined as the piece that conserves unitarity.

The function \mathcal{K} entering in the near-zone contributions has the explicit form

$$\mathcal{K} = |\Lambda|^{-2\bar{\nu}} \frac{\Gamma(2\bar{\nu})\Gamma(2\bar{\nu}+1)\Gamma(M_3 - \bar{\nu} + \frac{1}{2})\Gamma(M_2 - \bar{\nu} + \frac{1}{2})\Gamma(M_1 - \bar{\nu} + \frac{1}{2})}{\Gamma(-2\bar{\nu})\Gamma(1 - 2\bar{\nu})\Gamma(M_3 + \bar{\nu} + \frac{1}{2})\Gamma(M_2 + \bar{\nu} + \frac{1}{2})\Gamma(M_1 + \bar{\nu} + \frac{1}{2})} e^{\partial_{\bar{\nu}} F}, \quad (64)$$

spin, for both the helicity-preserving and the helicity-reversing scenarios. In this work, we are interested in introducing the leading $\ell = 2$ near-zone contributions to the scattering amplitude, up to 6th order in the Kerr spin. We however extract only the piece that does not present interference between the near and far-zones⁵, where interference effects are manifested starting at order a^6 . The first interference piece is purely imaginary at the level of the amplitude. (As an illustration of this in the helicity-preserving amplitude, see the green pieces in Eq. (B7) which appear, as mentioned, starting at $\mathcal{O}(a^6)$ and are anyways expected be canceled with non-Compton contributions in the two-body observables [39].)

As discussed in Ref. [95], the extraction of a spin polynomial piece that features an explicit tree-level

⁵Interference is used here to refer to the mixing between the near- and far-zone contributions when the exponential of the phase-shift is PM expanded.

scaling is ambiguous for the near-zone contribution because of the appearance of irrational functions of the Kerr spin parameter. In this work, we take a different philosophy and match instead the full $\ell = 2$ near-zone contribution to a contact term in the amplitude, at the spin orders outlined above. This matching captures of course the tree-level part of the near-zone contributions but has the advantage of encapsulating additional non-perturbative-in- χ Kerr finite-size effects. In summary, the Compton amplitude we present here is composed of the unambiguous tree-level contributions from the far-zone, plus the full, non-interfering $\ell = 2$ contributions from the near-zone, and up to $\mathcal{O}((a\omega)^6)$. Schematically this is shown in Fig. 1.

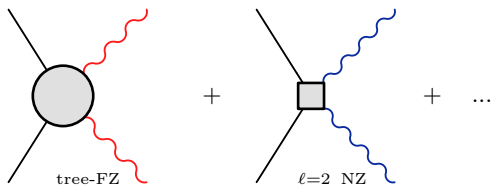


FIG. 1. Schematic representation of the different contributions to the Compton amplitude used in this paper.

The $\ell \rightarrow 2$ near-zone phase-shift is easily obtained using Eqs. (61), (64), (62) and (63). In a PM expansion,

$$e^{2i(s\delta_{\ell m}^{P,FZ} + s\delta_{\ell m}^{NZ})} = e^{i\Phi} \left(1 + \sum_{i=0} \beta_{\ell m, i}^{P,FZ} \chi^i \epsilon^{i+1} + \sum_{i=5,6} \beta_{2m, i}^{NZ}(\chi) \chi^i \epsilon^{i+1} + \sum_{i=5,6} \beta_{2m, i}^{\log, NZ}(\chi) \chi^i \epsilon^{i+1} \log \epsilon + \dots \right), \quad (67)$$

where the dots (\dots) stand for non-tree terms ignored in the far-zone, interference terms between the near and far-zones, and higher ϵ and higher ℓ contributions in both the near and the far-zones. We have also factored out the Newtonian phase $\Phi = -\frac{1}{2}\epsilon + \epsilon \log(2\epsilon)$, appearing in the far-zone phase-shift (60); we drop it from the matched amplitude presented below.

Notice that for the far-zone terms in Eq. (67), we made explicit the tree-level scaling of the spin multipole expansion (SME), and the coefficients $\beta_{\ell m, i}^{P,FZ}$ are then

⁶From a point-particle computation, this kind of poles appear as UV-divergent terms in the scattering amplitude that are removed using for instance a minimal subtraction scheme [73]. The near + far-zone BHPT result is finite as the BH finite size acts as UV regulator. Since here we are dropping the $\ell \rightarrow 2$ divergent terms in the near-zone, in order to be consistent when computing the Compton amplitude at higher loop (higher ϵ) orders, the UV divergences appearing in the point-particle computation needs to be canceled using the same prescription; that is, by matching the UV-divergent term exactly to the divergent $\ell \rightarrow 2$ piece in the far-zone amplitude (which comes with the opposite sign compared to the near-zone one), and dropping it from the final result.

it has the schematic form:

$$-2\delta_{\ell m}^{NZ}|_{\ell \rightarrow 2} = \sigma_{2, m}^{(6)}(\chi, \log \epsilon) \epsilon^6 + \sigma_{2, m}^{(7)}(\chi, \log \epsilon) \epsilon^7 + \frac{1}{\ell-2} \left[\tilde{\sigma}_{2, m}^{(6)}(\chi) \epsilon^6 + \tilde{\sigma}_{2, m}^{(7)}(\chi) \epsilon^7 \right] + \mathcal{O}(\epsilon^8), \quad (65)$$

where the PM-wave parameter ϵ , is defined in Eq. (5). The explicit expression for the $\sigma_{i, j}^{(k)}$ -coefficients can be obtained from Eq. (B1). These coefficients are particular functions of $\log \kappa$, and combinations of the polygamma functions of the form

$$\begin{aligned} \psi^{(n, m)}(\chi) &= \psi^{(n)}\left(\frac{im\chi}{\kappa}\right) + \psi^{(n)}\left(-\frac{im\chi}{\kappa}\right), \\ \tilde{\psi}^{(n, m)}(\chi) &= i \left[\psi^{(n)}\left(\frac{im\chi}{\kappa}\right) - \psi^{(n)}\left(-\frac{im\chi}{\kappa}\right) \right], \end{aligned} \quad (66)$$

where $\psi^{(n)}(z) = \frac{d^{n+1}}{dz^{n+1}} \log \Gamma(z)$, and we also explicitly highlight the presence of near-zone logarithmic tails $\sim \log \epsilon$.

The divergence in Eq. (65) in the $\ell \rightarrow 2$ limit is spurious and cancels with the analog far-zone contribution; we safely ignore it in the following⁶. The piece of the Compton amplitude we use in this paper is then obtained by considering the following terms in the expansion of the phase-shift

understood to be pure real numbers. These were reported explicitly in Ref. [95]; therefore, we do not include them here—there is still a parity label which have to be summed over as indicated in Eq. (58). For the near-zone on the other hand, the coefficients $\beta_{\ell m}^{NZ}(\chi)$ are now functions of the Kerr spin χ , which we keep in the physical region $\chi \leq 1$. We remark that in order to keep the PM expansion (expansion in ϵ) and the SME (expansion in $a\omega$) independent, the Kerr parameter χ entering in this coefficients needs to be interpreted purely as a number. Therefore, an additional expansion in small χ , will not change the PM scaling of the spin operators accompanied by such coefficients; we expand on this below. The explicit form of the $\beta_{\ell m}^{NZ}(\chi)$ coefficients can be easily obtained by expanding the exponential of the near-zone phase-shift given in Eq. (B1) up to the desired order. Analogously, the coefficients for the logarithmic tail in the near-zone, $\beta_{\ell m}^{\log, NZ}(\chi)$ are obtained from the $\log(\epsilon)$ contribution⁷.

⁷In an EFT description of Kerr BHs, these terms are of physical

We are now ready to match the amplitudes obtained by the pieces selected in Eqs. (67) and (59), using Eqs. (58) and (57), to covariant ansatzes. We start by postulating that for conservative scattering, at any order in the PM expansion and the SME, keeping these as independent expansions, the Compton amplitude, for both the helicity-preserving and helicity-reversing cases, can be expanded *entirely* in the spin basis

$$\{k_2 \cdot a, k_3 \cdot a, w \cdot a\}, \quad (68)$$

where k_2^μ (k_3^μ) is the momentum of the incoming (outgoing) wave, and the vector w^μ constructed from the

spinors of the massless momenta, $w^\mu = p_1 \cdot k_2 \frac{[3|\sigma^\mu|2\rangle}{[3|p_1|2\rangle]}$. The kinematic information in the amplitudes will be on the other hand captured by (in general complicated) functions of the optical parameter, $\xi = \sin^2(\theta/2)$.

Let us start with the helicity-preserving scenario. Amazingly, the terms extracted in Eq. (67) can still be captured with the aid of the generic ansatz presented in Ref. [94]:

$$-2A|_{\text{HP}} = A^{(0)}|_{\text{HP}} \left[e^{-(2w-k_3-k_2) \cdot a} + P_\xi(k_2 \cdot a, k_3 \cdot a, w \cdot a) \right], \quad (69)$$

where we recall that the contact term deforming the exponential is⁸

$$P_\xi = \sum_{m=0}^2 (-\xi)^{m-1} (w \cdot a)^{4-2m} (w \cdot a - k_2 \cdot a)^m (w \cdot a - k_3 \cdot a)^m r_{|a|}^{(m)}(k_2 \cdot a, k_3 \cdot a, w \cdot a) + \sum_{m=0}^{\infty} \left[\frac{(w \cdot a)^{2m+6}}{(-\xi)^{m+2}} p_{|a|}^{(m)}(k_2 \cdot a, k_3 \cdot a, w \cdot a) + (-\xi)^{m+2} (w \cdot a - k_2 \cdot a)^{m+3} (w \cdot a - k_3 \cdot a)^{m+3} q_{|a|}^{(m)}(k_2 \cdot a, k_3 \cdot a, w \cdot a) \right] \quad (70)$$

and up to S^6 , the polynomials $r_{|a|}, p_{|a|}, q_{|a|}$ are

$$\begin{aligned} r_{|a|}^{(m)} &= c_1^{(m)} - c_2^{(m)}(k_2+k_3) \cdot a - c_3^{(m)}w \cdot a + c_4^{(m)}|a|\omega \\ &+ c_5^{(m)}(w \cdot a - k_2 \cdot a)(w \cdot a - k_3 \cdot a) \\ &+ c_6^{(m)}(2w \cdot a - k_2 \cdot a - k_3 \cdot a)w \cdot a \\ &+ c_7^{(m)}(2w \cdot a - k_2 \cdot a - k_3 \cdot a)^2 \\ &+ c_8^{(m)}(w \cdot a)^2 - c_9^{(m)}(k_2 \cdot a + k_3 \cdot a)|a|\omega \\ &- c_{10}^{(m)}w \cdot a|a|\omega + \mathcal{O}(a^3), \end{aligned} \quad (71)$$

$$p_{|a|}^{(m)} = d_1^{(m)} + \mathcal{O}(a), \quad q_{|a|}^{(m)} = f_1^{(m)} + \mathcal{O}(a). \quad (72)$$

The difference with the tree-level matching presented in Refs. [94, 95] is that now the coefficients accompanying each spin-multipole moment $c_i^{(j)}(\chi)$ can now be functions of the Kerr spin parameter χ , which we interpret as a number, as mentioned above.

interest as they capture the renormalization group running of the tidal coefficients in the effective model [67, 73]. The constant in the ω term can still have a tidal interpretation but it is scheme dependent. The BHPT matching selects then a preferred renormalization group scheme in such a way the Compton free coefficients in Eq. (70) no longer present renormalization group running.

⁸Note some sign differences as compared to the original form written in Ref. [94] due to the metric signature conventions used in this paper: One can recover the original ansatz simply by replacing $\xi \rightarrow -\xi$ and dot products of the form $p \cdot q \rightarrow -p \cdot q$.

In Ref. [94], the operator $|a|\omega = \sqrt{a^2}\omega$ was interpreted as being responsible for capturing dissipative (${}_s\eta_{\ell m} \neq 1$) contributions in the super-extremal region of the Compton amplitude. Since in this work we are concerned with conservative (${}_s\eta_{\ell m} = 1$) contributions only, it would be natural for us to drop these contributions in the ansatz since $|a|\omega$ is not an element of the spin basis (68). These terms are nevertheless still useful in a conservative Compton ansatz. We can rewrite $|a|\omega = \chi\epsilon/2$. The factor χ can then be reabsorbed inside the free coefficients, and the resulting spin-multipole operator is interpreted as contributing one order lower in the SME but one order higher in the PM expansion. Terms obtained in this way are not relevant for the computation of the two-body observables at the PN orders we consider in this paper, as outlined in Table I, but are still illustrative to keep at the level of the Compton amplitude.

In order to match this ansatz to both the near and far-zone contributions from the BHPT computation, it is also natural to split the free coefficients as follows:

$$c_i^{(m)} \rightarrow c_i^{\text{NZ},(m)}(\chi) + c_i^{\text{log,NZ},(m)}(\chi) \log \epsilon + c_i^{\text{FZ},(m)}, \quad (73)$$

and analogously for the $d_i^{(j)}$ and $f_i^{(j)}$ coefficients. After the matching computation, the far-zone coefficients agree with those reported in Table 1 of Ref. [94] for $\alpha = 1$ and $\eta = 0$ (recall we are considering the conservative contributions only), which reduce the amplitude to agree with the far-zone amplitude reported in Ref. [155]. We included the far-zone solutions in Eq. (B6) for the reader's convenience. The near-zone contributions are reported in Eq. (B7), and as expected, these have a non-

trivial dependence on the Kerr spin parameter χ .

Let us remark that although χ appears in the denominator of these coefficients, the near-zone $\ell = 2$ contribution cannot be captured by a lower spin multipole moment ansatz for the helicity-preserving Compton amplitude as the angular dependence in the amplitude is unique for a given harmonic. This allows us to conclude that the matched contact terms in Eq. (70), with coefficients produced via Eq. (73) with explicit solution as obtained by replacing Eqs. (B6) and (B7), correspond indeed to $\mathcal{O}(a\omega)^{5,6}$ spin multipole moments. More remarkable is the fact that the construction of the two-body observables through the Compton will naturally inherit this SME; this is a feature that is not manifested for two-body observables constructed via GSF methods. For instance, if one takes directly the expressions for the 1SF observables reported for instance in Refs. [99, 106], the SME is totally obscured, and the only option one message such observables is to do a small-spin expansion, as we discuss in Sec. IV, which is not equivalent to the SME presented in this section.

Let us finally comment on the non-vanishing $|a|\omega$ terms which, although they do not play a role in our two-body analysis, it is still illustrative to understand their origin in the wave scattering computation. These are terms accompanied by the coefficients $c_8^{(i)}$. To obtain a non-vanishing contribution, we have purposely included an interference contribution given by a term of the form $\beta_{2,m,0}^{P,FZ} \times \beta_{2,m,6}^{NZ} \times \chi^6 \epsilon^8$. This gives a term contributing at sixth order in the spin-multipole expansion but at one loop in the PM expansion. The contribution of this interference term is given by the green terms in Eq. (B7). The remaining (real) contributions in the $c_8^{(i)}$ coefficients come from 1-loop contributions in the near-zone phase-shift (B1), more precisely from those terms proportional to π .

We now turn to the helicity-reversing amplitude. In this case, in the non-interfering scenario the non-zero contributions to the modes (59) come purely from the far zone due to the overall parity factor P inside the sums. The covariant amplitude obtained by matching the non-interfering far-zone contributions is the well-known exponential

$$-{}_2A|_{\text{HR}} = A^{(0)}|_{\text{HR}} \times e^{-(k_3 - k_2) \cdot a}, \quad (74)$$

which was checked up to eighth order in the spin multipole expansion in Ref. [95]. This therefore sets to zero any deformation of the helicity-reversing BCFW exponential, up to that spin order (see for instance Ref. [82] for an explicit Compton ansatz for the helicity-reversing amplitude).

B. Scattering angle

Having discussed the Compton amplitude, we now consider the scattering of two Kerr BHs with spins

a_1 and a_2 , aligned in the direction of the system's angular momentum. Compton contributions to the aligned-spin scattering angle are well known to be controlled by the triangle leading singularity [156], where as shown in Ref. [155, 156], on the support of the Teukolsky solutions, the helicity-reversing exponential (74) does not contribute to the scattering angle, leaving as only contribution that from the helicity-preserving amplitude. In the following, we also subtract the near-zone logarithmic tails from the Compton amplitude as these deserve a deeper understanding, especially considering that $\log \epsilon$ -tails can also be obtained from the far zone.

Using the ansatz (70), the scattering angle up to $\mathcal{O}(a^6)$ was computed in Ref. [155] for generic values of the free coefficients. Let us not import the total angle from that reference but instead consider its non-relativistic expansion as we are interested in making contact with the Hamiltonian formulation discussed above. In the PN expansion, we identify the map from the coefficients in Eq. (23) to those from the helicity-preserving Compton ansatz (70):

$$\begin{aligned} f_{50} &= -\frac{3}{128}(60c_2^{(1)} + 240c_2^{(2)} - 45c_3^{(0)} + 692), \\ g_{50} &= \frac{3}{128}(60c_2^{(1)} + 240c_2^{(2)} - 45c_3^{(0)} - 428), \\ f_{60} &= -\frac{25}{256}(27c_5^{(0)} - 27c_5^{(1)} + 45c_5^{(2)} + 45c_6^{(0)} - 45c_6^{(1)} \\ &\quad + 45c_6^{(2)} + 216c_7^{(0)} - 180c_7^{(1)} + 252c_7^{(2)} - 260), \\ g_{60} &= \frac{35}{256}(27c_5^{(0)} - 27c_5^{(1)} + 45c_5^{(2)} + 45c_6^{(0)} - 45c_6^{(1)} \\ &\quad + 45c_6^{(2)} + 216c_7^{(0)} - 180c_7^{(1)} + 252c_7^{(2)} + 76), \\ f_{51} &= \frac{105}{64}(3c_2^{(0)} + 6c_2^{(2)} + 128), \\ g_{51} &= -\frac{105}{64}(3c_2^{(0)} + 6c_2^{(2)} - 28), \end{aligned} \quad (75)$$

where the $c_i^{(j)}$ coefficients are understood to be decomposed as in Eq. (73) and discarding the near-zone logarithmic tails. Out of the non vanishing contributions, the $c_3^{(i)}$ and $c_6^{(i)}$ ones are subject of further analysis below as these are the ones contributing to the gauge-invariant observables at the PN orders indicated in Table I. Let us finally observe that although the body associated to the Compton amplitude in the triangle diagram is the small body, the information about the larger mass enters through a symmetrization of the triangle, i.e. when the Compton effects are attached to the heavier BH.

Non-aligned spin: Before we discuss the comparison of our findings with the GSF literature, let us take a moment to discuss the non-aligned spin scenario. In Ref. [155], observables for non-aligned spins with generic $c_i^{(j)}$ deformations of the Compton amplitude where computed from the eikonal phase at 2PM order using the formula derived in Refs. [45, 157]. We remark such results can be evaluated on the non-perturbative in

χ Teukolsky solutions presented here, via the splitting (73) and the explicit solution as obtained by replacing Eqs. (B6) and (B7); i.e. by allowing the $c_i^{(j)}$ coefficients to be functions of the Kerr spin parameter χ , as the effect of the derivatives on such $c_i^{(j)}(\chi)$ coefficients is effectively zero when using the eikonal formula, at least up to 2PM order.

IV. NLO S^5 AND S^6 : COMPARISON BETWEEN GSF AND COMPTON/TEUKOLSKY SOLUTIONS

A. Solving for the NLO S^5 unknowns

The NLO S^5 part of the scattering angle (23) contains two unknown coefficients, f_{50} and g_{50} . From the OSF redshift, we obtained the relation $f_{50} = -105/4 - g_{50}$ (see Eq. (41)). We could in principle solve for the remaining unknown from the 1SF redshift, if not for transcendental functions of the Kerr spin that appear at $\mathcal{O}(\chi^5 y^{15/2})$. These functions are likely due to the tidal deformations or other finite-size effects of the Kerr BH, and they make it difficult to separate the NLO S^5 PN contribution [95].

To illustrate this issue, we consider the $\mathcal{O}(u_p^{15/2} e^2)$ piece of the 1SF redshift (noting that the same conclusions in this subsection can be obtained from the circular-orbit part of the redshift or from higher orders in eccentricity), which is given by [107]

$$U^{(1)}|_{u_p^{15/2} e^2} = \frac{18317\chi^5}{5} + \frac{96}{5}(3\chi^3 + \chi)[\psi^{(0,2)}(\chi) + \log \kappa^2] + \chi^3 \left[\frac{576 \log u_p}{5} + \frac{20600396}{225} - \frac{37445\pi^2}{768} + \frac{576\gamma_E}{5} + \frac{576 \log 2}{5} \right] + \chi \left[\frac{21874 \log u_p}{35} + \frac{42404\gamma_E}{35} + \frac{932332 \log 2}{105} + \frac{2430 \log 3}{7} - \frac{86233969\pi^2}{6144} + \frac{10843142833}{44100} \right] + \frac{2687231\pi}{4410}, \quad (76)$$

where the polygamma functions $\psi^{(n,k)}(\chi)$ were defined in Eq. (66).

We consider three possibilities to use the GSF and Compton amplitudes results to solve for the f_{50} and g_{50} coefficients: 1) match the polynomial χ^5 piece only, 2) expand the polygamma functions in spin, or 3) match nonperturbatively in spin by treating f_{50} and g_{50} as effective functions of spin. We proceed to discuss these three possibilities.

1. Polynomial matching

One possible way to determine the f_{50} and g_{50} coefficients is by simply equating the spin powers in our computation of the redshift in Eq. (54), restricting to the desired PN and eccentricity order, to the 1SF result

in Eq. (76). This reduces to considering only the first term in Eq. (76) and discarding any other irrational contributions, yielding the constraint

$$a^5 u_p^{15/2} e^2 (200f_{50} + 296g_{50} + 6213) = 0. \quad (77)$$

Combined with the OSF constraint (40), one obtains

$$f_{50} = -\frac{519}{32}, \quad g_{50} = -\frac{321}{32}. \quad (78)$$

This solution for f_{50} and g_{50} as rational numbers is consistent with the expectation that LO and NLO PN contributions only contain rational numbers, as can be seen from the lower spin orders in Eq. (35) for example. In addition, both coefficients appear in the OSF redshift (cf. Eq. (A4)), which does not contain irrational numbers at any order.

Let us remark that the solution in Eq. (78) is automatically satisfied if one uses the Compton amplitude reported in Refs. [94, 158] to compute the 2PM angle, after removing the polygamma contributions (labeled with the α parameter), or simply by using the polynomial piece of the near+far-zone coefficients (B6) and (B7) in the first and second line of Eq. (75), using the splitting (73).

2. Small-spin expansion

Another possibility is to perform a small-spin expansion of the log and polygamma functions in Eq. (76). This is motivated by the fact that GSF results of Ref. [107] only assume that the spin value of the black hole is sub-extremal and as such should be valid in the Schwarzschild limit. In particular, one finds they agree explicitly with the $\mathcal{O}(\chi e^4)$ redshift derived in Refs. [104, 149], which suggests that this expansion produces sensible results.

The small-spin expansion of $\psi^{(0,2)}(\chi)$ and $\log \kappa^2$ from Eq. (76) is given by:

$$\log \kappa^2 = -\chi^2 - \frac{\chi^4}{2} - \frac{\chi^6}{3} + \mathcal{O}(\chi^8), \quad (79a)$$

$$\psi^{(0,2)}(\chi) = -2\gamma_E + 8\chi^2\zeta(3) + 8\chi^4[\zeta(3) - 4\zeta(5)] + 8\chi^6[\zeta(3) - 8\zeta(5) + 16\zeta(7)] + \mathcal{O}(\chi^8), \quad (79b)$$

where $\zeta(z)$ is the Riemann zeta function. With these expansions, the first line of Eq. (76) becomes

$$U^{(1)}|_{u_p^{15/2} e^2} = -\frac{192\gamma_E}{5}\chi + \chi^3 \left[\frac{768\zeta(3)}{5} - \frac{576\gamma_E}{5} \right] + \chi^5 \left[\frac{3072\zeta(3)}{5} - \frac{3072\zeta(5)}{5} + \frac{18029}{5} \right] + \chi^7 \left[\frac{3072\zeta(3)}{5} - 3072\zeta(5) + \frac{12288\zeta(7)}{5} - \frac{144}{5} \right] + \mathcal{O}(\chi^9) + [\dots], \quad (80)$$

where the dots represent the last three lines of Eq. (76).

Matching the $\mathcal{O}(\chi^5)$ part of the above equation to our PN calculation from Eq. (54) yields the following constraint:

$$a^5 u_p^{15/2} e^2 \left[\frac{3806}{5} + \frac{80f_{50}}{3} + \frac{592g_{50}}{15} + \frac{3072}{5}\zeta(3) - \frac{3072}{5}\zeta(5) \right] = 0, \quad (81)$$

which together with Eq. (40) lead to the solution

$$\begin{aligned} f_{50} &= 48\zeta(3) - 48\zeta(5) - \frac{21}{4} - \frac{519}{32}, \\ g_{50} &= -48\zeta(3) + 48\zeta(5) + \frac{21}{4} - \frac{321}{32}. \end{aligned} \quad (82)$$

We recognize the first two terms in each line as polygamma contributions, the third terms comes from the $\log \kappa$, and the last term correspond to the polynomial contribution. Notice the same conclusion can be obtained by using directly the Compton solutions given in Eq. (75), by replacing the splitting (73), together with the explicit near-zone and the far-zone solutions, (B7) and (B6), followed by the small-spin expansion, and extracting the χ -independent piece of such an expansion.

By inspection, the small-spin expansion presents several features: 1) the polygamma contributions always come accompanied by a transcendental number, which suggests those to be loop contributions at the level of the Compton amplitude; 2) at $\mathcal{O}(\chi^7)$, the expansion produces a pre-leading PN contribution at $\mathcal{O}(u_p^{15/2})$, even though the leading PN order starts at $\mathcal{O}(u_p^{17/2})$, as can be extrapolated from Table I; and 3) the $\mathcal{O}(\chi^5)$ piece could be interpreted as the polynomial term contributing to the tree-level Compton amplitude at fifth order in the SME, which is similar to what Ref. [94] considered but in that reference, the opposite $\chi \gg 1$ limit was taken.

3. Non-Perturbative spin matching

Since the polynomial matching is ambiguous due to polygamma identities, a third possibility is to do a non-perturbative in χ matching following the absorptive computations performed in Refs. [69, 96], such that the scattering angle coefficients f_{50} and g_{50} can be interpreted as functions of χ . We stress however that this matching cannot be done by direct comparison of Eq. (76) to Eq. (54) since the former contains lower-in-spin contributions at higher PM orders that mix with the NLO S^5 contributions we are after. It is here where the Compton matching of the previous section provides clarity, as the comparison to BHPT results has been obtained in a SME. Indeed, by replacing the non-perturbative solutions from Eqs. (B6) and (B7) into Eqs. (75) via (73), we obtain

$$\begin{aligned} f_{50} &= \frac{15}{128}(9c_3^{\text{NZ},(0)} - 100), \\ g_{50} &= -\frac{15}{128}(9c_3^{\text{NZ},(0)} + 124), \end{aligned} \quad (83)$$

where $c_3^{\text{NZ},(0)}$ is given in Eqs. (B7). These results perfectly match the polygamma and $\log \kappa$ contributions in (76). Additionally, these captures some of the χ^3 and χ^1 pieces in Eq. (76) that come from actual $\mathcal{O}((a\omega)^5)$ spin multipole operators in the Compton amplitude. The difference when replacing Eq. (83) into (54) and comparing with Eq. (76) for the given order in the PN and eccentricity expansions is

$$\begin{aligned} \Delta U|_{u_p^{15/2}e^2} &= \left[-\frac{20772764}{225} + \frac{576\gamma_E}{5} + \frac{37445\pi^2}{768} \right] \chi^3 \\ &+ \left[\frac{86233969\pi^2}{6144} - \frac{39716\gamma_E}{35} - \frac{10851864049}{44100} \right. \\ &\quad \left. - \frac{185660}{21} \log(2) - \frac{2430 \log(3)}{7} \right] \chi \\ &- \frac{2687231\pi}{4410}, \end{aligned} \quad (84)$$

which are purely $S^{0,1,3}$ contributions in the SME. In particular, these are $N^3\text{LO}$ pieces for the S^3 term, and $N^5\text{LO}$ for the S^1 term, which are 3-loop and 5-loop scattering angle computations, respectively, which are beyond the scope of this work.

Finally, one can check that the solutions for the f_{50} , g_{50} coefficients given in Eq. (83) satisfy the OSF constraint in Eq. (40), as expected since the Compton amplitude has the correct factorization properties into the Kerr 3-point spin exponential.

Furthermore, notice that although we previously assumed that the unknowns in the scattering angle ansatz are independent of the masses and spins, having the f_{50} and g_{50} coefficients depend on the spins as in the above solution is not a problem when computing the redshift or spin-precession frequency using Eq. (27). This is because the derivatives are taken with respect to the mass or spin of the secondary object, which are not affected by the dependence of the coefficients of a_1^5 on the mass and spin of the primary (Kerr BH). However, because of the symmetry under the exchange of the two bodies' labels, the coefficients of a_2^5 in the scattering angle ansatz (23) would be given by the solution (83) after replacing the Kerr spin by the spin of the lighter object. Thus, having the f_{50} and g_{50} coefficients be functions of spin would not change the calculations in this paper.

To summarize, the non-perturbative in χ matching has been possible thanks to 1) the SME of the Compton amplitude, which is inherited by the redshift observable, and 2) the inclusion of both near and far-zone contributions in the solution of the Teukolsky equation.

TABLE II. Summary of the matched scattering angle free coefficients at each order in spin, as determined by GSF and Compton/Teukolsky information. The explicit expression for $c_3^{\text{NZ},(0)}$ is given in Eq. (B7). The h_{22} coefficient is unconstrained as it requires currently unavailable 1SF results.

Matching prescription	Spin order	f -coefficients	g -coefficients	h -coefficients
Polynomial	NNLO S ³	$f_{30} = -180$ $f_{21} = -540$	$g_{30} = -100$ $g_{21} = -100$	$h_{30} = \frac{451}{3}$ $h_{21} = 371$
Polynomial	NNLO S ⁴	$f_{40} = 650$ $f_{31} = 2600$ $f_{22} = 3900$	$g_{40} = 400$ $g_{31} = 800$	$h_{40} = -\frac{631}{2}$ $h_{31} = -446$ h_{22}
Polynomial Small χ expansion Non-Pert. χ	NLO S ⁵	$f_{50} = -\frac{519}{32}$ $f_{50} = 48\zeta(3) - 48\zeta(5) - \frac{687}{32}$ $f_{50} = \frac{15}{128}(9c_3^{\text{NZ},(0)} - 100)$	$g_{50} = -\frac{321}{32}$ $g_{50} = -48\zeta(3) + 48\zeta(5) - \frac{153}{32}$ $g_{50} = -\frac{15}{128}(9c_3^{\text{NZ},(0)} + 124)$	
Polynomial / Non-Pert. χ	NLO S ⁶	$f_{60} = \frac{2205}{64}$ $f_{51} = 210$	$g_{60} = \frac{735}{64}$ $g_{51} = \frac{735}{16}$	

B. NLO S⁶ Results

In Sec. IID, we discussed how to fully fix the f_{60} , g_{60} , f_{51} and g_{51} coefficients directly from GSF observables, as transcendental functions do not appear in the redshift at NLO S⁶. The absence of irrational functions at this order is however only an accident for the aligned-spin scenario as, in general, the S⁶ Compton coefficients depend on such irrational functions. To illustrate this point, we carry the analogous S⁶ coefficient fixing using non-perturbative in χ Compton results only.

We proceed as follows: replacing the BHPT solutions for the near-zone (B7) + far-zone (B6) via the splitting (73) into Eq. (75), we obtain the following expressions for the unknowns:

$$\begin{aligned} f_{60} &= \frac{2205}{64}, & g_{60} &= \frac{735}{64}, \\ f_{51} &= 210, & g_{51} &= \frac{735}{16}. \end{aligned} \quad (85)$$

These are in perfect agreement with the ones reported in Eq. (43). However, the solutions as computed from the Compton approach expose a very non-trivial cancellation of the irrational-in-spin contributions for the f_{60} and g_{60} coefficients. That is, notice that the non-trivial Teukolsky terms contributing to f_{60} and g_{60} in Eq. (75) come from the $c_6^{(1)}$ and $c_6^{(2)}$ coefficients, which individually contain polygamma and $\log \kappa$ dependence as seen from Eq. (B7). This cancellation signals that the non-perturbative in χ matching is a good prescription to capture interesting features of Kerr BHs, which we further study in the next section. As a final remark, one can check that replacing the dictionary from Eqs. (75) into the eccentric redshift in Eq. (54) and precession frequency (56), and taking the test-mass limit ($\delta \rightarrow 1$),

the $c_i^{(j)}$ contact deformation drop out and one recovers the test-mass results given by Eqs. (A4) and (A7) respectively, at the given S^{5,6} orders.

For the reader's convenience, in Table II we collect the results for the matched scattering angle coefficients for the different spin orders considered in this work. The polynomial and the small- χ matching prescriptions can be obtained as special cases of the non-perturbative in χ prescription.

V. WORLDLINE DESCRIPTION FOR KERR

A. Worldline Compton amplitude vs on-shell Compton ansatz vs BHPT solutions

In the previous sections, we discussed a Compton amplitude with free coefficients that were matched to the UV BHPT solutions. In the spirit of having an EFT description for the Kerr BH, we would like to understand the nature of these free coefficients and classify the kind of BH finite-size effects they parametrize. Recall that BH finite-size effects are divided in two groups: tidal effects (present for both spinless and spinning BHs), and spin-induced multipole moments (present for spinning BHs only) [67]. The latter are characterized by their linear-in-curvature dependence whereas the former are quadratic (and higher) in curvature. In addition, these quadratic in curvature contribution can be static (time independent) or dynamic (time dependent), giving birth to the static and dynamical Love numbers for BHs, respectively.

From a worldline perspective, the dynamics of rotating

TABLE III. Free coefficients for the Compton amplitude derived in Ref. [91] at each order in the spin-multipole expansion.

Spin	Free coeff. helicity-preserving	Free coeff. helicity-reversing	Coeff. helicity-preserving ansatz (69)
S ²	C_2	C_2	
S ³	C_2, C_3	C_2, C_3	
S ⁴	$C_2, C_3, C_4, D_{4a, \dots, f}$	$C_2, C_3, C_4, D_{4a, \dots, f}, E_{4b}$	$c_1^{(i)}, i = 0, 1, 2$
S ⁵	$C_2, C_3, C_4, C_5, D_{4a, \dots, j}, E_{4a}, E_{5a, c, d}$	$C_2, C_3, C_4, C_5, D_{4a, \dots, j}, E_{4a}, E_{5a, \dots, e}$	$c_2^{(i)}, i = 0, 1, 2, c_3^{(i)}, i = 0, 1$

objects can be studied via the action [3, 159]

$$S = \int d\tau \left[p \cdot \dot{z} + \frac{1}{2} S^{\mu\nu} \Omega_{\mu\nu} + \beta_\mu p_\nu S^{\mu\nu} + \frac{\alpha}{2} (p^2 + \mathcal{M}^2) \right], \quad (86)$$

where \dot{z}^μ is the tangent to the worldline $z(\tau)$. In this action, α and β_μ are Lagrange multipliers imposing, respectively, the on-shell condition for the ‘‘dynamical mass function’’ \mathcal{M} , with respect to the magnitude of the momentum p^μ , and the covariant spin-supplementary condition $p_\mu S^{\mu\nu} = 0$. In a recent work [91], the dynamical mass function was presented to fifth order in spin and including quadratic-in-curvature contributions. It takes the form

$$\mathcal{M}^2 = m^2 + \delta\mathcal{M}_1^2 + \delta\mathcal{M}_2^2 + \mathcal{O}(R^3), \quad (87)$$

where $\delta\mathcal{M}_{1,2}^2$ are linear- and quadratic-in-Riemann contributions, respectively⁹. The explicit expressions for the dynamical mass function to fifth order in spin are given in Ref. [91] by Eqs. (8.54)–(8.58) for the linear-in-Riemann terms and by Eqs. (8.65)–(8.67) for the quadratic-in-Riemann pieces. The type of operators leads to a Compton amplitude whose coefficients can be classified as shown in Table III.

The Compton amplitudes presented in Ref. [91] sets $C_i = 1$ in order to match the Kerr 3-point exponential. One can in addition map the free coefficients in the Compton ansatz (69), imposing the exponential (74), to the worldline coefficients. Requiring spin-exponentiation for the helicity-reversing amplitude—as dictated by the non-interfering Teukolsky solutions—ensures that the helicity-reversing part of the worldline Compton amplitude provides zero contribution to the scattering

angle. The map is the following¹⁰

$$\begin{aligned} D_{4a} &= c_1^{(0)} - c_1^{(1)} + c_1^{(2)}, \\ D_{4b} &= \frac{1}{2} (E_{4b} - 2c_1^{(0)} + c_1^{(1)}), \\ D_{4c} &= -\frac{1}{6} E_{4b} + \frac{1}{4} c_1^{(0)}, \\ D_{4d} &= c_1^{(0)} - c_1^{(1)} + c_1^{(2)}, \\ D_{4e} &= \frac{1}{2} (-E_{4b} - 2c_1^{(0)} + c_1^{(1)}), \\ D_{4f} &= \frac{1}{6} E_{4b} + \frac{1}{4} c_1^{(0)}, \end{aligned} \quad (88)$$

at $\mathcal{O}(S^4)$, and

$$\begin{aligned} D_{5a} &= -\frac{1}{10} - 2c_2^{(0)} + 2c_2^{(1)} - 2c_2^{(2)}, \\ D_{5b} &= \frac{1}{60} (1 - 3E_{4a} - 16E_{5b} - 5E_{5c} + 120c_2^{(0)} - 60c_2^{(1)}), \\ D_{5c} &= \frac{1}{180} (18E_{5b} + 5E_{5c} + 3E_{5e} - 90c_2^{(0)}), \\ D_{5d} &= \frac{4}{15} + 2c_2^{(0)} - 2c_2^{(1)} + 2c_2^{(2)}, \\ D_{5e} &= \frac{1}{180} (E_{5a} - 15 - 48E_{5b} - 17E_{5c} - 360c_2^{(0)} + 180c_2^{(1)}), \\ D_{5f} &= \frac{1}{180} (18E_{5b} + 6E_{5c} - E_{5d} + 3E_{5e} + 90c_2^{(0)}), \\ D_{5g} &= \frac{1}{180} (-19 - 18E_{4a} + 3E_{5a} - E_{5c} + 180c_3^{(0)} - 90c_3^{(1)}), \\ D_{5h} &= \frac{1}{180} (6E_{5b} + E_{5c} - 2E_{5d} + 9E_{5e} - 45c_3^{(0)}), \\ D_{5i} &= \frac{1}{180} (21 + 27E_{4a} - 2E_{5a} - E_{5c} + 180c_3^{(0)} - 90c_3^{(1)}), \\ D_{5j} &= \frac{1}{180} (-6E_{5b} + E_{5d} - 9E_{5e} - 45c_3^{(0)}) \end{aligned} \quad (89)$$

at $\mathcal{O}(S^5)$. We stress that the map in Eqs. (88) and (89) holds on the support of the Teukolsky solutions, as we have used it to set to zero any contact deformation of the helicity-reversing exponential.

⁹Quadratic-in-curvature contributions from a QFT Lagrangian approach were presented in Ref. [80], where the free coefficients were related to the Compton coefficients from Eq. (69) in Table III of Ref. [155].

¹⁰Note that the map in Eqs. (88) and (89) for the Compton coefficients is a bit different from the one presented in Eq. (8.79) of the second version of Ref. [91] on arXiv. At $\mathcal{O}(S^4)$, it is due to dropping the $c_1^{(i)}$ coefficients in Ref. [91], whereas at $\mathcal{O}(S^5)$, the difference is due to some typos in that reference.

A natural choice for the coefficient $E_{4,b}$ is either to set it to zero or to reabsorb it into the D_4 coefficients via a field redefinition. From an on-shell approach, this is expected to be doable as there are only 6 free coefficients at this spin order that parametrize a crossing-symmetric Compton ansatz corresponding to the 6-contact deformations of the BCFW exponentials: 3 for the helicity-preserving amplitude and 3 for the helicity-reversing one (see Tables 1 and 2 of Ref. [82]). Therefore, this choice results in setting $D_{4,a,\dots,f} = 0$ when evaluating the near+far-zone Teukolsky solutions, which is nothing but the on-shell manifestation of the vanishing of the static tidal Love numbers for the Kerr BH, since such operators are of the form $(E_{SS})^2$ or $(B_{SS})^2$, which are the electric/magnetic components of the Weyl tensor $E_{\mu\nu}/B_{\mu\nu}$ contracted with the spin vector.

At $\mathcal{O}(S^5)$ —discarding the $|a\rangle$ operators—there are 10 crossing-symmetric contact deformations of the BCFW exponentials on-shell: 5 for the helicity-preserving amplitude and 5 for the helicity-reversing one [82]. This counting agrees with the 10 $D_{5a,\dots,j}$ coefficients in Eqs. (89); therefore, one expects to be able to reabsorb the 5 free $E_{5a,\dots,e}$ coefficients via field redefinitions. The operators with coefficients $D_{5g,h,i,j}$ are in general not vanishing when evaluating the near+far-zone Teukolsky solutions. Such operators are of dynamical type and as is well known, the dynamical Love numbers of Kerr BH are in general non-vanishing [67]. Hence, one expects such coefficients to be non-vanishing even after field redefinitions. It is interesting to note that the $D_{5g,h,i,j}$ coefficients are also proportional to $c_3^{(i)}$, which are also the coefficients with non-trivial polygamma and $\log \kappa\epsilon$ dependence, capturing dynamical finite-size effects.

More intriguing are the operators of type $D_{5a,\dots,f}$, as they are proportional to the $c_2^{(i)}$ coefficients, the latter vanishing on the Teukolsky solutions. These operators appear because of the breaking of the spherical symmetry by the Kerr spin, and feature a quadrupole-octupole mixing of the tidal fields $E_{\mu\nu}$ and $B_{\mu\nu}$. In Ref. [67], it was shown that this type of mixing for the lower linear- and cubic-in-spin orders produces coefficients proportional to those of the static Love operators, thus vanishing on the support of the Teukolsky solutions, while the even-in-spin contributions vanish by parity arguments. We find that starting at fifth order in spin, this mixing in general produces non-vanishing operators of Love type; for instance, $D_{5a} = -1/10$ and $D_{4d} = 4/15$ on the support of the Teukolsky solutions, which are also independent of any value of the linear-in-Riemann $E_{4,5,a,\dots}$ coefficients, thereby remain non-vanishing even after field redefinitions. In Subsection VC, we discuss a way to fix all the E_5 -coefficients in terms of E_{4a} only.

B. Scattering angle for a spinning test body in Kerr background

In this subsection, we compute the aligned-spin scattering angle for a spinning test body moving in a Kerr background, starting from the action in Eq. (86). We derive the integrand of the scattering angle without a PM expansion, to all orders in the Kerr spin, and to fifth order in the spin of the test body. Then, we compute the scattering angle in a PM expansion to 6PM order and spin expansion to sixth order in the Kerr spin, though we only write in Eq. (102) the 3PM angle, which was needed in Sec. II to obtain the NNLO S^3 and S^4 test-body coefficients. The angle we derive also provides an independent check of the mapping in Eqs. (88) and (89), and we use it in the following subsection to obtain additional constraints on the Wilson coefficients from GSF results.

The Mathisson-Papapetrou-Dixon (MPD) equations describe the motion of a multipolar test body in an arbitrary (vacuum) curved background [134, 160–162], and they can be written as

$$\frac{Dp_\mu}{d\tau} + \frac{1}{2}R_{\mu\nu\rho\sigma}\dot{z}^\nu S^{\rho\sigma} = F_\mu, \quad (90a)$$

$$\frac{DS^{\mu\nu}}{d\tau} - 2p^{[\mu}u^{\nu]} = N^{\mu\nu}, \quad (90b)$$

where F_μ and $N^{\mu\nu}$ are the ‘force’ and ‘torque’, along with the covariant SSC

$$p_\mu S^{\mu\nu} = 0, \quad (91)$$

which determines the tangent \dot{z}^μ to the worldline $z(\tau)$.

The 4-velocity u^μ is not in the same direction as \dot{z}^μ , but is related to the 4-momentum p^μ via

$$u^\mu = \frac{p^\mu}{\sqrt{-p^2}}, \quad (92)$$

where p^2 is related to the dynamical mass \mathcal{M} through the mass-shell constraint

$$p^2 = -\mathcal{M}^2(z, u, S). \quad (93)$$

The dynamical mass in terms of generic Wilson coefficients was obtained in Ref. [91] to fifth order in the test body’s spin.

One can verify that the same equations of motion (in a vacuum background) are produced by the action (86) with the Lagrange multiplier [74, 159]

$$\alpha = \frac{\dot{z} \cdot p}{p^2} = -\frac{\dot{z} \cdot u}{\mathcal{M}} = \frac{1}{\mathcal{M}}, \quad (94)$$

where we use the normalization condition $\dot{z} \cdot u = -1$. The force F_μ and torque $N^{\mu\nu}$ are given by

$$F_\mu = -\frac{\alpha}{2} \frac{D}{Dz^\mu} \mathcal{M}^2, \quad (95a)$$

$$\begin{aligned}
N^{\mu\nu} &= -\alpha \left(u^{[\mu} \frac{D}{Du_{\nu]}} + 2S^{[\mu}{}_{\lambda} \frac{D}{DS_{\nu]\lambda}} \right) \mathcal{M}^2 \\
&= -\alpha \left(u^{[\mu} \frac{D}{Du_{\nu]}} + \sigma^{[\mu} \frac{D}{D\sigma_{\nu]}} \right) \mathcal{M}^2, \quad (95b)
\end{aligned}$$

where the spin vector σ^μ is related to the spin tensor $S^{\mu\nu}$ via

$$\sigma^\mu = -\frac{1}{2} \eta^\mu{}_{\nu\rho\lambda} u^\nu S^{\rho\lambda}, \quad S^{\mu\nu} = \eta^{\mu\nu}{}_{\rho\lambda} u^\rho \sigma^\lambda, \quad (96)$$

with $\eta_{\mu\nu\rho\lambda}$ being the volume form. We denote the magnitude of the spin vector by $\sigma = \sqrt{\sigma^\mu \sigma_\mu}$, and define $s := \sigma/m$, where m is the mass of the test body, so that s has units of length like the Kerr spin a .

To solve for \dot{z}^μ , we first solve for the components of $u_\mu = (u_t, u_r, 0, u_\phi)$. We use the conserved quantities from the Killing vectors $t^\mu := (\partial_t)^\mu$ and $\phi^\mu := (\partial_\phi)^\mu$, which are the energy and angular momentum [163]

$$\begin{aligned}
E &= -p_\mu t^\mu - \frac{1}{2} S^{\mu\nu} \nabla_\mu t_\nu, \\
&= -\mathcal{M} u_t + \frac{M\sigma(a u_t + u_\phi)}{r^3}, \quad (97a)
\end{aligned}$$

$$\begin{aligned}
J &= p_\mu \phi^\mu + \frac{1}{2} S^{\mu\nu} \nabla_\mu \phi_\nu, \\
&= \mathcal{M} u_\phi + \frac{\sigma}{r^3} (a M u_\phi + a^2 M u_t - u_t r^3). \quad (97b)
\end{aligned}$$

These conserved quantities, together with the normalization condition $u^2 = -1$, can be solved for the three components of u^μ .

After that, we apply D/d τ on the SSC condition (91)

and use the MPD equations (90), yielding

$$S^{\mu\nu} F_\nu + N^{\mu\nu} p_\nu - \frac{1}{2} S^{\mu\nu} R_{\nu\lambda\rho\sigma} \dot{z}^\lambda S^{\rho\sigma} + 2p^{[\mu} \dot{z}^{\nu]} p_\nu = 0. \quad (98)$$

The last two terms can be written as follows:

$$2p^{[\mu} \dot{z}^{\nu]} p_\nu = \mathcal{M}^2 (\dot{z}^\mu - u^\mu), \quad (99a)$$

$$\begin{aligned}
-\frac{1}{2} S^{\mu\nu} R_{\nu\lambda\rho\sigma} \dot{z}^\lambda S^{\rho\sigma} &= \dot{z}^\mu {}^*R^*{}_{us us} + {}^*R^*{}_{sus} \\
&\quad + \dot{z} \cdot \sigma {}^*R^*{}_{uus}, \quad (99b)
\end{aligned}$$

where we used the double (left and right) dual of the Riemann tensor ${}^*R^*{}_{\mu\nu\rho\sigma} = \frac{1}{2} \eta_{\mu\nu}{}^{\kappa\lambda} R_{\kappa\lambda\tau\chi} \eta^{\tau\chi}{}_{\rho\sigma} \frac{1}{2}$.

For aligned spins, $\dot{z} \cdot \sigma = 0$, and the above equations can be solved for \dot{z}^μ , leading to

$$\dot{z}^\mu = \frac{\mathcal{M}^2 u^\mu - {}^*R^*{}_{sus} - S^{\mu\nu} F_\nu - N^{\mu\nu} p_\nu}{\mathcal{M}^2 + {}^*R^*{}_{us us}}. \quad (100)$$

This relation can then be evaluated for the components of $\dot{z}^\mu = (\dot{z}^t, \dot{z}^r, 0, \dot{z}^\phi)$, yielding the orbital equation $d\phi/dr = \dot{z}^\phi/\dot{z}^r$. Our result for $d\phi/dr$ agrees with the $\mathcal{O}(s^2)$ result given by Eq. (65) of Ref. [164]. In the Supplemental Material, we provide $d\phi/dr$ to all PM orders, all orders in the Kerr spin, and fifth order in the spin of the test body.

The scattering angle can be computed from the integral

$$\theta = \int d\phi = \int_0^{1/b} 2 \frac{d\phi}{du} du \quad (101)$$

where b is the impact parameter and we defined $u := M/r$. The integral can be evaluated in a PM expansion while taking the *partie-finie*, i.e., neglecting the divergent terms [8]. Performing the integration to 3PM order and expanding to sixth order in both spins, we obtain

$$\theta_{\text{test}} := \frac{GM}{b} \theta_{\text{test}}^{(1)} + \pi \frac{G^2 M^2}{b^2} \theta_{\text{test}}^{(2)} + \frac{G^3 M^3}{b^3} \theta_{\text{test}}^{(3)} + \mathcal{O}(G^4), \quad (102a)$$

$$\begin{aligned}
\theta_{\text{test}}^{(1)} &= \frac{2(v^2 + 1)}{v^2} - \frac{4(a+s)}{bv} + \frac{2(v^2 + 1)(a+s)^2}{b^2 v^2} - \frac{4(a+s)^3}{b^3 v} + \frac{2(v^2 + 1)(a+s)^4}{b^4 v^2} - \frac{4(a+s)^5}{b^5 v} \\
&\quad + \frac{2a(v^2 + 1)(a^5 + 6a^4 s + 15a^3 s^2 + 20a^2 s^3 + 15a s^4 + 6s^5)}{b^6 v^2} + \mathcal{O}(a^7, s^6), \quad (102b)
\end{aligned}$$

$$\begin{aligned}
\theta_{\text{test}}^{(2)} &= \frac{3}{v^2} + \frac{3}{4} - \frac{(3v^2 + 2)(4a + 3s)}{2bv^3} + \frac{3}{16b^2 v^4} [a^2 (15v^4 + 72v^2 + 8) + 8as (3v^4 + 15v^2 + 2) + 4s^2 (2v^4 + 11v^2 + 2)] \\
&\quad - \frac{3}{4b^3 v^3} [4a^3 (5v^2 + 4) + a^2 s (51v^2 + 44) + 40as^2 (v^2 + 1) + 4s^3 (2v^2 + 3)] \\
&\quad + \frac{15}{b^4 v^4 (1 - v^2)} \left\{ a^3 s \left(1 - \frac{5v^6}{4} - \frac{11v^4}{2} + \frac{23v^2}{4} \right) + a^2 s^2 \left(\frac{3}{2} - \frac{3v^6}{2} - \frac{59v^4}{8} + \frac{59v^2}{8} \right) + as^3 \left(1 - \frac{2v^6}{3} - \frac{13v^4}{3} + 4v^2 \right) \right. \\
&\quad \left. + a^4 \left(\frac{1}{4} - \frac{35v^6}{96} - \frac{145v^4}{96} + \frac{13v^2}{8} \right) + s^4 \left[\frac{1}{4} + v^2 \left(\frac{3}{4} - \frac{D_4^{\text{NLO}}}{32} \right) + v^4 \left(-\frac{3D_4^{\text{NLO}}}{32} + \frac{5D_4^{\text{NNLO}}}{64} - 1 \right) \right] \right\}
\end{aligned}$$

$$\begin{aligned}
& + v^6 \left(\frac{105D_{4c}}{128} - \frac{41D_4^{\text{NLO}}}{512} - \frac{5D_4^{\text{NNLO}}}{512} + \frac{35E_{4b}}{256} \right) \Big] \Big\} \\
& + \frac{15}{2b^5v^3(1-v^2)} \left\{ a^5 \left(\frac{7v^4}{2} - \frac{v^2}{2} - 3 \right) + a^4s \left(\frac{125v^4}{8} - \frac{11v^2}{8} - \frac{57}{4} \right) + a^3s^2(27v^4 - 27) + a^2s^3 \left(22v^4 + \frac{7v^2}{2} - \frac{51}{2} \right) \right. \\
& + as^4 \left[-12 + v^2 \left(\frac{3D_4^{\text{NLO}}}{4} - \frac{3D_4^{\text{NNLO}}}{8} + 4 \right) + v^4 \left(-\frac{63D_{4c}}{8} + \frac{39D_4^{\text{NLO}}}{32} - \frac{9D_4^{\text{NNLO}}}{32} - \frac{21E_{4b}}{16} + 8 \right) \right] \\
& + s^5 \left[-\frac{9}{4} + v^2 \left(\frac{3D_5^{\text{NLO}}}{8} + \frac{247}{160} \right) + v^4 \left(\frac{25D_5^{\text{NLO}}}{64} - \frac{7D_5^{\text{NNLO}}}{64} + \frac{1639}{1280} \right) \right] \Big\} \\
& + \frac{15}{4b^6v^4(1-v^2)^2} \left\{ a^6 \left(\frac{147v^8}{64} + \frac{245v^6}{32} - \frac{1309v^4}{64} + \frac{35v^2}{4} + \frac{7}{4} \right) + a^5s \left(\frac{49v^8}{4} + \frac{175v^6}{4} - \frac{455v^4}{4} + \frac{189v^2}{4} + \frac{21}{2} \right) \right. \\
& + a^4s^2 \left(\frac{105v^8}{4} + \frac{833v^6}{8} - \frac{1043v^4}{4} + \frac{833v^2}{8} + \frac{105}{4} \right) + a^3s^3(28v^8 + 133v^6 - 315v^4 + 119v^2 + 35) \\
& + a^2s^4 \left[\frac{105}{4} + v^2 \left(\frac{147}{2} - \frac{21D_4^{\text{NLO}}}{16} + \frac{7D_4^{\text{NNLO}}}{16} \right) + v^4 \left(\frac{441D_{4c}}{16} - \frac{441D_4^{\text{NLO}}}{64} + \frac{189D_4^{\text{NNLO}}}{64} + \frac{147E_{4b}}{32} - \frac{847}{4} \right) \right. \\
& + v^6 \left(98 - \frac{441D_{4c}}{64} + \frac{1449D_4^{\text{NLO}}}{256} - \frac{819D_4^{\text{NNLO}}}{256} - \frac{147E_{4b}}{128} \right) + v^8 \left(14 - \frac{1323D_{4c}}{64} + \frac{651D_4^{\text{NLO}}}{256} \right. \\
& \left. \left. - \frac{49D_4^{\text{NNLO}}}{256} - \frac{441E_{4b}}{128} \right) \right] + as^5 \left[\frac{21}{2} + v^2 \left(-\frac{7D_5^{\text{NLO}}}{8} + \frac{7D_5^{\text{NLO}S^6}}{40} + \frac{357}{16} \right) \right. \\
& + v^4 \left(-\frac{77D_5^{\text{NLO}}}{12} + \frac{49D_5^{\text{NNLO}}}{96} + \frac{63D_5^{\text{NLO}S^6}}{160} - \frac{49D_5^{\text{NNLO}S^6}}{80} - \frac{50211}{640} \right) \\
& + v^6 \left(\frac{2555D_5^{\text{NLO}}}{384} - \frac{49D_5^{\text{NNLO}}}{192} + \frac{147D_5^{\text{NLO}S^6}}{320} - \frac{399D_5^{\text{NLO}S^6}}{640} + \frac{49D_5^{\text{NNLO}S^6}}{64} + \frac{27027}{640} \right) \\
& \left. + v^8 \left(\frac{245D_5^{\text{NLO}}}{384} - \frac{49D_5^{\text{NNLO}}}{192} - \frac{147D_5^{\text{NLO}S^6}}{320} + \frac{7D_5^{\text{NLO}S^6}}{128} - \frac{49D_5^{\text{NNLO}S^6}}{320} + \frac{273}{80} \right) \right] \Big\} + \mathcal{O}(a^7, s^6), \quad (102c)
\end{aligned}$$

$$\theta_{\text{test}}^{(3)} = \frac{2(5v^6 + 45v^4 + 15v^2 - 1)}{3v^6} - \frac{4(3a + 2s)(5v^4 + 10v^2 + 1)}{bv^5}$$

$$\begin{aligned}
& + \frac{4}{b^2v^6} \left[a^2(7v^6 + 75v^4 + 45v^2 + 1) + 2as(5v^6 + 55v^4 + 35v^2 + 1) + s^2(3v^6 + 35v^4 + 25v^2 + 1) \right] \\
& - \frac{40(a+s)^2}{3b^3v^5} \left[a(21v^4 + 50v^2 + 9) + 2s(3v^4 + 10v^2 + 3) \right] \\
& + \frac{15}{b^4v^4(1-v^2)} \left\{ a^4 \left(48 - 6v^6 - 64v^4 + 20v^2 + \frac{2}{v^2} \right) + a^3s \left(\frac{496}{3} - \frac{56v^6}{3} - 208v^4 + \frac{160v^2}{3} + \frac{8}{v^2} \right) \right. \\
& + a^2s^2 \left(208 - 20v^6 - 240v^4 + 40v^2 + \frac{12}{v^2} \right) + as^3 \left(112 - 8v^6 - 112v^4 + \frac{8}{v^2} \right) \\
& + s^4 \left[\frac{2}{v^2} - \frac{8}{15}D_4^{\text{NLO}} + \frac{64}{3} + v^2 \left(-\frac{72}{25}D_4^{\text{NLO}} + \frac{48D_4^{\text{NNLO}}}{25} - \frac{20}{3} \right) + v^4 \left(\frac{4608D_{4c}}{175} - \frac{632D_4^{\text{NLO}}}{175} + \frac{96D_4^{\text{NNLO}}}{175} \right. \right. \\
& \left. \left. + \frac{768E_{4b}}{175} - 16 \right) + v^6 \left(\frac{512D_{4c}}{175} - \frac{152D_4^{\text{NLO}}}{525} - \frac{16D_4^{\text{NNLO}}}{525} + \frac{256E_{4b}}{525} - \frac{2}{3} \right) \right] \Big\} + \mathcal{O}(a^5, s^5), \quad (102d)
\end{aligned}$$

To simplify the above expressions, and since we are working with BHs, we set the coefficients $C_2 = C_3 = C_4 = C_5 = 1$, and truncated the spin expansions to the orders needed below, but our result in the Supplemental Material retains the dependence on all Wilson coefficients, in addition to including the 6PM expansion of the scattering angle.

In Eq. (102), we defined the following combinations of

Wilson coefficients:

$$D_4^{\text{NLO}} := 2D_{4a} + 2D_{4b} + 12D_{4c} + E_{4b}, \quad (103a)$$

$$D_4^{\text{NNLO}} := 12D_{4c} - 6D_{4e} - 12D_{4f} + E_{4b}, \quad (103b)$$

$$\begin{aligned}
D_5^{\text{NLO}} &:= 3D_{5b} + 6D_{5c} - 2D_{5d} - 2D_{5e} - 8D_{5f} \\
&\quad - 3D_{5h} + \frac{3}{20}E_{4a} + \frac{1}{5}E_{5b}, \quad (103c)
\end{aligned}$$

$$D_5^{\text{NNLO}} := 4D_{5d} + 4D_{5e} - 14D_{5f} - 12D_{5h} + 9D_{5i}$$

$$+ 9D_{5j} - \frac{6E_{4a}}{5} + \frac{7E_{5b}}{5}, \quad (103d)$$

$$D_5^{\text{NLO}S^6} := 5D_{5d} + 5D_{5e} + 20D_{5f} - 15D_{5h} - E_{5b}, \quad (103e)$$

$$D_5^{\text{NNLO}S^6} := 5D_{5d} + 5D_{5e} + 45D_{5f} - 2E_{5b}, \quad (103f)$$

$$D_5^{\text{N}^3\text{LO}S^6} := 5D_{5d} + 5D_{5e} + E_{5b}, \quad (103g)$$

such that in a PN expansion, the NLO S^4 scattering angle (or Hamiltonian) only depends on D_4^{NLO} while the NNLO only depends on D_4^{NLO} and D_4^{NNLO} , and similarly for the dependence of the S^5 contributions on D_5^{NLO} and D_5^{NNLO} . The contributions at sixth order in spin depend on different combinations of the D_5 and E_5 coefficients, denoted by $D_5^{\text{NLO}S^6}$, $D_5^{\text{NNLO}S^6}$, and $D_5^{\text{N}^3\text{LO}S^6}$.

The 2PM part of our scattering angle, to fourth order in the test body's spin, agrees with Ref. [117], and agrees after setting the Wilson coefficients to $D_{4a,\dots,f} = E_{4b} = 0$ with Ref. [38]. We also checked that our angle, at quadratic order in the test body's spin and up to 5PM order, agrees with the results of Ref. [165], which are valid to all orders in the Kerr spin. To our knowledge, our result at fifth order in the test body's spin is new, and so are the higher PM contributions at lower orders in spin.

C. Constraints on the Wilson coefficients

1. Worldline test-body scattering angle vs Compton angle

We can compare the scattering angle derived from the Compton ansatz in Eqs. (75) to the 2PM part of the test-body scattering angle in Eq. (102), which leads to the following relations:

$$D_4^{\text{NLO}} = 3c_1^{(0)} - c_1^{(1)} + 2c_1^{(2)} = 0, \quad (104a)$$

$$D_4^{\text{NNLO}} = 6c_1^{(0)} - 3c_1^{(1)} = 0, \quad (104b)$$

$$D_{4c} = -\frac{E_{4b}}{6} + \frac{c_1^{(0)}}{4} = -\frac{E_{4b}}{6}, \quad (104c)$$

$$\begin{aligned} D_5^{\text{NLO}} &= -\frac{19}{60} + \frac{3c_3^{(0)}}{4} - c_2^{(1)} - 4c_2^{(2)} \\ &= -\frac{19}{60} + \frac{3c_3^{(0)}}{4}, \end{aligned} \quad (104d)$$

$$\begin{aligned} D_5^{\text{NNLO}} &= \frac{11}{6} + \frac{39c_3^{(0)}}{4} - \frac{9c_3^{(1)}}{2} - 7c_2^{(1)} + 8c_2^{(2)} \\ &= \frac{11}{6} + \frac{39c_3^{(0)}}{4} - \frac{9c_3^{(1)}}{2}, \end{aligned} \quad (104e)$$

$$\begin{aligned} D_5^{\text{NLO}S^6} &= \frac{11}{12} + 15c_2^0 + \frac{15c_3^0}{4} - 5c_2^1 + 10c_2^2 \\ &= \frac{11}{12} + \frac{15c_3^0}{4}, \end{aligned} \quad (104f)$$

$$D_5^{\text{NNLO}S^6} = \frac{11}{12} + \frac{45c_2^0}{2} - 5c_2^1 + 10c_2^2 = \frac{11}{12}, \quad (104g)$$

$$D_5^{\text{N}^3\text{LO}S^6} = \frac{11}{12} - 5c_2^1 + 10c_2^2 = \frac{11}{12}, \quad (104h)$$

where the latter equality follows on the support of the Teukolsky solutions, obtained via the splitting Eq. (73) and the explicit solutions Eqs. (B6) and (B7).

If we combine the above solution with the maps obtained in Eqs. (88) and (89), then the D coefficients drop and we get that the E coefficients satisfy

$$2E_{5a} + 66E_{5b} + 32E_{5c} - 14E_{5d} + 33E_{5e} = 0, \quad (105a)$$

$$\begin{aligned} 27E_{4a} + 47E_{5d} - 14E_{5a} - 318E_{5b} - 173E_{5c} \\ - 231E_{5e} = 9, \end{aligned} \quad (105b)$$

$$30E_{5b} - E_{5a} - 4E_{5c} - 2E_{5d} + 15E_{5e} = 0, \quad (105c)$$

$$E_{5a} + 42E_{5b} + 37E_{5c} - 9E_{5d} + 27E_{5e} = 0, \quad (105d)$$

$$E_{5a} - 12E_{5b} - 17E_{5c} = 0. \quad (105e)$$

which can be solved for the E_5 coefficients in terms of E_{4a} leading to

$$\begin{aligned} E_{5a} &= -\frac{4}{7} + \frac{12E_{4a}}{7}, & E_{5b} &= -\frac{1}{28} + \frac{3E_{4a}}{28}, \\ E_{5d} &= -\frac{2}{7} + \frac{6E_{4a}}{7}, & E_{5c} &= -\frac{1}{119} + \frac{3E_{4a}}{119}, \\ E_{5e} &= -\frac{5}{714} + \frac{5E_{4a}}{238}. \end{aligned} \quad (106)$$

Substituting this solution into the map (89) leads to

$$D_{5a} = -\frac{1}{10}, \quad (107a)$$

$$D_{5b} = \frac{16}{595} - \frac{48E_{4a}}{595}, \quad (107b)$$

$$D_{5c} = -\frac{1}{255} + \frac{E_{4a}}{85}, \quad (107c)$$

$$D_{5d} = \frac{4}{15}, \quad (107d)$$

$$D_{5e} = -\frac{8}{105} - \frac{3E_{4a}}{140}, \quad (107e)$$

$$D_{5f} = -\frac{1}{420} + \frac{E_{4a}}{140}, \quad (107f)$$

$$D_{5g} = -\frac{88}{765} + c_3^{(0)} - \frac{c_3^{(1)}}{2} - \frac{73E_{4a}}{1020}, \quad (107g)$$

$$D_{5h} = \frac{1}{630} - \frac{c_3^{(0)}}{4} - \frac{E_{4a}}{210}, \quad (107h)$$

$$D_{5i} = \frac{659}{5355} + c_3^{(0)} - \frac{c_3^{(1)}}{2} + \frac{467E_{4a}}{3570}, \quad (107i)$$

$$D_{5j} = -\frac{1}{21420} - \frac{c_3^{(0)}}{4} + \frac{E_{4a}}{7140}. \quad (107j)$$

Thus, we obtain nonzero values for the D_5 Wilson coefficients, which is surprising given the results of Ref. [67], as discussed at the end of Subsection V A.

2. Constraints from GSF invariants

In Sec. II, we started from a scattering angle ansatz with unknowns coefficients, related it to a

Hamiltonian, then computed the redshift and spin-precession invariants and compared them to GSF results to solve for the unknowns. The same steps can be performed but using the test-body scattering we derived in the previous subsection, which includes Wilson coefficients.

Specifically, we take the scattering angle ansatz from Sec. II B and use the angle from Eq. (102) to determine the coefficients in the test-mass limit, at NLO S^4 , NNLO S^4 , NLO S^5 , and (partially) NLO S^6 . The result of the matching for the a_1^4 part of the scattering angle in terms of Wilson coefficients reads

$$\begin{aligned} \frac{\theta_{a_1^4}}{\Gamma} = \frac{a_1^4}{b^4} & \left\{ \frac{GM \left(\frac{2}{v^2} + 2 \right)}{b} + \frac{\pi G^2 M^2}{b^2 v^4} \left\{ \frac{15}{4} \right. \right. \\ & + v^2 \left[\frac{105\delta}{16} + \left(\frac{15\delta}{64} - \frac{15}{64} \right) D_4^{\text{NLO}} + \frac{345}{16} \right] \\ & + v^4 \left[\frac{175}{64} + \frac{175\delta}{64} + \left(\frac{15\delta}{16} - \frac{15}{16} \right) D_4^{\text{NLO}} \right. \\ & \left. \left. + \left(\frac{75}{128} - \frac{75\delta}{128} \right) D_4^{\text{NNLO}} \right] \right\} + \frac{G^3 M^3}{b^3 v^6} \left\{ 30 \right. \\ & + v^2 [200\delta + (4\delta - 4) D_4^{\text{NLO}} - 50\nu + 550] \\ & + v^4 \left[650 + 400\delta + \left(\frac{128\delta}{5} - \frac{128}{5} \right) D_4^{\text{NLO}} \right. \\ & \left. \left. + \left(\frac{72}{5} - \frac{72\delta}{5} \right) D_4^{\text{NNLO}} + h_{40}\nu \right] \right\}, \quad (108) \end{aligned}$$

and for the a_1^5 contribution

$$\begin{aligned} \frac{\theta_{a_1^5}}{\Gamma} = \frac{va_1^5}{b^5} & \left\{ -\frac{4GM}{bv} + \frac{\pi G^2 M^2}{b^2 v^3} \left\{ -\frac{45\delta}{16} - \frac{315}{16} \right. \right. \\ & \left. \left. + v^2 \left[\frac{45D_5^{\text{NLO}}}{32} - \frac{2019}{128} - \delta \left(\frac{45D_5^{\text{NLO}}}{32} + \frac{1341}{128} \right) \right] \right\} \right\}, \quad (109) \end{aligned}$$

where instead of the two unknowns f_{50} and g_{50} in Eq. (23), we now have one unknown, which is the combination D_5^{NLO} of Wilson coefficients. At the NLO S^6 , we get the following contribution:

$$\begin{aligned} \frac{\theta_{a_1^5 a_2}}{\Gamma} = \frac{a_1^5 a_2}{b^6} & \left\{ \frac{12GM}{bv^2} (1 + v^2) + \frac{\pi G^2 M^2}{b^2 v^4} \left\{ \frac{315}{8} \right. \right. \\ & + v^2 \left[\frac{26775}{128} - \frac{105D_5^{\text{NLO}}}{64} + \frac{21D_5^{\text{NLO} S^6}}{64} \right. \\ & \left. \left. + \delta \left(\frac{105D_5^{\text{NLO}}}{64} - \frac{21D_5^{\text{NLO} S^6}}{64} + \frac{5985}{128} \right) \right] \right\}, \quad (110) \end{aligned}$$

which replaces the f_{51} and g_{51} unknowns from Eq. (23) by D_5^{NLO} and $D_5^{\text{NLO} S^6}$.

Next, we obtain a Hamiltonian in terms of the scattering angle coefficients and compute from it the redshift and spin-precession invariants, expanded to first order in the mass ratio. Comparison with circular-orbit

GSF results allows us to obtain the following solution at $\mathcal{O}(S^4)$:

$$\begin{aligned} h_{40} = -\frac{631}{2}, \quad h_{31} = -446, \\ D_4^{\text{NLO}} = 0, \quad D_4^{\text{NNLO}} = 0, \end{aligned} \quad (111)$$

which is the same solution obtained in Sec. II for h_{40} and h_{31} , in addition to confirming that the $\mathcal{O}(S^4)$ Wilson coefficients are consistent with being zero for BHs [67, 117]. As for the D_5^{NLO} coefficient at $\mathcal{O}(S^5)$, we get

$$\text{polynomial:} \quad D_5^{\text{NLO}} = -\frac{19}{60}, \quad (112a)$$

$$\text{spin expansion:} \quad D_5^{\text{NLO}} = -\frac{81}{20} + \frac{512\zeta(3)}{15} - \frac{512\zeta(5)}{15}, \quad (112b)$$

where the first solution is obtained by matching our result to the polynomial piece of the 1SF redshift, while the second solution is obtained by first expanding the irrational functions in the 1SF redshift in a small-spin expansion, as explained in Sec. IV. Similarly, from the NLO S^6 part, we get

$$\text{polynomial:} \quad D_5^{\text{NLO} S^6} = \frac{11}{12}, \quad (113a)$$

$$\text{spin expansion:} \quad D_5^{\text{NLO} S^6} = -\frac{71}{4} + \frac{512\zeta(3)}{3} - \frac{512\zeta(5)}{3}, \quad (113b)$$

in addition to the same solution for f_{60} and g_{60} as in Eq. (43). These solutions are all in agreement with Eqs. (75) when combined with the constraints (104).

VI. CONCLUSIONS

Improving the accuracy of gravitational waveform models is crucial for the increasing sensitivity of current and future gravitational-wave detectors [166]. Since spin plays an important role in compact binary inspirals, in this paper, we looked into improving the spin description in binary dynamics, by deriving new PN results at high orders in spin.

In particular, in this work we studied the conservative, aligned-spin binary dynamics at NNLO S^3 and S^4 , in addition to the NLO S^5 and S^6 PN contributions for Kerr BHs, using a synergy of methods including worldline field theory, the Tutti-Frutti method, on-shell Compton amplitudes, and BHPT. We obtained several observables for binary systems, namely the scattering angle for hyperbolic orbits, and the redshift and spin-precession frequency for bound eccentric orbits without an eccentricity expansion.

Our result for the NNLO S^4 dynamics contains one unknown coefficient of order $\mathcal{O}(\nu a_1^2 a_2^2)$. Solving for that unknown using the Tutti-Frutti method requires 1SF results for the redshift at quadratic order in both

the secondary and Kerr spins, which are currently unavailable. We leave such a calculation for future investigation. The inclusion of higher-spin, and higher ℓ near-zone BHPT contributions is also left for future work.

At NLO S^5 , we encountered an ambiguity while solving for the unknown coefficients, due to transcendental functions of the Kerr spin appearing in the redshift at that order. We suggested three possibilities to determine the unknowns: matching the polynomial S^5 piece only, expanding in small spin, or a non-perturbative matching as a function of the Kerr spin; with the first two prescriptions obtained as special cases of the latter. While the polynomial and the small spin matching prescriptions are of theoretical interest, for instance for obtaining an all-orders-in-spin expression for the tree-level gravitational Compton amplitude, the non-perturbative matching is relevant for phenomenological applications as it has the advantage of encapsulating, via simple contact term in the Compton amplitude, Kerr BH finite-size effects that are present for spinning observables in binary systems, as derived directly in the alternative GSF computations.

Furthermore, from a parametrized worldline action, we derived a scattering angle for a spinning test body, to fifth order in its spin, in a Kerr background, and used it to obtain constraints on the Wilson coefficients through comparisons with both GSF and Compton amplitudes results. Our solutions for the Wilson coefficients are consistent between the two approaches, but they are in tension with recent EFT results [67]. Therefore, fully resolving the issues with the spin⁵ dynamics probably requires the derivation of the NLO S^5 PN contribution from first principles, and finding additional ways to fix the value of Wilson coefficients.

ACKNOWLEDGMENTS

We would like to thank Lucille Cangemi, Giorgio Di Russo, Diego Gallego, David Kosower, Jose Francisco Morales, Trevor Scheopner, and Zihan Zhou for useful Discussions. We are grateful to Trevor Scheopner for rechecking the Compton dictionary presented in Ref. [91], which he confirmed agrees with ours given in Eq. (89). We also thank the organizers of the workshop [Amplifying Gravity at All Scales](#), held in the summer of 2023 in Nordita, where the idea of constraining the Compton amplitude from eccentric gravitational self force computations was born. Y.F.B. thanks the hospitality of the physics department of the Universidad Pedagógica y Tecnológica de Colombia where part of the writing in the final stage of this work was done. This work made use of the tensor algebra package `xAct` [167, 168] in Mathematica, and the Black Hole Perturbation Toolkit [147].

The work of Y.F.B. and M.S. has been supported by the European Research Council under Advanced Investigator Grant ERC-AdG-885414. M.K.'s work is

supported by Perimeter Institute for Theoretical Physics. Research at Perimeter Institute is supported in part by the Government of Canada through the Department of Innovation, Science and Economic Development and by the Province of Ontario through the Ministry of Colleges and Universities. C.K. thanks David Kosower and the financial support from the Grant ERC-AdG-885414 during his visit to the IPhT during the spring of 2024. C.K. acknowledges support from Science Foundation Ireland under Grant number 21/PATH-S/9610.

Appendix A: Test-body redshift and spin-precession invariants for eccentric orbits

The equations of motion for a test mass on an equatorial orbit ($\theta = \pi/2$) in a Kerr background are given by (see, e.g., Ref. [169])

$$\Delta r^2 \frac{dt}{d\tau} = (r^2 E - a\sqrt{K})(r^2 + a^2) + \Delta a\sqrt{K}, \quad (\text{A1a})$$

$$r^4 \left(\frac{dr}{d\tau} \right)^2 = (r^2 E - a\sqrt{K})^2 - \Delta(r^2 + K), \quad (\text{A1b})$$

$$\Delta r \frac{d\phi}{d\tau} = rL - 2m_1\sqrt{K}, \quad (\text{A1c})$$

where $K = (L - aE)^2$ is Carter's constant and $\Delta := r^2 - 2m_1 r + a^2$, with m_1 and a being the mass and spin of the Kerr BH.

Using the Keplerian parametrization $r = m_1/[u_p(1 + e \cos \zeta)]$, we can obtain four equations of motion for $(d\tau/d\zeta, dt/d\zeta, dr/d\zeta, d\phi/d\zeta)$. Then, we solve $dr/d\zeta = 0$ at the turning points $r = [u_p(1 \pm e)]^{-1}$ for $E(u_p, e)$ and $L(u_p, e)$, in a spin expansion to $\mathcal{O}(a^6)$.

The periods of an eccentric orbit can be evaluated through the following integrals:

$$T_\tau^{(0)} := \oint d\tau = \int_0^{2\pi} \frac{d\tau}{d\zeta} d\zeta, \quad (\text{A2a})$$

$$T_r^{(0)} := \oint dt = \int_0^{2\pi} \frac{dt}{d\zeta} d\zeta, \quad (\text{A2b})$$

$$T_\phi^{(0)} := \oint d\phi = \int_0^{2\pi} \frac{d\phi}{d\zeta} d\zeta. \quad (\text{A2c})$$

The orbital frequency is $\Omega^{(0)} = T_\phi^{(0)}/T_r^{(0)}$, and we define the gauge invariant variables

$$y(u_p, e) := (m_1 \Omega^{(0)})^{3/2}, \quad (\text{A3a})$$

$$\lambda(u_p, e) := \frac{3y}{T_\phi^{(0)}/(2\pi) - 1}. \quad (\text{A3b})$$

We computed these periods, in addition to y and λ , in a PN and spin expansion to $\mathcal{O}(a^6 u_p^8)$, but without an eccentricity expansion. The results are lengthy, so we provide them in the Supplemental Material.

The redshift can be computed from the periods via $z^{(0)} := T_\tau^{(0)}/T_r^{(0)}$, with $U^{(0)} := 1/z^{(0)}$, leading to

$$\begin{aligned}
U^{(0)} = & 1 + \frac{3\varepsilon^2 u_p}{2} + \left(6\varepsilon^3 - \frac{21\varepsilon^4}{8}\right) u_p^2 + \left(\frac{55\varepsilon^6}{16} - 12\varepsilon^5 - 6\varepsilon^4 + 23\varepsilon^3\right) u_p^3 + \left(-\frac{525\varepsilon^8}{128} + \frac{75\varepsilon^7}{4} + 12\varepsilon^6 - 105\varepsilon^5 - 24\varepsilon^4\right. \\
& \left. + \frac{249\varepsilon^3}{2}\right) u_p^4 + \left(\frac{1197\varepsilon^{10}}{256} - \frac{105\varepsilon^9}{4} - \frac{57\varepsilon^8}{4} + \frac{969\varepsilon^7}{4} - \frac{27\varepsilon^6}{2} - 780\varepsilon^5 - 96\varepsilon^4 + \frac{5943\varepsilon^3}{8}\right) u_p^5 + \mathcal{O}(u_p^6) \\
& + \chi \varepsilon^3 \left[(-6 + 3\varepsilon) u_p^{5/2} + \left(36\varepsilon^2 - \frac{21\varepsilon^3}{2} + 18\varepsilon - 57\right) u_p^{7/2} + \left(\frac{165\varepsilon^5}{8} - \frac{375\varepsilon^4}{4} - 36\varepsilon^3 + 441\varepsilon^2 + 90\varepsilon - \frac{945}{2}\right) u_p^{9/2}\right. \\
& \left. + \left(-\frac{525\varepsilon^7}{16} + \frac{735\varepsilon^6}{4} + \frac{159\varepsilon^5}{4} - \frac{5745\varepsilon^4}{4} + \frac{531\varepsilon^3}{2} + 4176\varepsilon^2 + 420\varepsilon - \frac{30345}{8}\right) u_p^{11/2} + \mathcal{O}(u_p^{13/2}) \right] \\
& + \chi^2 \varepsilon^3 \left[\left(2 - \frac{3\varepsilon}{2}\right) u_p^3 + \left(\frac{39\varepsilon^3}{4} - 39\varepsilon^2 - 18\varepsilon + 54\right) u_p^4 + \left(\frac{711\varepsilon^4}{4} - \frac{585\varepsilon^5}{16} + 18\varepsilon^3 - \frac{1479\varepsilon^2}{2} - 120\varepsilon + \frac{1485}{2}\right) u_p^5\right. \\
& \left. + \left(\frac{2835\varepsilon^7}{32} - \frac{4115\varepsilon^6}{8} + \frac{327\varepsilon^5}{4} + \frac{6891\varepsilon^4}{2} - 1226\varepsilon^3 - \frac{37713\varepsilon^2}{4} - 672\varepsilon + \frac{16863}{2}\right) u_p^6 + \mathcal{O}(u_p^7) \right] \\
& + \chi^3 \varepsilon^3 \left[(-3\varepsilon^3 + 18\varepsilon^2 + 6\varepsilon - 22) u_p^{9/2} + \left(27\varepsilon^5 - \frac{645\varepsilon^4}{4} + 45\varepsilon^3 + \frac{1251\varepsilon^2}{2} + 60\varepsilon - \frac{2445}{4}\right) u_p^{11/2}\right. \\
& \left. + \left(-\frac{915\varepsilon^7}{8} + \frac{5901\varepsilon^6}{8} - \frac{1815\varepsilon^5}{4} - 4293\varepsilon^4 + 2583\varepsilon^3 + \frac{93279\varepsilon^2}{8} + 420\varepsilon - \frac{21315}{2}\right) u_p^{13/2} + \mathcal{O}(u_p^{15/2}) \right] \\
& + \chi^4 \varepsilon^3 \left[(3 - 3\varepsilon^2) u_p^5 + \left(-\frac{57\varepsilon^5}{8} + \frac{141\varepsilon^4}{2} - 63\varepsilon^3 - 276\varepsilon^2 + \frac{555}{2}\right) u_p^6\right. \\
& \left. + \left(\frac{1125\varepsilon^7}{16} - \frac{4587\varepsilon^6}{8} + \frac{1413\varepsilon^5}{2} + \frac{23421\varepsilon^4}{8} - 2919\varepsilon^3 - \frac{17211\varepsilon^2}{2} + \frac{33705}{4}\right) u_p^7 + \mathcal{O}(u_p^8) \right] \\
& + \chi^5 \varepsilon^3 \left[\left(-12\varepsilon^4 + 27\varepsilon^3 + \frac{117\varepsilon^2}{2} - 6\varepsilon - \frac{135}{2}\right) u_p^{13/2}\right. \\
& \left. + \left(-\frac{33\varepsilon^7}{2} + \frac{1841\varepsilon^6}{8} - 513\varepsilon^5 - \frac{4089\varepsilon^4}{4} + \frac{3659\varepsilon^3}{2} + \frac{31119\varepsilon^2}{8} - 84\varepsilon - \frac{17269}{4}\right) u_p^{15/2} + \mathcal{O}(u_p^{17/2}) \right] \\
& + \chi^6 \varepsilon^3 \left[\left(-3\varepsilon^3 - \frac{9\varepsilon^2}{2} + \frac{15}{2}\right) u_p^7 + \left(-\frac{75\varepsilon^6}{2} + \frac{351\varepsilon^5}{2} + \frac{501\varepsilon^4}{4} - 612\varepsilon^3 - \frac{4275\varepsilon^2}{4} + \frac{2835}{2}\right) u_p^8 + \mathcal{O}(u_p^9) \right], \quad (\text{A4})
\end{aligned}$$

where we recall that $\varepsilon := \sqrt{1 - e^2}$ and $\chi := a/m_1$.

The spin-precession frequency can be derived as in Ref. [169], utilizing Marck's parallel propagated frame [170]. The angular velocity of the gyro-fixed axes in the Marck frame is given by

$$\mathcal{T} = \frac{a + E\sqrt{K}}{r^2 + K}. \quad (\text{A5})$$

The instantaneous spin-precession frequency and its orbit average can then be computed using

$$\Omega_S^{\text{inst}} = \frac{d\tau}{dt} \left(\frac{d\phi}{d\tau} - \mathcal{T} \right), \quad \Omega_S^{(0)} = \frac{1}{T_r^{(0)}} \int_0^{T_r^{(0)}} \Omega_S^{\text{inst}} dt, \quad (\text{A6})$$

from which the spin-precession invariant is defined as $\psi^{(0)} := \Omega_S^{(0)}/\Omega^{(0)}$. Expanding to $\mathcal{O}(\chi^5 u_p^{13/2})$, but without an eccentricity expansion, we obtain

$$\begin{aligned}
\psi^{(0)} = & \frac{3u_p}{2} + \left(\frac{21}{8} - \frac{3\varepsilon^2}{2}\right) u_p^2 + \left(\frac{3\varepsilon^4}{16} - \frac{69\varepsilon^2}{8} + \frac{81}{8}\right) u_p^3 + \left(-\frac{3\varepsilon^6}{32} + \frac{33\varepsilon^4}{8} - \frac{1665\varepsilon^2}{32} + \frac{6549}{128}\right) u_p^4 + \mathcal{O}(u_p^5) \\
& + \chi \left[-u_p^{3/2} + \left(3\varepsilon^2 - \frac{9}{2}\right) u_p^{5/2} + \left(-\frac{9\varepsilon^4}{8} + \frac{117\varepsilon^2}{4} - \frac{63}{2}\right) u_p^{7/2} + \left(\frac{3\varepsilon^6}{4} - \frac{75\varepsilon^4}{4} + \frac{1965\varepsilon^2}{8} - \frac{3777}{16}\right) u_p^{9/2} + \mathcal{O}(u_p^{11/2}) \right] \\
& + \chi^2 \left[\left(2 - \frac{3\varepsilon^2}{2}\right) u_p^3 + \left(\frac{3\varepsilon^4}{8} - \frac{75\varepsilon^2}{2} + \frac{315}{8}\right) u_p^4 + \left(-\frac{33\varepsilon^6}{16} + \frac{285\varepsilon^4}{16} - \frac{969\varepsilon^2}{2} + \frac{7635}{16}\right) u_p^5 + \mathcal{O}(u_p^6) \right] \\
& + \chi^3 \left[\left(\frac{9\varepsilon^4}{4} + 24\varepsilon^2 - \frac{107}{4}\right) u_p^{9/2} + \left(\frac{15\varepsilon^6}{8} + \frac{201\varepsilon^4}{8} + \frac{4203\varepsilon^2}{8} - \frac{4449}{8}\right) u_p^{11/2} + \mathcal{O}(u_p^{13/2}) \right]
\end{aligned}$$

$$\begin{aligned}
& + \chi^4 \left[\left(-\frac{33\epsilon^4}{16} - \frac{75\epsilon^2}{8} + \frac{183}{16} \right) u_p^5 + \left(-\frac{47\epsilon^6}{32} - 60\epsilon^4 - \frac{10899\epsilon^2}{32} + \frac{6443}{16} \right) u_p^6 + \mathcal{O}(u_p^7) \right] \\
& + \chi^5 \left[\left(\frac{3\epsilon^4}{8} + \frac{9\epsilon^2}{4} - \frac{21}{8} \right) u_p^{11/2} + \left(3\epsilon^6 + \frac{93\epsilon^4}{2} + 123\epsilon^2 - \frac{345}{2} \right) u_p^{13/2} + \mathcal{O}(u_p^{15/2}) \right]. \tag{A7}
\end{aligned}$$

In both $U^{(0)}$ and $\psi^{(0)}$, we truncated the PN expansion at each order in spin to the orders needed for the calculations in Sec. II. In the Supplemental Material, we include the full 8PN expressions for $y(u_p, e)$, $\lambda(u_p, e)$, $z^{(0)}$ and $\psi^{(0)}$, to complement the 1SF 8PN results derived in Refs. [102, 107, 112, 113] for circular orbits or in an eccentricity expansion.

Appendix B: Full Compton Coefficients

In this appendix we present relevant expressions for the Compton amplitude derivation using Teukolsky solutions, presented in Sec. III. We start by presenting the extended form of the near-zone phase-shift given in Eq. (65). It reads

$$\begin{aligned}
-2\delta_{\ell m}^{\text{NZ}}|_{\ell \rightarrow 2} = & \left[\frac{m\chi}{18000} \left(10((m^2 - 4)\chi^2 + 4)((m^2 - 1)\chi^2 + 1)\psi^{(0,m)}(\chi) + (-605m^2 + 40\gamma_E(5m^2 - 8) + 824)\chi^2 \right. \right. \\
& + (-133m^4 + 605m^2 + 40\gamma_E(m^4 - 5m^2 + 4) - 412)\chi^4 + 160\gamma_E - 412 \left. \right) \\
& + \frac{1}{900}m\chi((5m^2 - 8)\chi^2 + (m^4 - 5m^2 + 4)\chi^4 + 4)\log(2\kappa\epsilon) \left. \right] \epsilon^6 \\
& + \left[\frac{1}{3402000} \left(-\frac{9m\chi}{\kappa}((5m^2 - 8)\chi^2 + (m^4 - 5m^2 + 4)\chi^4 + 4)(107\kappa\tilde{\psi}^{(0,m)}(\chi) + 210\tilde{\psi}^{(1,m)}(\chi)) \right. \right. \\
& + 210(9\pi m(5m^2 - 8)\chi^3 + (72 - 115m^2)\chi^2 + 5m^2(m^4 - 5m^2 + 4)\chi^6 + 9\pi m(m^4 - 5m^2 + 4)\chi^5 \\
& + (-20m^4 + 95m^2 - 36)\chi^4 + 36\pi m\chi - 36)\psi^{(0,m)}(\chi) + 114345\pi\kappa^2 m^3\chi^3 \\
& + 963\kappa((5m^2 - 8)\chi^2 + (m^4 - 5m^2 + 4)\chi^4 + 4) + 840\gamma_E(9\pi m(5m^2 - 8)\chi^3 + (72 - 115m^2)\chi^2 \\
& + 5m^2(m^4 - 5m^2 + 4)\chi^6 + 9\pi m(m^4 - 5m^2 + 4)\chi^5 + (-20m^4 + 95m^2 - 36)\chi^4 + 36\pi m\chi - 36) \\
& + 7m^2\chi^2(\chi^2(-3591\pi m^3\chi + 7930m^2 - 5(437m^4 - 2005m^2 + 1388))\chi^2 - 35125) + 42065) \\
& - 77868\kappa^4(\pi m\chi - 1) \left. \right) + \frac{1}{8100} \left((9\pi m(5m^2 - 8)\chi^3 + (72 - 115m^2)\chi^2 + 5m^2(m^4 - 5m^2 + 4)\chi^6 \right. \\
& + 9\pi m(m^4 - 5m^2 + 4)\chi^5 + (-20m^4 + 95m^2 - 36)\chi^4 + 36\pi m\chi - 36) \log(2\kappa\epsilon) \left. \right) \left. \right] \epsilon^7 + \\
& \left[\frac{\chi m \epsilon^6}{1800} (\chi^2(m^2 - 4) + 4)(\chi^2(m^2 - 1) + 1) + \frac{\epsilon^7}{16200} (\chi(9\pi m(\chi^2(m^2 - 4) + 4)(\chi^2(m^2 - 1) + 1) \right. \\
& \left. + \chi(\chi^2(5m^2(\chi^2(m^4 - 5m^2 + 4) - 4m^2 + 19) - 36) - 115m^2 + 72)) - 36) \right] \frac{1}{\ell - 2} + \mathcal{O}(\epsilon^8). \tag{B1}
\end{aligned}$$

We also present the explicit matched coefficients in the Compton ansatz, as obtained from the gravitational wave scattering Teukolsky solutions. The spurious pole cancellation conditions read:

$$c_3^{(2)} = 4/15 - c_3^{(0)} + c_3^{(1)} \tag{B2}$$

$$c_{10}^{(2)} = c_{10}^{(1)} - c_{10}^{(0)} \tag{B3}$$

$$d_1^{(0)} = -\frac{8}{45} + 4 \sum_{i=0}^2 (-1)^i c_7^{(i)} + \sum_{j=5}^6 \sum_{i=0}^2 (-1)^i c_j^{(i)} \tag{B4}$$

$$f_1^{(0)} = \frac{4}{45} + \sum_{i=0}^2 \sum_{j \in \{6,8\}} (-1)^i c_j^{(i)}, \tag{B5}$$

with the c-coefficients spitted as in Eq. (73). The far-zone solutions are

$$\begin{aligned}
c_j^{\text{FZ},(i)} &= 0, \quad i = 0, 1, 2, \quad j = 1, 2, 4, 5, 7, 9, 10, \\
d_1^{\text{FZ},(0)} &= 0, \\
c_3^{\text{FZ},(0)} &= \frac{64}{15}, \quad c_3^{\text{FZ},(1)} = \frac{16}{3}, \quad c_3^{\text{FZ},(2)} = \frac{4}{3} \\
c_6^{\text{FZ},(0)} &= \frac{128}{45}, \quad c_6^{\text{FZ},(1)} = \frac{32}{9}, \quad c_6^{\text{FZ},(2)} = \frac{8}{9}, \\
c_8^{\text{FZ},(0)} &= -\frac{512}{45}, \quad c_8^{\text{FZ},(1)} = -\frac{160}{9}, \quad c_8^{\text{FZ},(2)} = -\frac{64}{9}, \\
f_1^{\text{FZ},(0)} &= -\frac{4}{9},
\end{aligned} \tag{B6}$$

whereas the non-perturbative in χ , $\ell = 2$ near-zone solutions are

$$\begin{aligned}
c_j^{\text{NZ},(i)} &= 0, \quad c_j^{\log, \text{NZ},(i)}, \quad i = 0, 1, 2, \quad j = 2, 4, 5, 7, 9, \\
c_3^{\text{NZ},(0)} &= \frac{32(10(3\chi^2 + 1)\psi^{(0,2)}(\chi) + 20(3\chi^2 + 1)\log(2\kappa) - 30\chi^4 + 3(40\gamma_E - 133)\chi^2 + 40\gamma_E - 103)}{225\chi^4} \\
c_3^{\text{NZ},(1)} &= \frac{1}{225\chi^4} \left(4 \left(-3\chi^2 \left(10\psi^{(0,1)}(\chi) - 120\psi^{(0,2)}(\chi) + 100\chi^2 + 1523 \right) + 8(5\psi^{(0,1)}(\chi) + 15\psi^{(0,2)}(\chi) - 206) \right) \right) \\
c_3^{\text{NZ},(2)} &= 4/15 - c_3^{\text{NZ},(0)} + c_3^{\text{NZ},(1)} \\
c_3^{\log, \text{NZ},(0)} &= \frac{128(3\chi^2 + 1)}{45\chi^4}, \quad c_3^{\log, \text{NZ},(1)} = \frac{16(33\chi^2 + 16)}{45\chi^4}, \quad c_3^{\log, \text{NZ},(2)} = 4/15 - c_3^{\log, \text{NZ},(0)} + c_3^{\log, \text{NZ},(1)} \\
c_6^{\log, \text{NZ},(0)} &= \frac{2}{3}c_3^{\log, \text{NZ},(0)}, \quad c_6^{\log, \text{NZ},(1)} = \frac{2}{3}c_3^{\log, \text{NZ},(1)}, \quad c_6^{\log, \text{NZ},(2)} = \frac{32(9\chi^2 + 8)}{135\chi^4}, \\
c_6^{\text{NZ},(0)} &= \frac{2}{3}c_3^{\text{NZ},(0)}, \quad c_6^{\text{NZ},(1)} = \frac{2}{3}c_3^{\text{NZ},(1)} \\
c_6^{\text{NZ},(2)} &= \frac{1}{675\chi^4} \left(8 \left(-3\chi^2 \left(10\psi^{(0,1)}(\chi) - 40\psi^{(0,2)}(\chi) + 20\chi^2 + 459 \right) + 8(5\psi^{(0,1)}(\chi) + 5\psi^{(0,2)}(\chi) - 103) \right) \right. \\
&\quad \left. + 20(9\chi^2 + 8)\log(2\kappa) + 40\gamma_E(9\chi^2 + 8) \right) \\
c_8^{\log, \text{NZ},(0)} &= -\frac{128(4(3\chi^2 + 1)\chi^2 + (6\chi^4 - 97\chi^2 - 9))}{405\chi^6}, \quad c_8^{\log, \text{NZ},(1)} = -\frac{32(4(\chi^2 + 2)\chi^2 + (29\chi^4 - 273\chi^2 - 36))}{135\chi^6} \\
c_8^{\log, \text{NZ},(2)} &= \frac{32(15\chi^4 + (-24\chi^4 + 158\chi^2 + 36))}{135\chi^6} \\
c_8^{\text{NZ},(0)} &= -\frac{64(3\chi^2 + 1) \left(210\kappa\tilde{\psi}^{(1,2)}(\chi) + 107(\chi^2 - 1)\tilde{\psi}^{(0,2)}(\chi) \right)}{4725\chi^5(\chi^2 - 1)} \\
&\quad + \frac{1}{42525\chi^6} \left(32 \left(-210(6\chi^4(2 + 1) + \chi^2(4 - 97) - 9)(\psi^{(0,2)}(\chi) + 2\log(2\kappa)) \right. \right. \\
&\quad \left. \left. + \chi^2(84(103 - 40\gamma_E) + (-2889\kappa + 81480\gamma_E - 255521)) + 2520\chi^6(1 + 5) \right. \right. \\
&\quad \left. \left. - 84\chi^4(60\gamma_E(2 + 1) - 399 - 52) + 9(-107\kappa + 840\gamma_E - 2163) \right) \right) \\
c_8^{\text{NZ},(1)} &= \frac{8}{4725\chi^5(\chi^2 - 1)} \left(210\kappa \left((3\chi^2 - 4)\tilde{\psi}^{(1,1)}(\chi) - 16(3\chi^2 + 1)\tilde{\psi}^{(1,2)}(\chi) \right) \right. \\
&\quad \left. + 107(3\chi^4 - 7\chi^2 + 4)\tilde{\psi}^{(0,1)}(\chi) - 1712(3\chi^4 - 2\chi^2 - 1)\tilde{\psi}^{(0,2)}(\chi) \right) \\
&\quad - \frac{1}{14175\chi^6} \left(8 \left(70 \left((39\chi^4 + 4(4 - 3\chi^2)\chi^2 - 43\chi^2 - 36)\psi^{(0,1)}(\chi) + 8(9\chi^4 - 96\chi^2 - 9)\psi^{(0,2)}(\chi) \right. \right. \right. \\
&\quad \left. \left. + 6(29\chi^4 + 4(\chi^2 + 2)\chi^2 - 273\chi^2 - 36)\log(2\kappa) + 963\kappa(7\chi^2 + 4) + 84(-193\chi^2 + 40\gamma_E(\chi^2 + 2) - 206)\chi^2 \right) \right)
\end{aligned} \tag{B7}$$

$$\begin{aligned}
& +727629\chi^2 - 7(4500\chi^2 + 7021)\chi^4 + 840\gamma_E(29\chi^4 - 273\chi^2 - 36) + 77868) \\
c_8^{\text{NZ},(2)} &= \frac{840\kappa \left((3\chi^2 - 4)\tilde{\psi}^{(1,1)}(\chi) - 6(3\chi^2 + 1)\tilde{\psi}^{(1,2)}(\chi) \right) + 428(3\chi^4 - 7\chi^2 + 4)\tilde{\psi}^{(0,1)}(\chi) - 2568(3\chi^4 - 2\chi^2 - 1)\tilde{\psi}^{(0,2)}(\chi)}{1575\chi^5(\chi^2 - 1)} \\
& + \frac{4}{14175\chi^6} \left(14\chi^2 \left(3\chi^2 \left(-195\psi^{(0,1)}(\chi) - 90\psi^{(0,1)}(\chi) + 750\chi^2 + 2527 \right) + 645\psi^{(0,1)}(\chi) + 4365\psi^{(0,1)}(\chi) - 61882 \right) \right. \\
& + 210\chi^2 \left(3\chi^2(2\psi^{(0,1)}(\chi) + 8\psi^{(0,1)}(\chi) + 40\gamma - 121) - 8\psi^{(0,1)}(\chi) + 8\psi^{(0,1)}(\chi) - 36\chi^4 \right) \\
& + 378(20\psi^{(0,1)}(\chi) + 15\psi^{(0,1)}(\chi) - 412) + 963\kappa(\chi^4 - 8\chi^2 - 6) + 840(-9\chi^4 + 158\chi^2 + 36)\log(2\kappa) \\
& \left. - 2100\gamma(21\chi^4 - 130\chi^2 - 27) \right) \\
c_{10}^{\text{log,NZ},(0)} &= \frac{64(12\pi + (24\gamma_E - 25)i)(3\chi^2 + 1)}{135\chi^5}, \quad c_{10}^{\text{log,NZ},(1)} = \frac{8(12\pi + (24\gamma_E - 25)i)(33\chi^2 + 16)}{135\chi^5}, \\
c_{10}^{\text{NZ},(0)} &= \frac{16(12\pi + (24\gamma_E - 25)i)(10(3\chi^2 + 1)\psi^{(0,2)}(\chi) + 20(3\chi^2 + 1)\log(2\kappa) - 30\chi^4 - 399\chi^2 + 40\gamma_E(3\chi^2 + 1) - 103)}{675\chi^5} \\
c_{10}^{\text{NZ},(1)} &= \frac{2}{675\chi^5} (12\pi + (24\gamma_E - 25)i) \left(-3\chi^2 \left(10\psi^{(0,1)}(\chi) - 120\psi^{(0,2)}(\chi) + 100\chi^2 + 1523 \right) \right. \\
& \left. + 8(5\psi^{(0,1)}(\chi) + 15\psi^{(0,2)}(\chi) - 206) + 20(33\chi^2 + 16)\log(2\kappa) + 40\gamma_E(33\chi^2 + 16) \right) \\
c_{10}^{\text{NZ},(2)} &= c_{10}^{\text{NZ},(1)} - c_{10}^{\text{NZ},(0)}, \quad c_{10}^{\text{log,NZ},(2)} = c_{10}^{\text{log,NZ},(1)} - c_{10}^{\text{log,NZ},(0)} \\
d_1^{\text{NZ},(0)} &= -\frac{8}{45} + 4 \sum_{i=0}^2 (-1)^i c_7^{\text{NZ},(i)} + \sum_{j=5}^6 \sum_{i=0}^2 (-1)^i c_j^{\text{NZ},(i)}, \quad d_1^{\text{log,NZ},(0)} = -\frac{8}{45} + 4 \sum_{i=0}^2 (-1)^i c_7^{\text{log,NZ},(i)} + \sum_{j=5}^6 \sum_{i=0}^2 (-1)^i c_j^{\text{log,NZ},(i)} \\
f_1^{\text{NZ},(0)} &= \frac{4}{45} + \sum_{i=0}^2 \sum_{j \in \{6,8\}} (-1)^i c_j^{\text{NZ},(i)}, \quad f_1^{\text{log,NZ},(0)} = \frac{4}{45} + \sum_{i=0}^2 \sum_{j \in \{6,8\}} (-1)^i c_j^{\text{log,NZ},(i)}, \tag{B8}
\end{aligned}$$

For the reader's convenience, we include the expressions for these coefficients in the supplementary Material.

-
- [1] L. Blanchet, Gravitational Radiation from Post-Newtonian Sources and Inspiralling Compact Binaries, *Living Rev. Rel.* **17**, 2 (2014), arXiv:1310.1528 [gr-qc].
 - [2] G. Schäfer and P. Jaranowski, Hamiltonian formulation of general relativity and post-Newtonian dynamics of compact binaries, *Living Rev. Rel.* **21**, 7 (2018), arXiv:1805.07240 [gr-qc].
 - [3] M. Levi and J. Steinhoff, Spinning gravitating objects in the effective field theory in the post-Newtonian scheme, *JHEP* **09**, 219, arXiv:1501.04956 [gr-qc].
 - [4] R. A. Porto, The effective field theorist's approach to gravitational dynamics, *Phys. Rept.* **633**, 1 (2016), arXiv:1601.04914 [hep-th].
 - [5] M. Levi, Effective Field Theories of Post-Newtonian Gravity: A comprehensive review, *Rept. Prog. Phys.* **83**, 075901 (2020), arXiv:1807.01699 [hep-th].
 - [6] K. Westpfahl and M. Goller, Gravitational scattering of two relativistic particles in post-linear approximation, *Lett. Nuovo Cim.* **26**, 573 (1979).
 - [7] L. Bel, T. Damour, N. Deruelle, J. Ibanez, and J. Martin, Poincaré-invariant gravitational field and equations of motion of two pointlike objects: The postlinear approximation of general relativity, *Gen. Rel. Grav.* **13**, 963 (1981).
 - [8] T. Damour, Gravitational scattering, post-Minkowskian approximation and Effective One-Body theory, *Phys. Rev. D* **94**, 104015 (2016), arXiv:1609.00354 [gr-qc].
 - [9] T. Damour, High-energy gravitational scattering and the general relativistic two-body problem, *Phys. Rev. D* **97**, 044038 (2018), arXiv:1710.10599 [gr-qc].
 - [10] Y. Mino, M. Sasaki, and T. Tanaka, Gravitational radiation reaction to a particle motion, *Phys. Rev. D* **55**, 3457 (1997), arXiv:gr-qc/9606018.
 - [11] T. C. Quinn and R. M. Wald, An Axiomatic approach to electromagnetic and gravitational radiation reaction of particles in curved space-time, *Phys. Rev. D* **56**, 3381 (1997), arXiv:gr-qc/9610053.
 - [12] L. Barack and A. Pound, Self-force and radiation reaction in general relativity, *Rept. Prog. Phys.* **82**, 016904 (2019), arXiv:1805.10385 [gr-qc].
 - [13] A. Pound and B. Wardell, Black hole perturbation theory and gravitational self-force 10.1007/978-981-15-4702-7_38-1 (2021), arXiv:2101.04592 [gr-qc].
 - [14] S. Foffa, Gravitating binaries at 5PN in the post-Minkowskian approximation, *Phys. Rev. D* **89**, 024019 (2014), arXiv:1309.3956 [gr-qc].
 - [15] S. Foffa, P. Mastrolia, R. Sturani, and C. Sturm, Effective field theory approach to the gravitational two-

- body dynamics, at fourth post-Newtonian order and quintic in the Newton constant, *Phys. Rev. D* **95**, 104009 (2017), [arXiv:1612.00482 \[gr-qc\]](#).
- [16] G. Kälin and R. A. Porto, From Boundary Data to Bound States, *JHEP* **01**, 072, [arXiv:1910.03008 \[hep-th\]](#).
- [17] J. Blümlein, A. Maier, P. Marquard, and G. Schäfer, Testing binary dynamics in gravity at the sixth post-Newtonian level, *Phys. Lett. B* **807**, 135496 (2020), [arXiv:2003.07145 \[gr-qc\]](#).
- [18] J. Blümlein, A. Maier, P. Marquard, and G. Schäfer, Fourth post-Newtonian Hamiltonian dynamics of two-body systems from an effective field theory approach, *Nucl. Phys. B* **955**, 115041 (2020), [arXiv:2003.01692 \[gr-qc\]](#).
- [19] J. Blümlein, A. Maier, P. Marquard, and G. Schäfer, The fifth-order post-Newtonian Hamiltonian dynamics of two-body systems from an effective field theory approach, *Nucl. Phys. B* **983**, 115900 (2022), [Erratum: *Nucl. Phys. B* 985, 115991 (2022)], [arXiv:2110.13822 \[gr-qc\]](#).
- [20] J. Blümlein, A. Maier, P. Marquard, and G. Schäfer, The 6th post-Newtonian potential terms at $O(G_N^4)$, *Phys. Lett. B* **816**, 136260 (2021), [arXiv:2101.08630 \[gr-qc\]](#).
- [21] G. Kälin, Z. Liu, and R. A. Porto, Conservative Dynamics of Binary Systems to Third Post-Minkowskian Order from the Effective Field Theory Approach, *Phys. Rev. Lett.* **125**, 261103 (2020), [arXiv:2007.04977 \[hep-th\]](#).
- [22] G. Kälin and R. A. Porto, Post-Minkowskian Effective Field Theory for Conservative Binary Dynamics, *JHEP* **11**, 106, [arXiv:2006.01184 \[hep-th\]](#).
- [23] C. Dlapa, G. Kälin, Z. Liu, and R. A. Porto, Dynamics of binary systems to fourth Post-Minkowskian order from the effective field theory approach, *Phys. Lett. B* **831**, 137203 (2022), [arXiv:2106.08276 \[hep-th\]](#).
- [24] C. Dlapa, G. Kälin, Z. Liu, and R. A. Porto, Conservative Dynamics of Binary Systems at Fourth Post-Minkowskian Order in the Large-Eccentricity Expansion, *Phys. Rev. Lett.* **128**, 161104 (2022), [arXiv:2112.11296 \[hep-th\]](#).
- [25] G. Cho, R. A. Porto, and Z. Yang, Gravitational radiation from inspiralling compact objects: Spin effects to the fourth post-Newtonian order, *Phys. Rev. D* **106**, L101501 (2022), [arXiv:2201.05138 \[gr-qc\]](#).
- [26] C. Dlapa, G. Kälin, Z. Liu, J. Neef, and R. A. Porto, Radiation Reaction and Gravitational Waves at Fourth Post-Minkowskian Order, *Phys. Rev. Lett.* **130**, 101401 (2023), [arXiv:2210.05541 \[hep-th\]](#).
- [27] C. Dlapa, G. Kälin, Z. Liu, and R. A. Porto, Local in Time Conservative Binary Dynamics at Fourth Post-Minkowskian Order, *Phys. Rev. Lett.* **132**, 221401 (2024), [arXiv:2403.04853 \[hep-th\]](#).
- [28] G. Mogull, J. Plefka, and J. Steinhoff, Classical black hole scattering from a worldline quantum field theory, *JHEP* **02**, 048, [arXiv:2010.02865 \[hep-th\]](#).
- [29] G. U. Jakobsen, G. Mogull, J. Plefka, and J. Steinhoff, Classical Gravitational Bremsstrahlung from a Worldline Quantum Field Theory, *Phys. Rev. Lett.* **126**, 201103 (2021), [arXiv:2101.12688 \[gr-qc\]](#).
- [30] G. U. Jakobsen, G. Mogull, J. Plefka, and J. Steinhoff, Gravitational Bremsstrahlung and Hidden Supersymmetry of Spinning Bodies, *Phys. Rev. Lett.* **128**, 011101 (2022), [arXiv:2106.10256 \[hep-th\]](#).
- [31] G. U. Jakobsen, G. Mogull, J. Plefka, and J. Steinhoff, SUSY in the sky with gravitons, *JHEP* **01**, 027, [arXiv:2109.04465 \[hep-th\]](#).
- [32] G. U. Jakobsen and G. Mogull, Conservative and Radiative Dynamics of Spinning Bodies at Third Post-Minkowskian Order Using Worldline Quantum Field Theory, *Phys. Rev. Lett.* **128**, 141102 (2022), [arXiv:2201.07778 \[hep-th\]](#).
- [33] G. U. Jakobsen, G. Mogull, J. Plefka, B. Sauer, and Y. Xu, Conservative Scattering of Spinning Black Holes at Fourth Post-Minkowskian Order, *Phys. Rev. Lett.* **131**, 151401 (2023), [arXiv:2306.01714 \[hep-th\]](#).
- [34] G. U. Jakobsen, G. Mogull, J. Plefka, and B. Sauer, Dissipative Scattering of Spinning Black Holes at Fourth Post-Minkowskian Order, *Phys. Rev. Lett.* **131**, 241402 (2023), [arXiv:2308.11514 \[hep-th\]](#).
- [35] M. Driesse, G. U. Jakobsen, G. Mogull, J. Plefka, B. Sauer, and J. Usovitsch, Conservative Black Hole Scattering at Fifth Post-Minkowskian and First Self-Force Order, *Phys. Rev. Lett.* **132**, 241402 (2024), [arXiv:2403.07781 \[hep-th\]](#).
- [36] N. Arkani-Hamed, T.-C. Huang, and Y.-t. Huang, Scattering amplitudes for all masses and spins, *JHEP* **11**, 070, [arXiv:1709.04891 \[hep-th\]](#).
- [37] N. E. J. Bjerrum-Bohr, P. H. Damgaard, G. Festuccia, L. Planté, and P. Vanhove, General Relativity from Scattering Amplitudes, *Phys. Rev. Lett.* **121**, 171601 (2018), [arXiv:1806.04920 \[hep-th\]](#).
- [38] A. Guevara, A. Ochirov, and J. Vines, Scattering of Spinning Black Holes from Exponentiated Soft Factors, *JHEP* **09**, 056, [arXiv:1812.06895 \[hep-th\]](#).
- [39] D. A. Kosower, B. Maybee, and D. O’Connell, Amplitudes, Observables, and Classical Scattering, *JHEP* **02**, 137, [arXiv:1811.10950 \[hep-th\]](#).
- [40] C. Cheung, I. Z. Rothstein, and M. P. Solon, From Scattering Amplitudes to Classical Potentials in the Post-Minkowskian Expansion, *Phys. Rev. Lett.* **121**, 251101 (2018), [arXiv:1808.02489 \[hep-th\]](#).
- [41] Y. F. Bautista and A. Guevara, From Scattering Amplitudes to Classical Physics: Universality, Double Copy and Soft Theorems, (2019), [arXiv:1903.12419 \[hep-th\]](#).
- [42] A. Guevara, A. Ochirov, and J. Vines, Black-hole scattering with general spin directions from minimal-coupling amplitudes, *Phys. Rev. D* **100**, 104024 (2019), [arXiv:1906.10071 \[hep-th\]](#).
- [43] Z. Bern, C. Cheung, R. Roiban, C.-H. Shen, M. P. Solon, and M. Zeng, Scattering Amplitudes and the Conservative Hamiltonian for Binary Systems at Third Post-Minkowskian Order, *Phys. Rev. Lett.* **122**, 201603 (2019), [arXiv:1901.04424 \[hep-th\]](#).
- [44] N. E. J. Bjerrum-Bohr, A. Cristofoli, and P. H. Damgaard, Post-Minkowskian Scattering Angle in Einstein Gravity, *JHEP* **08**, 038, [arXiv:1910.09366 \[hep-th\]](#).
- [45] Z. Bern, A. Luna, R. Roiban, C.-H. Shen, and M. Zeng, Spinning black hole binary dynamics, scattering amplitudes, and effective field theory, *Phys. Rev. D* **104**, 065014 (2021), [arXiv:2005.03071 \[hep-th\]](#).
- [46] A. Cristofoli, P. H. Damgaard, P. Di Vecchia, and C. Heissenberg, Second-order Post-Minkowskian scattering in arbitrary dimensions, *JHEP* **07**, 122, [arXiv:2003.10274 \[hep-th\]](#).

- [47] N. E. J. Bjerrum-Bohr, P. H. Damgaard, L. Planté, and P. Vanhove, Classical gravity from loop amplitudes, *Phys. Rev. D* **104**, 026009 (2021), [arXiv:2104.04510 \[hep-th\]](#).
- [48] E. Herrmann, J. Parra-Martinez, M. S. Ruf, and M. Zeng, Radiative classical gravitational observables at $\mathcal{O}(G^3)$ from scattering amplitudes, *JHEP* **10**, 148, [arXiv:2104.03957 \[hep-th\]](#).
- [49] Z. Bern, J. Parra-Martinez, R. Roiban, M. S. Ruf, C.-H. Shen, M. P. Solon, and M. Zeng, Scattering Amplitudes and Conservative Binary Dynamics at $\mathcal{O}(G^4)$, *Phys. Rev. Lett.* **126**, 171601 (2021), [arXiv:2101.07254 \[hep-th\]](#).
- [50] P. Di Vecchia, C. Heissenberg, R. Russo, and G. Veneziano, The eikonal approach to gravitational scattering and radiation at $\mathcal{O}(G^3)$, *JHEP* **07**, 169, [arXiv:2104.03256 \[hep-th\]](#).
- [51] Z. Bern, J. Parra-Martinez, R. Roiban, M. S. Ruf, C.-H. Shen, M. P. Solon, and M. Zeng, Scattering Amplitudes, the Tail Effect, and Conservative Binary Dynamics at $\mathcal{O}(G^4)$, *Phys. Rev. Lett.* **128**, 161103 (2022), [arXiv:2112.10750 \[hep-th\]](#).
- [52] Y. F. Bautista, A. Guevara, C. Kavanagh, and J. Vines, Scattering in black hole backgrounds and higher-spin amplitudes. Part I, *JHEP* **03**, 136, [arXiv:2107.10179 \[hep-th\]](#).
- [53] A. Cristofoli, R. Gonzo, D. A. Kosower, and D. O’Connell, Waveforms from amplitudes, *Phys. Rev. D* **106**, 056007 (2022), [arXiv:2107.10193 \[hep-th\]](#).
- [54] E. Herrmann, J. Parra-Martinez, M. S. Ruf, and M. Zeng, Gravitational Bremsstrahlung from Reverse Unitarity, *Phys. Rev. Lett.* **126**, 201602 (2021), [arXiv:2101.07255 \[hep-th\]](#).
- [55] G. Travaglini *et al.*, The SAGEX review on scattering amplitudes, *J. Phys. A* **55**, 443001 (2022), [arXiv:2203.13011 \[hep-th\]](#).
- [56] N. E. J. Bjerrum-Bohr, P. H. Damgaard, L. Plante, and P. Vanhove, The SAGEX review on scattering amplitudes Chapter 13: Post-Minkowskian expansion from scattering amplitudes, *J. Phys. A* **55**, 443014 (2022), [arXiv:2203.13024 \[hep-th\]](#).
- [57] D. A. Kosower, R. Monteiro, and D. O’Connell, The SAGEX review on scattering amplitudes Chapter 14: Classical gravity from scattering amplitudes, *J. Phys. A* **55**, 443015 (2022), [arXiv:2203.13025 \[hep-th\]](#).
- [58] Z. Bern, E. Herrmann, R. Roiban, M. S. Ruf, A. V. Smirnov, V. A. Smirnov, and M. Zeng, Amplitudes, Supersymmetric Black Hole Scattering at $\mathcal{O}(G^5)$, and Loop Integration, (2024), [arXiv:2406.01554 \[hep-th\]](#).
- [59] A. Luna, N. Moynihan, D. O’Connell, and A. Ross, Observables from the Spinning Eikonal, (2023), [arXiv:2312.09960 \[hep-th\]](#).
- [60] S. Mougiakakos and P. Vanhove, Schwarzschild metric from Scattering Amplitudes to all orders in G_N , (2024), [arXiv:2405.14421 \[hep-th\]](#).
- [61] C. Cheung, J. Parra-Martinez, I. Z. Rothstein, N. Shah, and J. Wilson-Gerow, Gravitational Scattering and Beyond from Extreme Mass Ratio Effective Field Theory, (2024), [arXiv:2406.14770 \[hep-th\]](#).
- [62] C. Cheung, J. Parra-Martinez, I. Z. Rothstein, N. Shah, and J. Wilson-Gerow, Effective Field Theory for Extreme Mass Ratio Binaries, *Phys. Rev. Lett.* **132**, 091402 (2024), [arXiv:2308.14832 \[hep-th\]](#).
- [63] D. Kosmopoulos and M. P. Solon, Gravitational self force from scattering amplitudes in curved space, *JHEP* **03**, 125, [arXiv:2308.15304 \[hep-th\]](#).
- [64] L. Barack *et al.*, Comparison of post-Minkowskian and self-force expansions: Scattering in a scalar charge toy model, *Phys. Rev. D* **108**, 024025 (2023), [arXiv:2304.09200 \[hep-th\]](#).
- [65] O. Long, C. Whittall, and L. Barack, Black hole scattering near the transition to plunge: Self-force and resummation of post-Minkowskian theory, (2024), [arXiv:2406.08363 \[gr-qc\]](#).
- [66] D. Bini, A. Geralico, C. Kavanagh, A. Pound, and D. Usseglio, Post-Minkowskian self-force in the low-velocity limit: scalar field scattering, (2024), [arXiv:2406.15878 \[gr-qc\]](#).
- [67] M. V. S. Saketh, Z. Zhou, and M. M. Ivanov, Dynamical tidal response of Kerr black holes from scattering amplitudes, *Phys. Rev. D* **109**, 064058 (2024), [arXiv:2307.10391 \[hep-th\]](#).
- [68] M. M. Ivanov and Z. Zhou, Vanishing of Black Hole Tidal Love Numbers from Scattering Amplitudes, *Phys. Rev. Lett.* **130**, 091403 (2023), [arXiv:2209.14324 \[hep-th\]](#).
- [69] M. V. S. Saketh, J. Steinhoff, J. Vines, and A. Buonanno, Modeling horizon absorption in spinning binary black holes using effective worldline theory, *Phys. Rev. D* **107**, 084006 (2023), [arXiv:2212.13095 \[gr-qc\]](#).
- [70] H. S. Chia, Z. Zhou, and M. M. Ivanov, Bring the Heat: Tidal Heating Constraints for Black Holes and Exotic Compact Objects from the LIGO-Virgo-KAGRA Data, (2024), [arXiv:2404.14641 \[gr-qc\]](#).
- [71] Z. Bern, J. Parra-Martinez, R. Roiban, E. Sawyer, and C.-H. Shen, Leading Nonlinear Tidal Effects and Scattering Amplitudes, *JHEP* **05**, 188, [arXiv:2010.08559 \[hep-th\]](#).
- [72] G. Kälin, Z. Liu, and R. A. Porto, Conservative Tidal Effects in Compact Binary Systems to Next-to-Leading Post-Minkowskian Order, *Phys. Rev. D* **102**, 124025 (2020), [arXiv:2008.06047 \[hep-th\]](#).
- [73] M. M. Ivanov, Y.-Z. Li, J. Parra-Martinez, and Z. Zhou, Gravitational Raman Scattering in Effective Field Theory: A Scalar Tidal Matching at $\mathcal{O}(G^3)$, *Phys. Rev. Lett.* **132**, 131401 (2024), [arXiv:2401.08752 \[hep-th\]](#).
- [74] J. Vines, Scattering of two spinning black holes in post-Minkowskian gravity, to all orders in spin, and effective-one-body mappings, *Class. Quant. Grav.* **35**, 084002 (2018), [arXiv:1709.06016 \[gr-qc\]](#).
- [75] M.-Z. Chung, Y.-T. Huang, J.-W. Kim, and S. Lee, The simplest massive S-matrix: from minimal coupling to Black Holes, *JHEP* **04**, 156, [arXiv:1812.08752 \[hep-th\]](#).
- [76] R. Aoude, K. Haddad, and A. Helset, On-shell heavy particle effective theories, *JHEP* **05**, 051, [arXiv:2001.09164 \[hep-th\]](#).
- [77] Y. F. Bautista and N. Siemonsen, Post-Newtonian waveforms from spinning scattering amplitudes, *JHEP* **01**, 006, [arXiv:2110.12537 \[hep-th\]](#).
- [78] S. De Angelis, R. Gonzo, and P. P. Novichkov, Spinning waveforms from KMOC at leading order, (2023), [arXiv:2309.17429 \[hep-th\]](#).
- [79] R. Aoude, K. Haddad, and A. Helset, Searching for Kerr in the 2PM amplitude, *JHEP* **07**, 072, [arXiv:2203.06197 \[hep-th\]](#).
- [80] Z. Bern, D. Kosmopoulos, A. Luna, R. Roiban, and F. Teng, Binary Dynamics through the Fifth Power of Spin at $\mathcal{O}(G^2)$, *Phys. Rev. Lett.* **130**, 201402 (2023),

- arXiv:2203.06202 [hep-th].
- [81] R. Aoude, K. Haddad, and A. Helset, Classical Gravitational Spinning-Spinless Scattering at $O(G_2S_\infty)$, *Phys. Rev. Lett.* **129**, 141102 (2022), arXiv:2205.02809 [hep-th].
- [82] K. Haddad, Recursion in the classical limit and the neutron-star Compton amplitude, *JHEP* **05**, 177, arXiv:2303.02624 [hep-th].
- [83] M. Chiodaroli, H. Johansson, and P. Pichini, Compton black-hole scattering for $s \leq 5/2$, *JHEP* **02**, 156, arXiv:2107.14779 [hep-th].
- [84] L. Cangemi, M. Chiodaroli, H. Johansson, A. Ochirov, P. Pichini, and E. Skvortsov, Kerr Black Holes From Massive Higher-Spin Gauge Symmetry, *Phys. Rev. Lett.* **131**, 221401 (2023), arXiv:2212.06120 [hep-th].
- [85] N. E. J. Bjerrum-Bohr, G. Chen, and M. Skowronek, Classical spin gravitational Compton scattering, *JHEP* **06**, 170, arXiv:2302.00498 [hep-th].
- [86] A. Brandhuber, G. R. Brown, G. Chen, J. Gowdy, and G. Travaglini, Resummed spinning waveforms from five-point amplitudes, *JHEP* **02**, 026, arXiv:2310.04405 [hep-th].
- [87] F. Alessio, Kerr binary dynamics from minimal coupling and double copy, *JHEP* **04**, 058, arXiv:2303.12784 [hep-th].
- [88] S. Akhtar, A. Manna, and A. Manu, Classical observables using exponentiated spin factors: electromagnetic scattering, *JHEP* **05**, 148, arXiv:2401.15574 [hep-th].
- [89] J.-H. Kim, J.-W. Kim, and S. Lee, Massive twistor worldline in electromagnetic fields, (2024), arXiv:2405.17056 [hep-th].
- [90] M. Ben-Shahar, Scattering of spinning compact objects from a worldline EFT, *JHEP* **03**, 108, arXiv:2311.01430 [hep-th].
- [91] T. Scheopner and J. Vines, Dynamical Implications of the Kerr Multipole Moments for Spinning Black Holes, (2023), arXiv:2311.18421 [gr-qc].
- [92] L. Cangemi and P. Pichini, Classical limit of higher-spin string amplitudes, *JHEP* **06**, 167, arXiv:2207.03947 [hep-th].
- [93] T. Azevedo, D. E. A. Matamoros, and G. Menezes, Compton scattering from superstrings, (2024), arXiv:2403.08899 [hep-th].
- [94] Y. F. Bautista, A. Guevara, C. Kavanagh, and J. Vines, Scattering in black hole backgrounds and higher-spin amplitudes. Part II, *JHEP* **05**, 211, arXiv:2212.07965 [hep-th].
- [95] Y. F. Bautista, G. Bonelli, C. Iossa, A. Tanzini, and Z. Zhou, Black hole perturbation theory meets CFT2: Kerr-Compton amplitudes from Nekrasov-Shatashvili functions, *Phys. Rev. D* **109**, 084071 (2024), arXiv:2312.05965 [hep-th].
- [96] R. A. Porto, Absorption effects due to spin in the worldline approach to black hole dynamics, *Phys. Rev. D* **77**, 064026 (2008), arXiv:0710.5150 [hep-th].
- [97] S. L. Detweiler, A Consequence of the gravitational self-force for circular orbits of the Schwarzschild geometry, *Phys. Rev. D* **77**, 124026 (2008), arXiv:0804.3529 [gr-qc].
- [98] D. Bini and T. Damour, High-order post-Newtonian contributions to the two-body gravitational interaction potential from analytical gravitational self-force calculations, *Phys. Rev. D* **89**, 064063 (2014), arXiv:1312.2503 [gr-qc].
- [99] C. Kavanagh, A. C. Ottewill, and B. Wardell, Analytical high-order post-Newtonian expansions for extreme mass ratio binaries, *Phys. Rev. D* **92**, 084025 (2015), arXiv:1503.02334 [gr-qc].
- [100] S. Hopper, C. Kavanagh, and A. C. Ottewill, Analytical self-force calculations in the post-Newtonian regime: eccentric orbits on a Schwarzschild background, *Phys. Rev. D* **93**, 044010 (2016), arXiv:1512.01556 [gr-qc].
- [101] D. Bini, T. Damour, and A. Geralico, Confirming and improving post-Newtonian and effective-one-body results from self-force computations along eccentric orbits around a Schwarzschild black hole, *Phys. Rev. D* **93**, 064023 (2016), arXiv:1511.04533 [gr-qc].
- [102] C. Kavanagh, A. C. Ottewill, and B. Wardell, Analytical high-order post-Newtonian expansions for spinning extreme mass ratio binaries, *Phys. Rev. D* **93**, 124038 (2016), arXiv:1601.03394 [gr-qc].
- [103] D. Bini, T. Damour, A. Geralico, and C. Kavanagh, Detweiler's redshift invariant for spinning particles along circular orbits on a Schwarzschild background, *Phys. Rev. D* **97**, 104022 (2018), arXiv:1801.09616 [gr-qc].
- [104] D. Bini and A. Geralico, New gravitational self-force analytical results for eccentric equatorial orbits around a Kerr black hole: redshift invariant, *Phys. Rev. D* **100**, 104002 (2019), arXiv:1907.11080 [gr-qc].
- [105] D. Bini, A. Geralico, and J. Steinhoff, Detweiler's redshift invariant for extended bodies orbiting a Schwarzschild black hole, *Phys. Rev. D* **102**, 024091 (2020), arXiv:2003.12887 [gr-qc].
- [106] C. Munna and C. R. Evans, High-order post-Newtonian expansion of the redshift invariant for eccentric-orbit nonspinning extreme-mass-ratio inspirals, *Phys. Rev. D* **106**, 044004 (2022), arXiv:2203.13832 [gr-qc].
- [107] C. Munna, High-order post-Newtonian expansion of the generalized redshift invariant for eccentric-orbit, equatorial extreme-mass-ratio inspirals with a spinning primary, *Phys. Rev. D* **108**, 084012 (2023), arXiv:2307.11158 [gr-qc].
- [108] S. R. Dolan, N. Warburton, A. I. Harte, A. Le Tiec, B. Wardell, and L. Barack, Gravitational self-torque and spin precession in compact binaries, *Phys. Rev. D* **89**, 064011 (2014), arXiv:1312.0775 [gr-qc].
- [109] D. Bini and T. Damour, Two-body gravitational spin-orbit interaction at linear order in the mass ratio, *Phys. Rev. D* **90**, 024039 (2014), arXiv:1404.2747 [gr-qc].
- [110] S. Akcay, D. Dempsey, and S. R. Dolan, Spin-orbit precession for eccentric black hole binaries at first order in the mass ratio, *Class. Quant. Grav.* **34**, 084001 (2017), arXiv:1608.04811 [gr-qc].
- [111] C. Kavanagh, D. Bini, T. Damour, S. Hopper, A. C. Ottewill, and B. Wardell, Spin-orbit precession along eccentric orbits for extreme mass ratio black hole binaries and its effective-one-body transcription, *Phys. Rev. D* **96**, 064012 (2017), arXiv:1706.00459 [gr-qc].
- [112] D. Bini, T. Damour, A. Geralico, C. Kavanagh, and M. van de Meent, Gravitational self-force corrections to gyroscope precession along circular orbits in the Kerr spacetime, *Phys. Rev. D* **98**, 104062 (2018), arXiv:1809.02516 [gr-qc].
- [113] D. Bini and A. Geralico, New gravitational self-force analytical results for eccentric equatorial orbits around a Kerr black hole: gyroscope precession, *Phys. Rev. D*

- 100**, 104003 (2019), [arXiv:1907.11082 \[gr-qc\]](#).
- [114] C. Munna and C. R. Evans, Post-Newtonian expansion of the spin-precession invariant for eccentric-orbit nonspinning extreme-mass-ratio inspirals to 9PN and e16, *Phys. Rev. D* **106**, 044058 (2022), [arXiv:2206.04085 \[gr-qc\]](#).
- [115] D. Bini, T. Damour, and A. Geralico, Novel approach to binary dynamics: application to the fifth post-Newtonian level, *Phys. Rev. Lett.* **123**, 231104 (2019), [arXiv:1909.02375 \[gr-qc\]](#).
- [116] D. Bini, T. Damour, and A. Geralico, Binary dynamics at the fifth and fifth-and-a-half post-Newtonian orders, *Phys. Rev. D* **102**, 024062 (2020), [arXiv:2003.11891 \[gr-qc\]](#).
- [117] N. Siemonsen and J. Vines, Test black holes, scattering amplitudes and perturbations of Kerr spacetime, *Phys. Rev. D* **101**, 064066 (2020), [arXiv:1909.07361 \[gr-qc\]](#).
- [118] A. Antonelli, C. Kavanagh, M. Khalil, J. Steinhoff, and J. Vines, Gravitational spin-orbit and aligned spin₁-spin₂ couplings through third-subleading post-Newtonian orders, *Phys. Rev. D* **102**, 124024 (2020), [arXiv:2010.02018 \[gr-qc\]](#).
- [119] T. Damour, Classical and quantum scattering in post-Minkowskian gravity, *Phys. Rev. D* **102**, 024060 (2020), [arXiv:1912.02139 \[gr-qc\]](#).
- [120] S. Mano, H. Suzuki, and E. Takasugi, Analytic solutions of the Regge-Wheeler equation and the postMinkowskian expansion, *Prog. Theor. Phys.* **96**, 549 (1996), [arXiv:gr-qc/9605057](#).
- [121] S. Mano, H. Suzuki, and E. Takasugi, Analytic solutions of the Teukolsky equation and their low frequency expansions, *Prog. Theor. Phys.* **95**, 1079 (1996), [arXiv:gr-qc/9603020](#).
- [122] A. Le Tiec, L. Blanchet, and B. F. Whiting, The First Law of Binary Black Hole Mechanics in General Relativity and Post-Newtonian Theory, *Phys. Rev. D* **85**, 064039 (2012), [arXiv:1111.5378 \[gr-qc\]](#).
- [123] L. Blanchet, A. Buonanno, and A. Le Tiec, First law of mechanics for black hole binaries with spins, *Phys. Rev. D* **87**, 024030 (2013), [arXiv:1211.1060 \[gr-qc\]](#).
- [124] A. Le Tiec, First Law of Mechanics for Compact Binaries on Eccentric Orbits, *Phys. Rev. D* **92**, 084021 (2015), [arXiv:1506.05648 \[gr-qc\]](#).
- [125] L. Blanchet and A. Le Tiec, First Law of Compact Binary Mechanics with Gravitational-Wave Tails, *Class. Quant. Grav.* **34**, 164001 (2017), [arXiv:1702.06839 \[gr-qc\]](#).
- [126] R. Fujita, S. Isoyama, A. Le Tiec, H. Nakano, N. Sago, and T. Tanaka, Hamiltonian Formulation of the Conservative Self-Force Dynamics in the Kerr Geometry, *Class. Quant. Grav.* **34**, 134001 (2017), [arXiv:1612.02504 \[gr-qc\]](#).
- [127] The ancillary file `alignedspin_binary_NLOS6.m` contains the scattering angle, Hamiltonian, redshift, and spin-precession invariant, for aligned-spin binary dynamics up to NLO S⁶.
The file `testbody_observables.m` contains the scattering angle, redshift, and spin-precession invariant for a test body in a Kerr background.
The file `ComptonCoefficients.m` contains the Compton amplitude coefficients determined by matching to Teukolsky solutions.
- [128] S. Akcay, A. Le Tiec, L. Barack, N. Sago, and N. Warburton, Comparison Between Self-Force and Post-Newtonian Dynamics: Beyond Circular Orbits, *Phys. Rev. D* **91**, 124014 (2015), [arXiv:1503.01374 \[gr-qc\]](#).
- [129] J. Vines, J. Steinhoff, and A. Buonanno, Spinning-black-hole scattering and the test-black-hole limit at second post-Minkowskian order, *Phys. Rev. D* **99**, 064054 (2019), [arXiv:1812.00956 \[gr-qc\]](#).
- [130] T. Damour, P. Jaranowski, and G. Schäfer, Fourth post-Newtonian effective one-body dynamics, *Phys. Rev. D* **91**, 084024 (2015), [arXiv:1502.07245 \[gr-qc\]](#).
- [131] M. H. L. Pryce, The mass-centre in the restricted theory of relativity and its connexion with the quantum theory of elementary particles, *Proceedings of the Royal Society of London. Series A. Mathematical and Physical Sciences* **195**, 62 (1948).
- [132] T. D. Newton and E. P. Wigner, Localized states for elementary systems, *Reviews of Modern Physics* **21**, 400 (1949).
- [133] W. Tulczyjew, Equations of motion of rotating bodies in general relativity theory, *Acta Phys. Polon.* **18**, 37 (1959), [Erratum: *Acta Phys. Polon.* **18**, 534 (1959)].
- [134] W. G. Dixon, Dynamics of extended bodies in general relativity. I. Momentum and angular momentum, *Proc. Roy. Soc. Lond. A* **314**, 499 (1970).
- [135] W. G. Dixon, Dynamics of extended bodies in general relativity. II. Moments of the charge-current vector, *Proc. Roy. Soc. Lond. A* **319**, 509 (1970).
- [136] T. Damour and G. Schaefer, Higher Order Relativistic Periastron Advances and Binary Pulsars, *Nuovo Cim. B* **101**, 127 (1988).
- [137] M. Khalil, Gravitational spin-orbit dynamics at the fifth-and-a-half post-Newtonian order, *Phys. Rev. D* **104**, 124015 (2021), [arXiv:2110.12813 \[gr-qc\]](#).
- [138] A. Antonelli, C. Kavanagh, M. Khalil, J. Steinhoff, and J. Vines, Gravitational spin-orbit coupling through third-subleading post-Newtonian order: from first-order self-force to arbitrary mass ratios, *Phys. Rev. Lett.* **125**, 011103 (2020), [arXiv:2003.11391 \[gr-qc\]](#).
- [139] M. K. Mandal, P. Mastrolia, R. Patil, and J. Steinhoff, Gravitational spin-orbit Hamiltonian at NNNLO in the post-Newtonian framework, *JHEP* **03**, 130, [arXiv:2209.00611 \[hep-th\]](#).
- [140] J.-W. Kim, M. Levi, and Z. Yin, N³LO spin-orbit interaction via the EFT of spinning gravitating objects, *JHEP* **05**, 184, [arXiv:2208.14949 \[hep-th\]](#).
- [141] J.-W. Kim, M. Levi, and Z. Yin, N³LO quadratic-in-spin interactions for generic compact binaries, *JHEP* **03**, 098, [arXiv:2209.09235 \[hep-th\]](#).
- [142] J.-W. Kim, M. Levi, and Z. Yin, Quadratic-in-spin interactions at fifth post-Newtonian order probe new physics, *Phys. Lett. B* **834**, 137410 (2022), [arXiv:2112.01509 \[hep-th\]](#).
- [143] M. K. Mandal, P. Mastrolia, R. Patil, and J. Steinhoff, Gravitational quadratic-in-spin Hamiltonian at NNNLO in the post-Newtonian framework, *JHEP* **07**, 128, [arXiv:2210.09176 \[hep-th\]](#).
- [144] M. Levi, S. Mougiakakos, and M. Vieira, Gravitational cubic-in-spin interaction at the next-to-leading post-Newtonian order, *JHEP* **01**, 036, [arXiv:1912.06276 \[hep-th\]](#).
- [145] M. Levi and F. Teng, NLO gravitational quartic-in-spin interaction, *JHEP* **01**, 066, [arXiv:2008.12280 \[hep-th\]](#).
- [146] M. Levi and Z. Yin, Completing the fifth PN precision frontier via the EFT of spinning gravitating objects,

- JHEP **04**, 079, arXiv:2211.14018 [hep-th].
- [147] Black Hole Perturbation Toolkit, (bhptoolkit.org).
- [148] C. Darwin, The Gravity Field of a Particle, *Proceedings of the Royal Society of London Series A* **249**, 180 (1959).
- [149] D. Bini, T. Damour, and A. Geralico, High post-Newtonian order gravitational self-force analytical results for eccentric equatorial orbits around a Kerr black hole, *Phys. Rev. D* **93**, 124058 (2016), arXiv:1602.08282 [gr-qc].
- [150] F. Cachazo and A. Guevara, Leading Singularities and Classical Gravitational Scattering, *JHEP* **02**, 181, arXiv:1705.10262 [hep-th].
- [151] S. R. Dolan, Scattering and Absorption of Gravitational Plane Waves by Rotating Black Holes, *Class. Quant. Grav.* **25**, 235002 (2008), arXiv:0801.3805 [gr-qc].
- [152] F. Fucito and J. F. Morales, Post Newtonian emission of gravitational waves from binary systems: a gauge theory perspective, *JHEP* **03**, 106, arXiv:2311.14637 [gr-qc].
- [153] R. Flume, F. Fucito, J. F. Morales, and R. Poghossian, Matone's relation in the presence of gravitational couplings, *JHEP* **04**, 008, arXiv:hep-th/0403057.
- [154] M. Matone, Instantons and recursion relations in N=2 SUSY gauge theory, *Phys. Lett. B* **357**, 342 (1995), arXiv:hep-th/9506102.
- [155] Y. F. Bautista, Dynamics for super-extremal Kerr binary systems at $\mathcal{O}(G^2)$, *Phys. Rev. D* **108**, 084036 (2023), arXiv:2304.04287 [hep-th].
- [156] A. Guevara, Holomorphic Classical Limit for Spin Effects in Gravitational and Electromagnetic Scattering, *JHEP* **04**, 033, arXiv:1706.02314 [hep-th].
- [157] D. Kosmopoulos and A. Luna, Quadratic-in-spin Hamiltonian at $\mathcal{O}(G^2)$ from scattering amplitudes, *JHEP* **07**, 037, arXiv:2102.10137 [hep-th].
- [158] L. Cangemi, M. Chiodaroli, H. Johansson, A. Ochirov, P. Pichini, and E. Skvortsov, Compton Amplitude for Rotating Black Hole from QFT, (2023), arXiv:2312.14913 [hep-th].
- [159] J. Vines, D. Kunst, J. Steinhoff, and T. Hinderer, Canonical Hamiltonian for an extended test body in curved spacetime: To quadratic order in spin, *Phys. Rev. D* **93**, 103008 (2016), [Erratum: Phys.Rev.D 104, 029902 (2021)], arXiv:1601.07529 [gr-qc].
- [160] M. Mathisson, Republication of: New mechanics of material systems, *General relativity and gravitation* **42**, 1011 (2010).
- [161] A. Papapetrou, Spinning test particles in general relativity. 1., *Proc. Roy. Soc. Lond. A* **209**, 248 (1951).
- [162] A. I. Harte, Motion in classical field theories and the foundations of the self-force problem, *Fund. Theor. Phys.* **179**, 327 (2015), arXiv:1405.5077 [gr-qc].
- [163] J. Ehlers and E. Rudolph, Dynamics of extended bodies in general relativity center-of-mass description and quasirigidity, *General Relativity and Gravitation* **8**, 197 (1977).
- [164] D. Bini, A. Geralico, and J. Vines, Hyperbolic scattering of spinning particles by a Kerr black hole, *Phys. Rev. D* **96**, 084044 (2017), arXiv:1707.09814 [gr-qc].
- [165] P. H. Damgaard, J. Hoogeveen, A. Luna, and J. Vines, Scattering angles in Kerr metrics, *Phys. Rev. D* **106**, 124030 (2022), arXiv:2208.11028 [hep-th].
- [166] M. Pürrer and C.-J. Haster, Gravitational waveform accuracy requirements for future ground-based detectors, *Phys. Rev. Res.* **2**, 023151 (2020), arXiv:1912.10055 [gr-qc].
- [167] J. M. Martín-García, xAct: Efficient tensor computer algebra, <http://www.xact.es/>.
- [168] J. M. Martín-García, xPerm: fast index canonicalization for tensor computer algebra, *Computer physics communications* **179**, 597 (2008), arXiv:0803.0862 [cs.SC].
- [169] D. Bini, A. Geralico, and R. T. Jantzen, Gyroscope precession along bound equatorial plane orbits around a Kerr black hole, *Phys. Rev. D* **94**, 064066 (2016), arXiv:1607.08427 [gr-qc].
- [170] J.-A. Marck, Parallel-tetrad on null geodesics in kerr-newman space-time, *Physics Letters A* **97**, 140 (1983).